creative commons
COMMONS DEED

저작자표시-비영리-변경금지 2.0 대한민국

이용자는 아래의 조건을 따르는 경우에 한하여 자유롭게

- 이 저작물을 복제, 배포, 전송, 전시, 공연 및 방송할 수 있습니다.

다음과 같은 조건을 따라야 합니다:

저작자표시. 귀하는 원저작자를 표시하여야 합니다.

비영리. 귀하는 이 저작물을 영리 목적으로 이용할 수 없습니다.

변경금지. 귀하는 이 저작물을 개작, 변형 또는 가공할 수 없습니다.

- 귀하는, 이 저작물의 재이용이나 배포의 경우, 이 저작물에 적용된 이용허락조건을 명확하게 나타내어야 합니다.
- 저작권자로부터 별도의 허가를 받으면 이러한 조건들은 적용되지 않습니다.

저작권법에 따른 이용자의 권리는 위의 내용에 의하여 영향을 받지 않습니다.

이것은 이용허락규약(Legal Code)을 이해하기 쉽게 요약한 것입니다.

Disclaimer

dCollection

공학박사 학위논문

Bimetallic Catalysts Supported on Mesoporous Carbon for Hydrogenation of Succinic Acid to γ-Butyrolactone and 1,4-Butanediol

숙신산의 수소화 반응으로부터
감마부티로락톤과 1,4-부탄디올을 제조하기
위한 중형기공성 탄소에 담지된 이종금속 촉매

2017년 2월

서울대학교 대학원

화학생물공학부

강 기 혁

Abstract

Bimetallic Catalysts Supported on Mesoporous Carbon for Hydrogenation of Succinic Acid to γ-Butyrolactone and 1,4-Butanediol

Ki Hyuk Kang

School of Chemical and Biological Engineering

The Graduate School

Seoul National University

1,4-Butanediol (BDO) is a versatile chemical that can be used in a wide range of industrial applications. BDO has been used as an organic solvent and a fine chemical for production of adhesives, fibers, and polyurethanes. Recently, BDO has received much attention as an important raw material for thermoplastic polymers such as polybutylene succinate (PBS) and polybutylene terephthalate (PBT). As the consumption of these polymers is growing faster in electronics and automobile industries, in particular, the global demand for BDO is expected to increase rapidly.

BDO has been produced through several conventional routes;

hydrogenation of maleic anhydride, isomerization of propylene oxide, and acetoxylation of butadiene. These processes rely on petrochemical feedstocks derived from fossil fuel. Due to the limited amount of fossil fuel, however, current research trend for BDO production moves toward the utilization of renewable energy sources such as biomass. In this respect, conversion of succinic acid to BDO by catalytic hydrogenation has attracted recent attraction as a promising process, because succinic acid can be obtained from bio-refinery process.

Hydrogenation of succinic acid to BDO occurs via two-step hydrogenation reactions as shown in Fig. 1. Succinic acid is first transformed into γ-butyrolactone (GBL) by hydrogenation, and then BDO or tetrahydrofuran (THF) is formed through consecutive hydrogenation of GBL. For the catalytic conversion of succinic acid, various noble metal catalysts such as Pd, Pt, Rh, Ru, and Re have been investigated. Among these catalysts, rhenium has been considered as the most efficient monometallic catalyst for the selective formation of BDO. However, several studies have shown that rhenium alone was not sufficient to obtain high yield for BDO.

In an attempt to improve BDO production by hydrogenation of succinic acid, Re-based bimetallic catalysts, including Re-Pt/C, Re-Pd/C, Re-Pd/TiO_2, and Re-Ru/C, have been investigated. Nonetheless, the researches have rarely elucidated the effect of interaction between rhenium and other metal on the selective formation of BDO from succinic acid. This is because combination of rhenium and noble metal causes difficulty in structural and chemical analyses. For example, rhenium can be miscible with noble metals such as Pt,

Pd, and Ru to form a solid-solution due to their similar atomic sizes and surface energies, which complicates characterization. Moreover, since rhenium does not cause dissociative hydrogen chemisorption at low temperature, either modified hydrogen chemisorption or CO chemisorption method is essential for determining metal dispersion of Re-based catalyst.

In addition, only a few studies have focused on the modification of carbon support for hydrogenation of succinic acid to BDO. It has been reported that addition of non-metal elements such as sulfur, boron, and phosphorous into carbon affects physicochemical properties of carbon support [24-30]. In particular, boron can be easily substituted for carbon atom during carbon growth process, which significantly changes structural and electronic properties of carbon lattice. Thus, it is expected that boron-containing carbon effectively interacts with active metal species to enhance reducibility and hydrogen adsorption behavior of supported metal catalyst.

To utilize transition metals for production of BDO, we have studied for a bifunctional metal catalyst supported on mesoporous carbon, which contained rhenium and copper. Interestingly, this catalyst showed a considerable catalytic activity in the hydrogenation of succinic acid to GBL and BDO via dimethyl succinate (DMS) in the presence of methanol. Although the catalyst contains transition metal, yield for GBL and BDO over the catalyst was comparable to that over noble metal-based catalysts, due to its bifunctional catalysis. Thus, a systematic investigation on the catalyst based on a combination of transition metal and noble metal for hydrogenation of succinic acid to GBL and BDO would be worthwhile.

In this work, Re-based metal catalysts were supported on mesoporous

carbon, and they were applied to the liquid-phase hydrogenation of succinic acid to BDO.

First of all, A series of Re-Ru bimetallic catalysts supported on mesoporous carbon (denoted as (0.6-x)Re-xRu/MC) were prepared by a single-step surfactant-templating method and a subsequent incipient wetness impregnation method with a variation of ruthenium loading (x, mol%), and they were applied to the liquid-phase hydrogenation of succinic acid to 1,4-butanediol (BDO). The effect of metal content on the catalytic activities and physicochemical properties of (0.6-x)Re-xRu/MC catalysts was investigated. It was found that a Re-Ru miscible phase was formed in the catalysts during the reduction process, and it was responsible for strong interaction between rhenium and ruthenium. It was also revealed that reducibility, metal dispersion, and oxidation state of (0.6-x)Re-xRu/MC catalysts were affected by Re:Ru molar ratio. In particular, the oxidation state was closely related to the hydrogen adsorption behavior of the catalysts. The amount of weak hydrogen-binding sites increased with increasing the ratios of metallic rhenium (Re^0) and ruthenium (Ru^0) with respect to total metallic species in the reduced (0.6-x)Re-xRu/MC catalysts. Catalytic performance in the hydrogenation of succinic acid to BDO over (0.6-x)Re-xRu/MC showed a volcano-shaped trend with respect to Re:Ru molar ratio. This result was well correlated with the amount of weak hydrogen-binding sites of the catalysts. Among the catalysts tested, 0.3Re-0.3Ru/MC with the largest amount of weak hydrogen-binding sites showed the best catalytic performance in the BDO production by hydrogenation of succinic acid.

A series of Re-Ru bimetallic catalysts supported on mesoporous boron-

modified carbon (denoted as Re-Ru/xBMC, x = B/C molar ratio) were prepared by a single-step surfactant-templating method and a subsequent incipient wetness impregnation method, and they were used for liquid-phase hydrogenation of succinic acid to 1,4-butandiol (BDO). The effect of boron addition on the catalytic activities and physicochemical properties of Re-Ru/xBMC catalysts was investigated. It was found that the addition of boron into carbon support affected surface area, metal dispersion, and reducibility of rhenium and ruthenium species in the Re-Ru/xBMC catalysts. It was also observed that boron species in carbon framework existed in several different phases such as substituted boron, partial oxidized boron, and boron oxide. In particular, the amount of substituted boron species was closely related to the hydrogen adsorption behavior of Re-Ru/xBMC catalysts. The amount of weak hydrogen-binding sites increased with increasing the amount of substituted boron species of the catalysts. Yield for BDO in the hydrogenation of succinic acid showed a volcano-shaped trend with respect to B/C molar ratio. This result was in good agreement with the amount of weak hydrogen-binding sites of the catalysts. It was revealed that TOF_{BDO} increased with increasing the amount of weak hydrogen-binding sites of Re-Ru/xBMC catalysts. Among the catalysts, Re-Ru/0.04BMC with the largest amount of weak hydrogen-binding sites served as an efficient catalyst in the selective formation of BDO by hydrogenation of succinic acid.

A mesoporous rhenium-copper-carbon composite catalyst (Re-Cu-MC) was prepared by a facile single-step surfactant-templating method. For comparison, a series of mesoporous carbon-supported catalysts (Re/Cu-MC, Cu/Re-MC, and Re-Cu/MC) were also prepared. The catalysts were applied to

the liquid-phase hydrogenation of succinic acid to γ-butyrolactone (GBL) and 1,4-butanediol (BDO). The effect of preparation method on the physicochemical properties and catalytic activities of the catalysts was investigated. It was found that the catalysts based on metal-carbon composite (Re-Cu-MC, Re/Cu-MC, and Cu/Re-MC) were favorable for enhancing textural properties and metal-support interaction of the catalysts. Surface atomic ratios of metal species (Re/C and Cu/C) on the catalyst surface increased with increasing metal-support interaction. Yield for GBL and BDO increased with decreasing average metal particle size of the catalysts. It was revealed that metal particle size of the catalysts served as a key factor determining the catalytic activity and stability in the reaction. Among the catalysts tested, Re-Cu-MC catalyst with the smallest average metal particle size showed the best catalytic performance in the hydrogenation of succinic acid to GBL and BDO.

In summary, various Re-based metal catalysts supported on mesoporous carbon were prepared, and they were applied to the liquid-phase hydrogenation of succinic acid to BDO. The catalysts were characterized by nitrogen adsorption-desorption, TPR, XRD, CO chemisorption, TEM, STEM-EDX mapping, Raman, XPS, and H_2-TPD analyses.

Keywords: Hydrogenation of succinic acid, 1,4-Butanediol, Bimetallic catalyst, Mesoporous carbon, Re-Ru catalyst, Boron-modified carbon, Re-Cu catalyst, Dimethyl succinate, Bifunctional catalyst

Student Number: 2014-30247

Contents

List of Tables

List of Figures

Chapter 1. Introduction

1.1. γ-Butyrolactone and 1,4-butanediol

γ-Butyrolactone (GBL) and 1,4-butanediol (BDO) have attracted much attention as important starting materials for petrochemical industries. GBL is a promising raw chemical for *N*-methyl-2-pyrrolidone (NMP) and 2-pyrrolidone in the pharmaceutical industry [1,2]. One of the first technologies for GBL production is the DuPont process using maleic acid as a reactant. The largest share of global demand for GBL still relies on this process.

BDO is an important raw material for producing polybutylene terephthalate (PBT) which is mostly used in automobile and electronic industries [3-5]. Traditionally, BDO has been produced via petrochemical-based routes such as Reppe [6], Mitsubishi-Kasei [7], and Arco processes [8] (Table 1.1.1). These processes rely on petrochemical feedstocks derived from fossil fuel. Due to the limited amount of fossil fuel, however, current research trend for BDO production moves toward the utilization of renewable energy sources such as biomass. In this respect, conversion of succinic acid to BDO by catalytic hydrogenation has received recent attraction as a promising process, because succinic acid can be easily obtained from bio-refinery process [9,10] (Fig. 1.1.1). With the development of bio-refinery processes, succinic acid is recognized as one of the promising C_4 platform chemicals that can replace maleic anhydride [11,12].

Table 1.1.1.

Conventional processes for 1,4-butanediol production

Process	Reactant	Catalyst
Reppe	Acetylene	Raney Ni
LyondellBasell	Propylene oxide	Tri-alkyl phosphine
Mitsubishi	Butadiene	Ni-Zn-O_y
BP Amoco	n-Butane	Pd/TiO_2
Hydrogenation of succinic acid	Succinic acid	Pd/Carbon

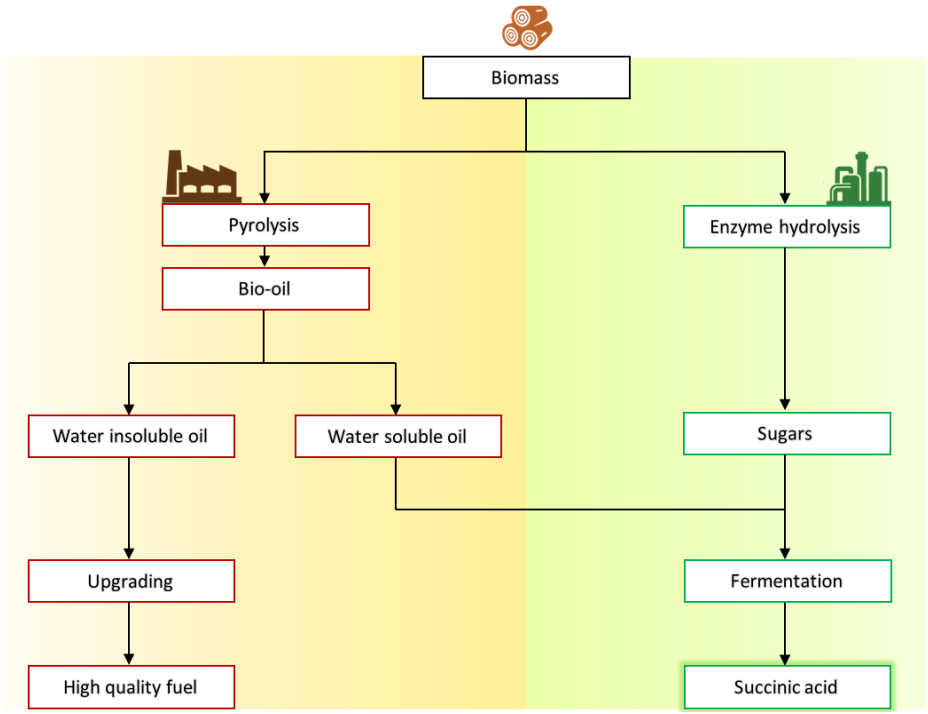

Fig. 1.1.1. Production of succinic acid from bio-refinery process.

1.2. Hydrogenation of succinic acid

Succinic acid has been used in the food industry. In addition, succinic acid is a major building block chemical and the global market of its derivatives is estimated to be 270 kt/year [4]. Traditionally, succinic acid has produced by catalytic hydrogenation of maleic acid or maleic anhydride derived catalytic hydrogenation, as shown in Fig. 1.2.1. Because these processes use the limited amount of fossil fuel, current research trend for BDO production moves toward the utilization of renewable energy sources such as biomass. Although the cost of fermentative production of succinic acid increased by the required nutrients and operation processes, the succinic acid will become economically more viable due to current improvements in the bio-refinery process [11].

Succinic acid is called a C4 platform chemical because it can be converted to various derivatives. The derivatives differ in the degree of hydrogenation of succinic acid, as shown in Fig. 1.2.2. Among the derivatives, a main group of possible derivatives consists of GBL, BDO, and THF by continuous hydrogenation reaction. Hydrogenation of succinic acid to BDO occurs via two-step hydrogenation reactions (Fig. 1.2.3). Succinic acid is first transformed into GBL by hydrogenation, and then BDO or tetrahydrofuran (THF) is formed through consecutive hydrogenation of GBL [3].

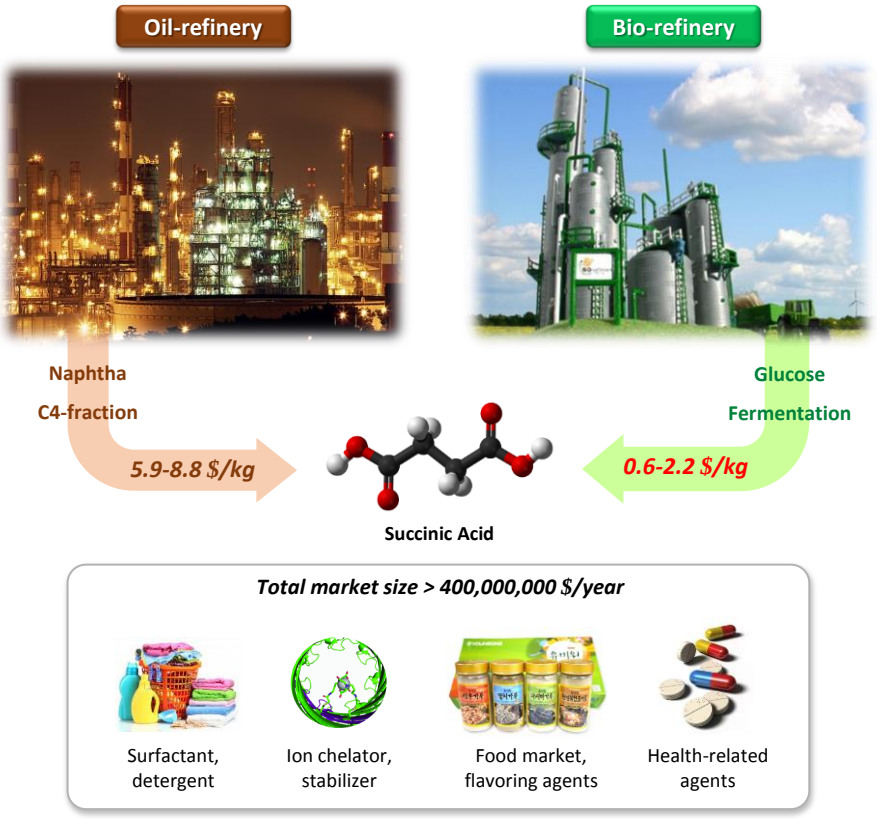

Fig. 1.2.1. The production routes and applications of succinic acid.

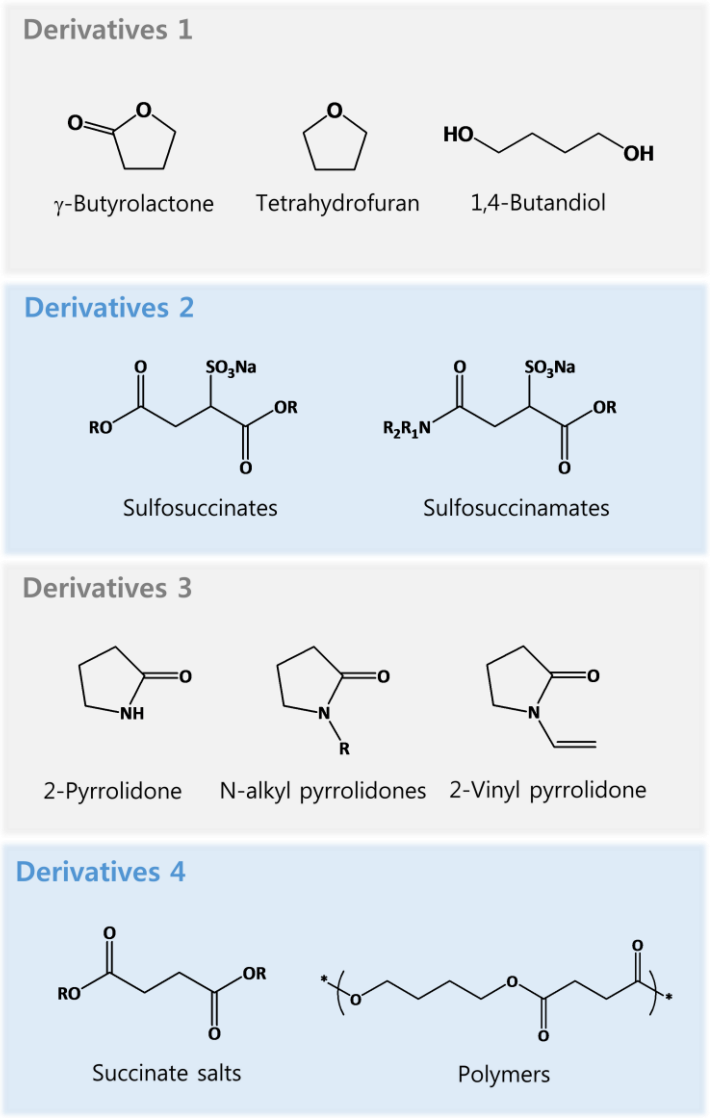

Fig. 1.2.2. Succinic acid derivatives.

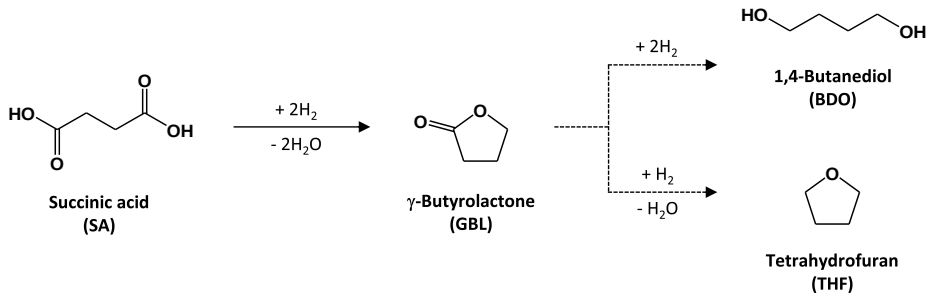

Fig. 1.2.3. Reaction pathway for hydrogenation of succinic acid.

1.3. Heterogeneous catalysts

For the catalytic conversion of succinic acid, various noble metal catalysts such as Pd [13-15], Pt [16], Rh [16], Ru [16,17], and Re [16] have been investigated. Among these catalysts, rhenium has been considered as the most efficient monometallic catalyst for the selective formation of BDO. However, several studies have shown that rhenium alone was not sufficient to obtain high yield for BDO [18-21]. In an attempt to improve BDO production by hydrogenation of succinic acid, Re-based bimetallic catalysts, including Re-Pt/C [22], Re-Pd/C [22,23], Re-Pd/TiO_2 [24], and Re-Ru/C [25], have been investigated. Nonetheless, the researches have rarely elucidated the effect of interaction between rhenium and other metal on the selective formation of BDO from succinic acid. This is because combination of rhenium and noble metal causes difficulty in structural and chemical analyses. For example, rhenium can be miscible with noble metals such as Pt, Pd, and Ru to form a solid-solution due to their similar atomic sizes and surface energies [26,27], which complicates characterization. Moreover, since rhenium does not cause dissociative hydrogen chemisorption at low temperature [28,29], either modified hydrogen chemisorption or CO chemisorption method is essential for determining metal dispersion of Re-based catalyst. In this respect, a systematic investigation on the effect of interaction between rhenium and other metal on the catalytic activities and physicochemical properties of Re-based bimetallic catalyst would be worthwhile.

To improve physicochemical properties of metal catalysts, various

support materials have been used in the dehydrogenation of succinic acid. For example, TiO_2 was suggested as a support for Re-based catalysts to increase stability under hydrothermal conditions, which prevented metal leaching from the catalysts [30]. In case of Pd catalysts supported on silica materials such as SBA-15 and MCM-41, product selectivity was highly dependent on their pore geometry [31]. In particular, carbon is known as a suitable support for noble metal catalysts due to its high surface area and acid resistant nature [32].

However, only a few studies have focused on the modification of carbon support for hydrogenation of succinic acid to BDO. It has been reported that addition of non-metal elements such as sulfur, boron, and phosphorous into carbon affects physicochemical properties of carbon support [33-38]. In particular, boron can be easily substituted for carbon atom during carbon growth process, which significantly changes structural and electronic properties of carbon lattice [33,34]. Thus, it is expected that boron-containing carbon effectively interacts with active metal species to enhance reducibility and hydrogen adsorption behavior of supported metal catalyst [33-35]. Therefore, a systematic investigation on the effect of boron addition into carbon on the catalytic activities and physicochemical properties of Re-Ru bimetallic catalyst supported on boron-modified carbon in the hydrogenation of succinic acid would be worthwhile.

The noble metal catalysts have been mainly used for hydrogenation of succinic acid to GBL. Nonetheless, these catalysts are not still satisfactory for mass production of GBL and BDO through hydrogenation of succinic acid. To overcome these problems, we have reported a bifunctional metal catalyst supported on mesoporous carbon, which contained rhenium and copper [39].

Interestingly, this catalyst showed a considerable catalytic activity in the hydrogenation of succinic acid to GBL and BDO via dimethyl succinate (DMS) in the presence of methanol. Although the catalyst contains transition metal, yield for GBL and BDO over the catalyst was comparable to that over noble metal-based catalysts, due to its bifunctional catalysis. Thus, a systematic investigation on the catalyst based on a combination of transition metal and noble metal for hydrogenation of succinic acid to GBL and BDO would be worthwhile. Fig. 1.3.1 shows the reaction pathways for hydrogenation of succinic acid to GBL and BDO via DMS in the presence of methanol. According to the mechanism, GBL is produced by hydrogenation of succinic acid, and consecutive hydrogenation of GBL leads to the formation of BDO and THF. On the other hand, succinic acid also reacts with methanol to produce DMS by methylation, and BDO is finally formed through demethylation of DMS [31]. Hydrogenation of succinic acid to BDO via GBL and methylation of succinic acid to DMS mostly occur by rhenium species, while demethylation of DMS to BDO is strongly affected by copper species [39]. Therefore, it can be inferred that rhenium and copper species in the catalyst may serve as crucial active sites in the hydrogenation of succinic acid to GBL and BDO via DMS.

It is known that dispersion of active sites can be controlled by modifying textural property and metal-support interaction of the catalyst [40]. In this respect, we have investigated mesoporous metal-carbon composite catalysts such as Re-C and Ru-C for practical application to hydrogenation of succinic acid [41]. However, the previous preparation methods for mesoporous metal-carbon composite catalysts required many preparation

steps and H_2SO_4 post-treatment step to yield mesoporosity of carbon, which caused aggregation and leaching of the metal particles. In other words, a more facile preparation method for metal-carbon composite catalyst is necessary to improve activity and stability of the catalyst. Therefore, it is expected that a mesoporous rhenium-copper-composite catalyst prepared by a simple one-pot route may serve as an efficient catalyst for hydrogenation of succinic acid to GBL and BDO.

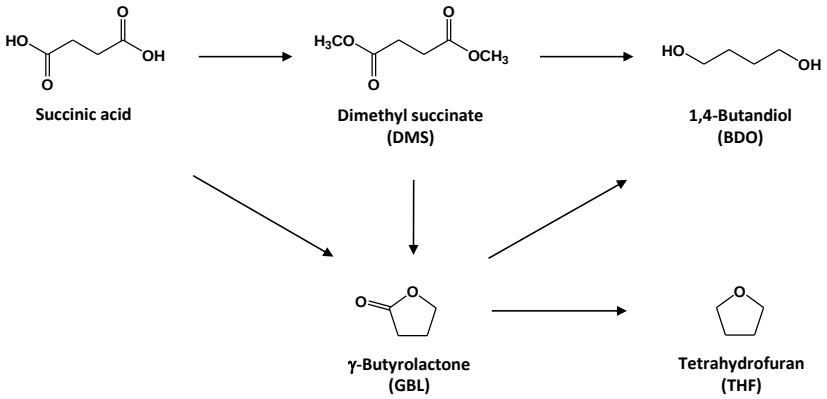

Fig. 1.3.1. Reaction pathway for hydrogenation of succinic acid.

Chapter 2. Experimental

2.1. Preparation of catalysts

2.1.1. Re-Ru bimetallic catalysts supported on mesoporous carbon

A series of Re-Ru bimetallic catalysts supported on mesoporous carbon were prepared by a single-step surfactant-templating method and a subsequent incipient wetness impregnation method (Fig. 2.1.1). For the preparation of mesoporous carbon (MC), 5 g of P123 copolymer (Sigma-Aldrich) was dissolved in deionized water (130 ml) at room temperature under vigorous stirring. 2.1 g of sucrose (Sigma-Aldrich) as a carbon precursor and 20 ml of HCl solution (35%) were then added into the solution. Subsequently, 1.9 ml of H_2SO_4 solution (95%) was added into the solution to promote later cross-linkage of P123 with tetraethoxysilane (TEOS). After maintaining the solution with stirring for 1 h, 9.3 ml of TEOS (Sigma-Aldrich) as a structure-directing agent was slowly added into the mixed solution. The resulting solution was stirred at 37 ˚C for 24 h, and it was then kept at 100 ˚C for 24 h without stirring for self-assembly of micelle structure. The resultant was dried at 100 ˚C for 48 h, and then carbonized at 800 ˚C for 4 h at a heating rate of 5 ˚C/min in a nitrogen stream (50 ml/min). The obtained carbon-silica composite was then treated with 300 ml of HF solution (5%) for 24 h to remove silica template, and it was finally filtered and dried. The resulting mesoporous

carbon was denoted as MC.

For co-impregnation of rhenium and ruthenium onto MC support, known amounts of $ReCl_5$ (Sigma-Aldrich) and $RuCl_3 \cdot xH_2O$ (Sigma-Aldrich) as metal precursors were dissolved in 5 ml of acetone. During this process, Re:Ru molar ratio was adjusted to be 1:0, 0.75:0.25, 0.50:0.50, 0.25:0.75, and 0:1, while the total loading of two metals was fixed at 0.6 mol% in all the samples to maintain the same number of active sites. The acetone solution containing metal precursors was then introduced to MC by an incipient wetness impregnation method. After drying the impregnated sample at 60 ˚C, it was calcined at 500 ˚C for 4 h with a heating rate of 5 ˚C/min under N_2 flow (50 ml/min) to remove chlorine and organic impurities. The prepared Re-Ru bimetallic catalysts were denoted as (0.6-x)Re-xRu/MC (x = 0, 0.15, 0.3, 0.45, and 0.6), where x represented the ruthenium content (mol%).

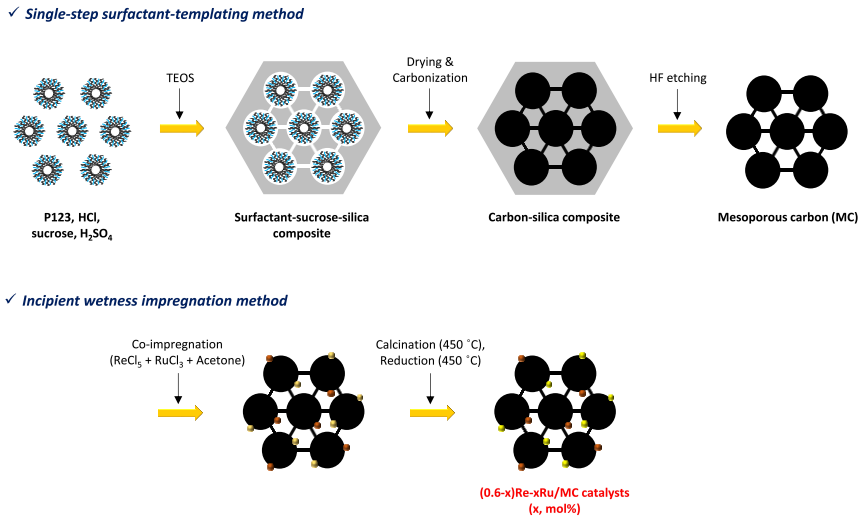

Fig. 2.1.1. Schematic procedures for the preparation of Re-Ru bimetallic catalysts supported on mesoporous carbon.

2.1.2. Re-Ru bimetallic catalysts supported on mesoporous boron-modified carbon

The synthesis of mesoporous boron-modified carbon was done according to our previously reported methods with slight modification (Fig. 2.1.2). Copolymer P123 (Sigma-Aldrich) and aqueous HCl were initially dissolved in distilled water with vigorous stirring. After P123 was completely dissolved, sucrose (Sigma-Aldrich) and aqueous H_2SO_4 were added into the homogeneous solution. Subsequently, a known amount of boric acid as a structural modifier was introduced into the solution. During this process, B/C molar ratio was adjusted to be 0, 0.02, 0.04, 0.08, and 0.12. TEOS (Sigma-Aldrich) was then added into the mixed solution, and the solution was kept at 37 ˚C under vigorous stirring for 1 day for self-assembly reaction. The resulting white solution was heated to 100 ˚C and it was maintained at the same temperature for 1 day. Afterward, the dark brown suspension was transferred to unsealed bottle and it was dried at 100 ˚C for 2 days. Carbonization was done at 800 ˚C for 4 h in a flow of N_2. The residual silica in the solid resultant was removed by HF solution. Template-free carbon product was filtered, and finally, it was washed with distilled water and ethanol. The resulting mesoporous boron-modified carbon was designated as xBMC (x = 0, 0.02, 0.04, 0.08, and 0.12), where x represented B/C molar ratio.

A set of Re-Ru catalysts supported on mesoporous boron-modified carbon (BMC) were prepared by an incipient wetness impregnation method.

The acetone solution containing rhenium chloride (Sigma-Aldrich) and ruthenium chloride (Sigma-Aldrich) was introduced to xBMC supports for impregnation. According to the previous study in Section 2.1.1, an optimal molar ratio of Re:Ru was modulated to be 1:1. The loading of each metal species was fixed at 0.3 mol%. After the impregnation, the resultant samples were dried in air overnight, followed by calcination at 500 ˚C at 4 h using a N_2 stream. The prepared catalysts were denoted as Re-Ru/xBMC (x = 0, 0.02, 0.04, 0.08, and 0.12).

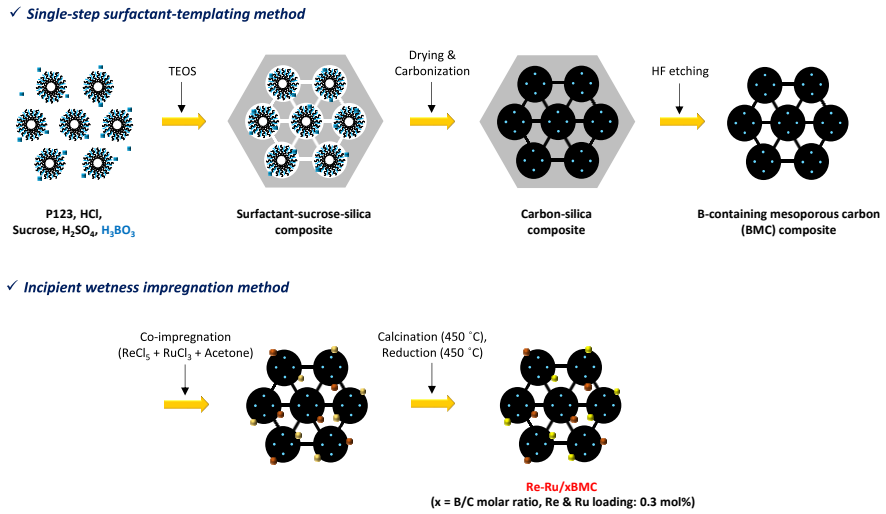

Fig. 2.1.2. Schematic procedures for the preparation of Re-Ru bimetallic catalysts supported on mesoporous boron-modified carbon.

2.1.3. Mesoporous Re-Cu-carbon composite catalysts

A mesoporous rhenium-copper-carbon composite catalyst (Re-Cu-MC) was prepared by a facile single-step surfactant-templating method. Fig. 2.1.3 shows the schematic procedures for the preparation of Re-Cu-MC composite catalyst. 3.3 g of $(EO)_{20}(PO)_{70}(EO)_{20}$ triblock copolymer (Pluronic P123, Sigma-Aldrich) was dissolved in 1.3 M HCl solution (100 ml) at 37 ˚C with vigorous stirring. 1.4 g of carbon precursor (sucrose, Sigma-Aldrich) and 1.2 ml of H_2SO_4 solution were then added into the solution with stirring for 1 h. Known amounts of rhenium precursor (rhenium chloride, Sigma-Aldrich) and copper precursor (copper chloride, Sigma-Aldrich) were added into the mixed solution. Rhenium and copper contents were fixed at 5 wt% and 20 wt%, respectively. After the metal precursors were completely dissolved, 6.0 g of silica precursor (TEOS, Sigma-Aldrich) was slowly added into the solution. The resulting solution was stirred at 37 ˚C for 24 h, and it was then kept at 100 ˚C for 24 h without stirring to induce self-assembly of micelle structure. The resultant was dried at 100 ˚C for 48 h, and the obtained composite solid was then carbonized at 800 ˚C for 4 h at a heating rate of 5 ˚C/min in a nitrogen stream (100 ml/min). The solid product was further treated with 5 wt% HF solution for 20 h to remove silica template, and then it was filtered and dried. The resulting rhenium-copper-carbon composite catalyst was denoted as Re-Cu-MC.

For comparison, a series of mesoporous carbon-supported catalysts (Re/Cu-MC, Cu/Re-MC, and Re-Cu/MC) were prepared. The rhenium

catalyst supported on copper-carbon composite (Re/Cu-MC) was prepared by a facile single-step surfactant-templating method and a subsequent impregnation method. A mesoporous copper-carbon composite (Cu-MC) was first prepared by the similar methods described above without a rhenium precursor. Rhenium precursor (rhenium chloride, Sigma-Aldrich) was then impregnated on Cu-MC by an incipient wetness impregnation method using an acetone solution. After drying the supported catalyst in a vacuum oven at 40 ˚C, it was calcined at 600 ˚C in a nitrogen stream. The resulting catalyst was denoted as Re/Cu-MC.

The copper catalyst supported on rhenium-carbon composite (Cu/Re-MC) was prepared by the similar methods as Re/Cu-MC catalyst. A mesoporous rhenium-carbon composite (Re-MC) was prepared, and copper precursor (copper chloride, Sigma-Aldrich) was then impregnated on Re-MC using an acetone solution. The resultant was dried and it was calcined at 600 ˚C in a nitrogen stream. The resulting catalyst was denoted as Cu/Re-MC.

The rhenium-copper catalyst supported on mesoporous carbon (Re-Cu/MC) was also prepared according to the similar methods described above. A mesoporous carbon support (MC) was first prepared by a single-step surfactant-templating method without metal precursors. Rhenium and copper were then impregnated on MC using an acetone solution. The catalyst was dried and it was calcined at 600 ˚C in a nitrogen stream. The resulting catalyst was denoted as Re-Cu/MC. Rhenium and copper contents in all the catalysts were fixed at 5 wt% and 20 wt%, respectively. Prior to the catalytic reaction, all the catalysts were reduced with a mixed stream of nitrogen (47.5 ml/min) and hydrogen (2.5 ml/min) at 600 ˚C for 4 h.

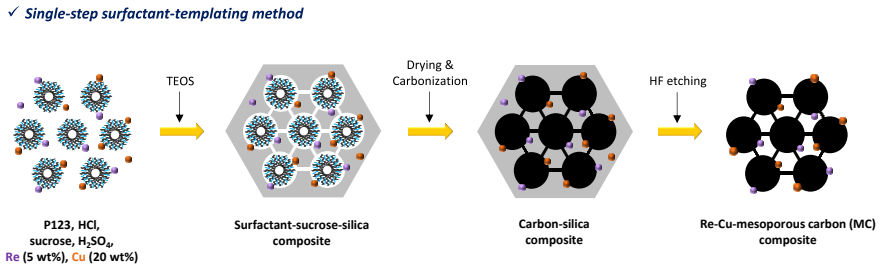

Fig. 2.1.3. Schematic procedures for the preparation of Mesoporous Re-Cu-carbon composite catalyst.

2.2. Characterization

2.2.1. Textural properties

Textural properties of calcined (0.6-x)Re-xRu/MC (x = 0, 0.15, 0.3, 0.45, and 0.6) catalysts were investigated by nitrogen adsorption-desorption measurements using a BELSORP-mini II instrument (BEL Japan). Surface areas of the catalysts were calculated by the Brunauer-Emmett-Teller (BET) method.

The molar ratios of metals of the catalysts were determined by ICP-MS analyses (ELAN 6100, Perkin-Elmer SCIEX).

2.2.2. Reducibility

Temperature-programmed reduction (TPR) analyses of the calcined catalysts were conducted in a flow reactor system equipped with a quartz reactor. 10 mg of the catalysts was pretreated with N_2 flow (50 ml/min) at 200 ˚C for 1 h, and subsequently, TPR profiles were obtained using a thermal conductivity detector (TCD) at temperatures ranging from room temperature to 600 ˚C with a heating rate of 5 ˚C/min under 5% H_2/N_2 flow (50 ml/min).

2.2.3. Crystalline structure

X-ray diffraction (XRD) patterns of the reduced catalysts were

collected by a D-Max2500-PC diffractometer (Rigaku) using Cu-Kα radiation (λ = 1.541 Å) operated at 50 kV and 100 mA.

2.2.4. Metal dispersion

CO chemisorption experiments were performed using a BELCAT-B instrument (BEL Japan). 10 mg of calcined catalyst was reduced at 500 ˚C for 4 h with a heating rate of 5 ˚C/min, and then 5% CO/He mixed gas was periodically injected at 100 ˚C. Metal surface area, metal dispersion, and average metal particle size were calculated from the amount of carbon monoxide adsorbed on the reduced catalyst by assuming that one carbon monoxide molecule occupies one surface metal atom.

2.2.5. Morphological feature

Morphology and particle size distribution of the reduced catalysts were examined by transmission electron microscopy (TEM) analyses (JEM-3010, JEOL). The particle size was calculated on the basis of projected area of particle in the TEM image by assuming that the shape of metal particle is sphere. The projected area, *A*, was converted to particle diameter, *D*, using $D = 2(A/\pi)^{1/2}$. To confirm the detailed distribution of rhenium and ruthenium of the reduced catalysts, energy dispersive X-ray spectroscopy (EDX) mapping analyses were conducted using a scanning transmission electron microscopy (STEM) apparatus (JEM-2100F, JEOL).

2.2.6. Chemical state studies

Binding energies and surface atomic compositions of rhenium and ruthenium in the reduced catalysts were examined by X-ray photoelectron spectroscopy (XPS) analyses using a AXIS-HSI instrument (KRATOS) equipped with a Mg/Al anode source. For XPS analyses, the calcined catalysts were reduced using an ex-situ reduction system at 500 ˚C for 4 h under 5% H_2/N_2 flow (50 ml/min), and the catalysts were then transported to glass jar with sample holder in argon atmosphere glove box to minimize air exposure. After outgassing the glass jar in a vacuum oven, the sample holder was transferred to the XPS chamber as quickly as possible. All the XPS spectra were calibrated using C 1s peak (284.5 eV) as a reference.

Raman spectroscopy analyses (T64000, Horiba) were carried out within the range of 1000-2000 cm^{-1} using Ar laser to examine graphite carbon structure.

2.2.7. Hydrogen adsorption studies

H_2 temperature-programmed desorption (H_2-TPD) analyses of the reduced catalysts were conducted using a BELCAT-B instrument (BEL Japan). 10 mg of calcined catalyst was reduced at 500 ˚C for 4 h with a heating rate of 5 ˚C/min under 5% H_2/Ar flow (50 ml/min), and then purged with Ar flow (50 ml/min) for 10 min at 500 ˚C. After cooling the reduced catalyst to 200 ˚C under Ar flow (50 ml/min), 5% H_2/Ar mixed gas (50 ml/min) was injected for

30 min at 200 ˚C. To remove physisorbed hydrogen, the sample was purged at 200 ˚C with Ar flow (50 ml/min), and subsequently, H_2-TPD measurements were conducted within temperature range of 200-700 ˚C at a heating rate of 5 ˚C/min under Ar flow (50 ml/min).

2.3. Hydrogenation of succinic acid

2.3.1. Hydrogenation of succinic acid to BDO via GBL

Liquid-phase hydrogenation of succinic acid to BDO was conducted in a stainless steel autoclave reactor with a volume of 200 ml (Fig. 2.3.1). Prior to the reaction, the catalysts were reduced using an ex-situ reduction system at 500 ˚C for 4 h with a heating rate of 5 ˚C/min under 5% H_2/N_2 flow (50 ml/min). In order to avoid air exposure, reduced catalyst (0.1 g), succinic acid (0.25 g), and 1,4-dioxane (50 ml, an inert aprotic solvent) were charged into the reactor in an argon atmosphere glove box. The closed reactor filled with argon was then mounted to the autoclave chamber as quickly as possible. After purging the reactor with nitrogen, it was pressurized up to 50 bar using hydrogen. The sealed autoclave was heated to the reaction temperature (200 ℃), and then pressurized up to 80 bar using hydrogen. Catalytic reaction was conducted with constant stirring (700 rpm) for 7 h. After the reaction, the reactor was cooled to room temperature and depressurized. Reaction products were analyzed with a gas chromatograph (Younglin, ACME-6100) equipped with a flame ionization detector (FID). Conversion of succinic acid, selectivity for product, and yield for product were calculated according to the following equations.

$$\text{Conversion of succinic acid (\%)} = \frac{\text{mole of succinic acid reacted}}{\text{mole of succinic acid supplied}} \times 100$$

$$\text{Selectivity for product (\%)} = \frac{\text{mole of product formed}}{\text{mole of succinic acid reacted}} \times 100$$

Yield for product (%) = (Conversion of succinic acid) × (Selectivity for product) / 100

Turnover frequency (TOF) and TOF for BDO (TOF_{BDO}) were calculated on the basis of moles of succinic acid converted at ca. 10% conversion and moles of BDO formed at ca. 70% yield for GBL, respectively. The moles of surface metal atoms used for TOF and TOF_{BDO} calculation were obtained by CO chemisorption experiments.

Table 2.3.1

Reaction condition for hydrogenation of succinic acid

Operation variable	Condition
Temperature	200 ℃
Pressure	80 bar H_2
Agitation speed	700 rpm
Solvent	50 ml 1,4-dioxane (aprotic)
Reactant	0.25 g succinic acid
Catalyst	0.1 g

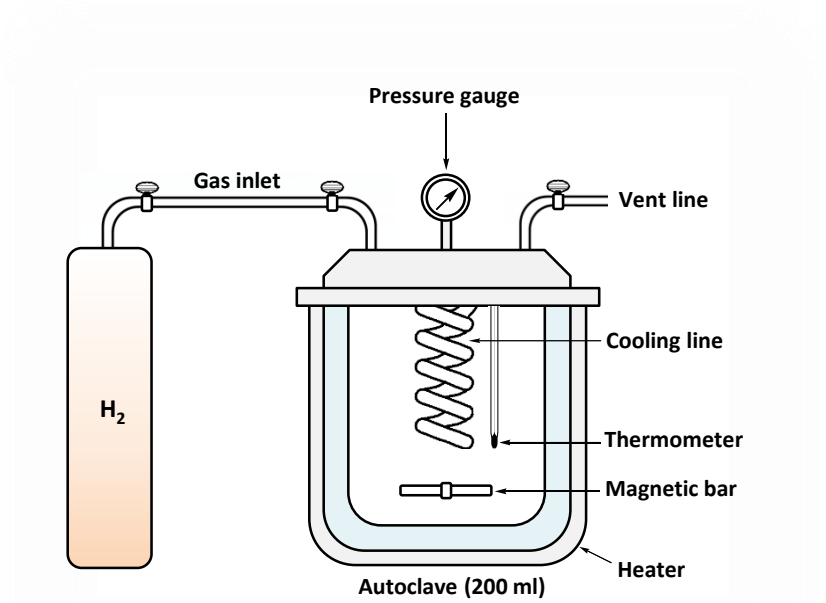

Fig. 2.3.1. Reaction apparatus for hydrogenation of succinic acid.

2.3.2. Hydrogenation of succinic acid to BDO via DMS

Liquid-phase hydrogenation of succinic acid to GBL and BDO was conducted in a stainless steel autoclave reactor with a volume of 200 ml. Methanol (25 ml), succinic acid (0.25 g), and reduced catalyst (0.1 g) were initially charged into the reactor, and then 1,4-dioxane (25 ml) as an inert aprotic solvent was charged to mitigate drastic vaporization of methanol. After purging the reactor with nitrogen, it was pressurized up to 50 bar using hydrogen. After heating the reactor to the reaction temperature (200 ℃), the autoclave was pressurized up to 80 bar using hydrogen. Catalytic reaction was carried out with constant stirring (700 rpm) for 20 h. After the reaction, the reactor was cooled to room temperature and depressurized. Reaction products were analyzed with a gas chromatograph (Younglin, ACME-6100) equipped with a flame ionization detector (FID).

Chapter 3. Results and Discussion

3.1. Re-Ru bimetallic catalysts supported on mesoporous carbon

3.1.1. Textural properties of catalysts

Textural properties of (0.6-x)Re-xRu/MC (x = 0, 0.15, 0.3, 0.45, and 0.6) catalysts were examined by nitrogen adsorption-desorption measurements as shown in Fig. 3.1.1. All the catalysts exhibited IV-type isotherms indicative of mesoporous structure. H3-type hysteresis loops were also observed in the isotherms, which was attributed to the capillary condensation of nitrogen molecules in the well-developed mesopores of carbon support. Detailed textural properties of (0.6-x)Re-xRu/MC (x = 0, 0.15, 0.3, 0.45, and 0.6) catalysts are listed in Table 3.1.1 and Table 3.1.2. It was found that the actual Re:Ru loadings and molar ratios of the prepared catalysts were in good agreement with the designed values. Total metal loadings were also well fixed at 0.6 mol%. All the catalysts retained high surface area (>812 m^2/g), large pore volume (>1.06 cm^3/g), and large average pore diameter (>5.0 nm), which means that mesoporous carbon structure were successfully formed by a single-step surfactant-templating method. Interestingly, surface area and pore volume of the catalysts decreased with increasing rhenium loading. This might be because pore blockage by rhenium was more severe than that by

ruthenium due to the difference in atomic radius of rhenium (137 pm) and ruthenium (134 pm).

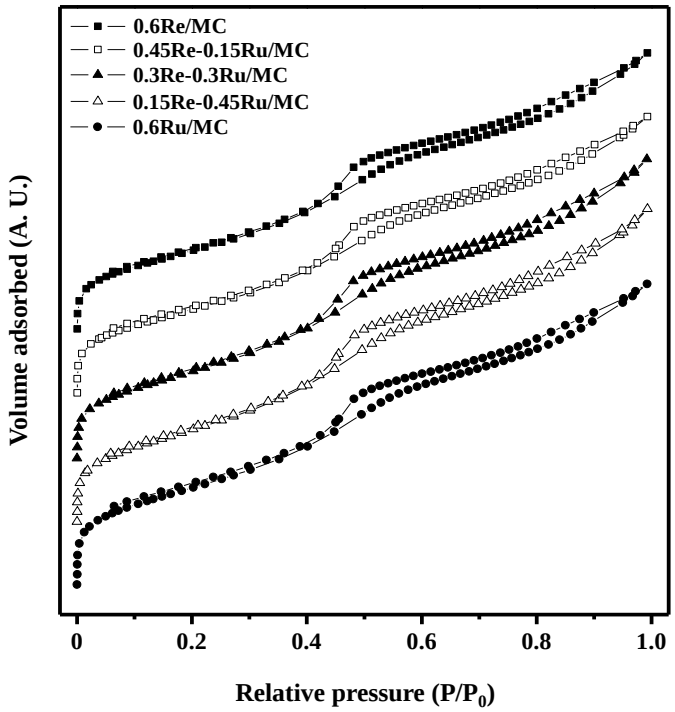

Fig. 3.1.1. Nitrogen adsorption-desorption isotherms of (0.6-x)Re-xRu/MC (x = 0, 0.15, 0.3, 0.45, and 0.6) catalysts.

Table 3.1.1

ICP-MS results of (0.6-x)Re-xRu/MC (x = 0, 0.15, 0.3, 0.45, and 0.6) catalysts

Catalyst	Re : Ru loading (mol%)[a]	Re : Ru molar ratio
0.6Re/MC	0.59 : 0	1 : 0
0.45Re-0.15Ru/MC	0.44 : 0.15	0.74 : 0.26
0.3Re-0.3Ru/MC	0.29 : 0.31	0.49 : 0.51
0.15Re-0.45Ru/MC	0.15 : 0.45	0.25 : 0.75
0.6Ru/MC	0 : 0.6	0 : 1

[a] Determined by ICP-MS measurement

Table 3.1.2

Textural properties of (0.6-x)Re-xRu/MC (x = 0, 0.15, 0.3, 0.45, and 0.6) catalysts

Catalyst	Surface area $(m^2/g)^a$	Pore volume $(cm^3/g)^b$	Pore diameter $(nm)^c$
0.6Re/MC	812	1.06	5.2
0.45Re-0.15Ru/MC	838	1.07	5.1
0.3Re-0.3Ru/MC	861	1.14	5.3
0.15Re-0.45Ru/MC	899	1.18	5.3
0.6Ru/MC	923	1.19	5.0

[a] Calculated by the BET equation
[b] Total pore volume at $P/P_0 = 0.99$
[c] Average pore diameter

3.1.2. Reduction behaviors of catalysts

A In order to investigate the reduction behaviors of (0.6-x)Re-xRu/MC (x = 0, 0.15, 0.3, 0.45, and 0.6) catalysts, TPR measurements were conducted as shown in Fig. 3.1.2. It was found that 0.6Re/MC and 0.6Ru/MC catalysts exhibited asymmetrical reduction peaks at 340 ˚C and 264 ˚C, respectively; the former was attributed to the reduction of rhenium species [42], while the latter was attributed to the reduction of ruthenium species [43]. The reduction peak of 0.45Re-0.15Ru/MC catalyst moved toward lower temperature and showed more narrow shape than that of 0.6Re/MC. In case of bimetallic catalysts containing noble metals such as Pd, Pt, and Ru, the noble metals can affect the reduction of the other metal due to hydrogen transfer from their reduced species [44-47]. Therefore, it can be inferred that hydrogen adsorbed on reduced ruthenium species was transferred to unreduced neighboring rhenium species during the reduction process, which promoted the reduction of rhenium species. It is interesting to note that (0.6-x)Re-xRu/MC (x = 0.15, 0.3, and 0.45) catalysts retained only one reduction peak corresponding to co-reduction of rhenium and ruthenium without any reduction peaks for bulk rhenium and ruthenium species, indicating that most of ruthenium atoms were distributed in the periphery of unreduced rhenium atoms throughout the catalyst. Furthermore, the reduction bands of (0.6-x)Re-xRu/MC (x = 0.15, 0.3, and 0.45) catalysts were changed to the symmetrical shape compared to those of 0.6Re/MC and 0.6Ru/MC. It is known that the symmetrical peak shape can be induced from uniform reduction process caused by homogeneity

of metal particle size [48]. Thus, it is inferred that the particles of both rhenium and ruthenium species were homogeneously formed in the Re-Ru bimetallic catalysts. The amounts of hydrogen uptake calculated from the TPR profiles of (0.6-x)Re-xRu/MC (x = 0, 0.15, 0.3, 0.45, and 0.6) catalysts are summarized in Table 3.1.3. It was found that (0.6-x)Re-xRu/MC (x = 0.15, 0.3, and 0.45) catalysts showed the larger amount of hydrogen uptake than 0.6Re/MC and 0.6Ru/MC, indicating that the interaction between rhenium and ruthenium species might modify the reducibility of both metal species. However, the amount of hydrogen uptake of (0.6-x)Re-xRu/MC (x = 0.15, 0.3, 0.45, and 0.6) catalysts determined by TPR measurements exceeded the theoretical ratio of hydrogen with respect to rhenium (3.5) and ruthenium (2) for complete reduction [48]. This was due to hydrogen spillover induced by metal surface on carbon material [49]. Therefore, it is difficult to determine the reduction degree of (0.6-x)Re-xRu/MC (x = 0.15, 0.3, 0.45, and 0.6) catalysts by only TPR results.

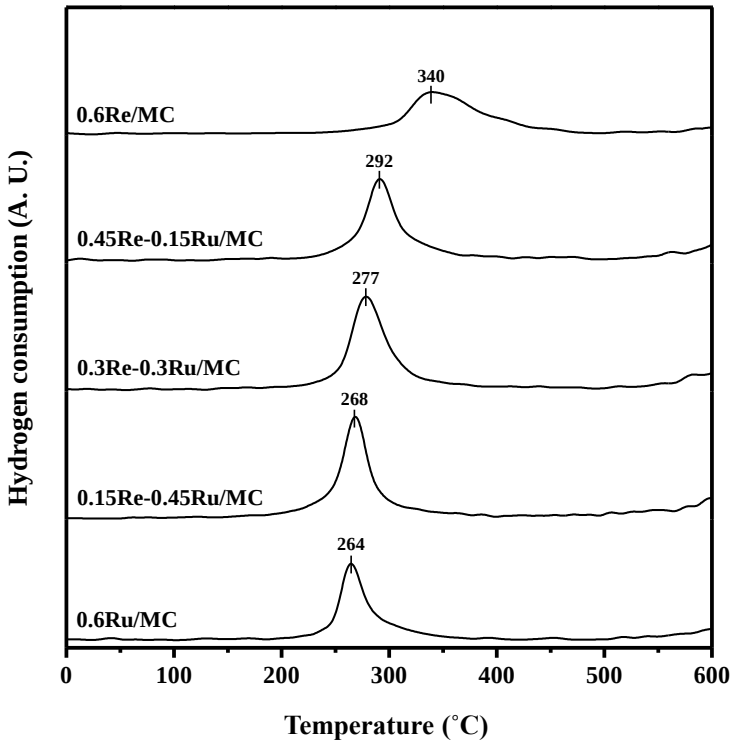

Fig. 3.1.2. TPR profiles of (0.6-x)Re-xRu/MC (x = 0, 0.15, 0.3, 0.45, and 0.6) catalysts.

Table 3.1.3

TPR chemisorption results of (0.6-x)Re-xRu/MC (x = 0, 0.15, 0.3, 0.45, and 0.6) catalysts

Catalyst	Amount of hydrogen uptake (mol-H_2/mol-metal)[a]
0.6Re/MC	2.73
0.45Re-0.15Ru/MC	3.29
0.3Re-0.3Ru/MC	4.10
0.15Re-0.45Ru/MC	3.50
0.6Ru/MC	3.03

[a] Calculated from peak area of TPR profiles in Fig. 3.1.2

3.1.3. Crystalline structures of reduced catalysts

Crystalline phases of the reduced (0.6-x)Re-xRu/MC (x = 0, 0.15, 0.3, 0.45, and 0.6) catalysts were examined by XRD measurements as presented in Fig. 3.1.3. All the catalysts showed diffraction peaks for graphitic carbon structure at $2\theta = 23.5^{o}$ and 43.8^{o} [50]. The diffraction peaks corresponding to (101) planes of metallic rhenium (dashed line) and ruthenium (solid line) were clearly observed in the XRD patterns of 0.6Re/MC and 0.6Ru/MC catalysts, respectively, although the diffraction peak of 0.6Ru/MC was overlapped with that (43.8^{o}) of the carbon support. On the other hand, any diffraction peaks for rhenium and ruthenium species were not detected in the (0.6-x)Re-xRu/MC (x = 0.15, 0.3, and 0.45) catalysts. This result might be because particle sizes of metallic rhenium and ruthenium in the catalysts were too small to be detected by XRD. According to the literatures [26-28], rhenium and ruthenium species can interact in all range of chemical composition due to their similar crystal structure, atomic radius, and electronegativity. Thus, it is inferred that the interaction between rhenium and ruthenium species affected the development of particles during the reduction process, which might induce the decrement of metal particle size of Re-Ru bimetallic catalysts compared to rhenium or ruthenium monometallic catalyst.

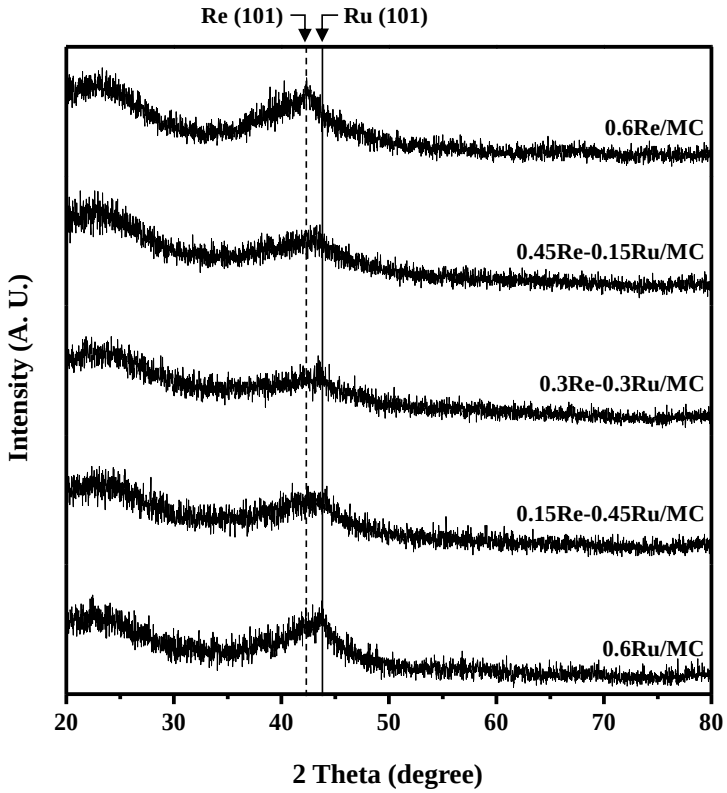

Fig. 3.1.3. XRD patterns of reduced (0.6-x)Re-xRu/MC (x = 0, 0.15, 0.3, 0.45, and 0.6) catalysts.

3.1.4. Metal dispersion of reduced catalysts

To investigate the effect of Re-Ru interaction on the metal dispersion, CO chemisorption measurements for the reduced (0.6-x)Re-xRu/MC (x = 0, 0.15, 0.3, 0.45, and 0.6) catalysts were conducted. As listed in Table 3.1.4, metal surface area and metal dispersion increased in the order of 0.6Re/MC < 0.6Ru/MC < 0.45Re-0.15Ru/MC < 0.15Re-0.45Ru/MC < 0.3Re-0.3Ru/MC, while average metal particle size decreased in the order of 0.6Re/MC > 0.6Ru/MC > 0.45Re-0.15Ru/MC > 0.15Re-0.45Ru/MC > 0.3Re-0.3Ru/MC. It was found that all the catalysts retained small metal particle size in the range of 5.1-7.9 nm, indicating that metallic rhenium and ruthenium particles were finely dispersed in the mesoporous carbon framework. It is noteworthy that average metal particle sizes of (0.6-x)Re-xRu/MC (x = 0.15, 0.3, and 0.45) catalysts were smaller than those of 0.6Re/MC and 0.6Ru/MC. This might be because aggregation of each rhenium and ruthenium particle was effectively suppressed by forming a Re-Ru metallic bond during the reduction process, as discussed in the XRD results.

The above result was further confirmed by TEM analyses. Fig. 3.1.4 shows the TEM images and particle size distributions of reduced (0.6-x)Re-xRu/MC (x = 0, 0.15, 0.3, 0.45, and 0.6) catalysts. All the catalysts retained an ordered mesoporous carbon structure and well-dispersed metal particles as presented in the TEM images. However, (0.6-x)Re-xRu/MC (x = 0.15, 0.3, and 0.45) catalysts showed more narrow particle size distributions than 0.6Re/MC and 0.6Ru/MC, indicating that metal particles of Re-Ru bimetallic

catalysts were uniformly distributed, as discussed in the TPR results. It is noteworthy that all the reduced catalysts retained a few metal particles which were larger than pore sizes of the calcined catalysts (Table 3.1.1). This means that some metal particles grown during the reduction process caused the partial pore blockage of carbon supports. It was revealed that average metal particle size measured by TEM decreased in the order of 0.6Re/MC > 0.6Ru/MC > 0.45Re-0.15Ru/MC > 0.15Re-0.45Ru/MC > 0.3Re-0.3Ru/MC, which was well consistent with the trend of average metal particle size determined by CO chemisorption. However, average metal particle sizes of all catalysts determined by CO chemisorption were larger than those measured by TEM. This overestimation might be because the catalysts were partially reduced under the reduction condition at 500 ˚C for 4 h. Among the catalysts, 0.3Re-0.3Ru/MC showed the largest metal dispersion and smallest average metal particle size.

In order to confirm the distribution of rhenium and ruthenium species, STEM-EDX analyses were carried out. Fig. 3.1.5 showed the STEM and EDX mapping images for one metal particle of reduced 0.3Re-0.3Ru/MC catalyst. Rhenium and ruthenium species were distinguishable in the EDX mapping images. It is noticeable that rhenium atom and ruthenium atom were co-presented in the metal particle domain of 0.3Re-0.3Ru/MC catalyst. On the basis of TPR, XRD, and EDX mapping results, it is believed that a Re-Ru miscible phase was formed in the reduced 0.3Re-0.3Ru/MC catalyst and this was responsible for strong interaction between metallic rhenium and ruthenium species.

Table 3.1.4

CO chemisorption results of reduced (0.6-x)Re-xRu/MC (x = 0, 0.15, 0.3, 0.45, and 0.6) catalysts

Catalyst	Metal surface area (m^2/g-cat.)[a]	Metal dispersion (%)[a]	Average metal particle size (nm)[a]
0.6Re/MC	3.15	17.6	7.9
0.45Re-0.15Ru/MC	3.62	20.3	6.8
0.3Re-0.3Ru/MC	4.74	26.9	5.1
0.15Re-0.45Ru/MC	4.09	23.2	5.9
0.6Ru/MC	3.36	19.2	6.9

[a] Calculated from CO chemisorption measurement by assuming a stoichiometry factor of $CO/metal_{atom} = 1$

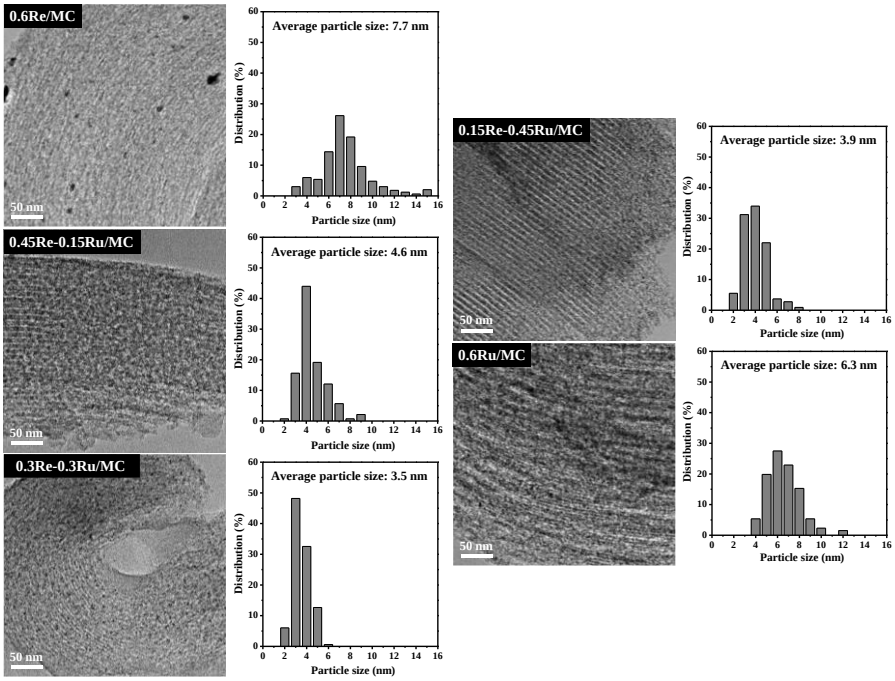

Fig. 3.1.4. TEM images and particle size distributions of reduced (0.6-x)Re-xRu/MC (x = 0, 0.15, 0.3, 0.45, and 0.6) catalysts.

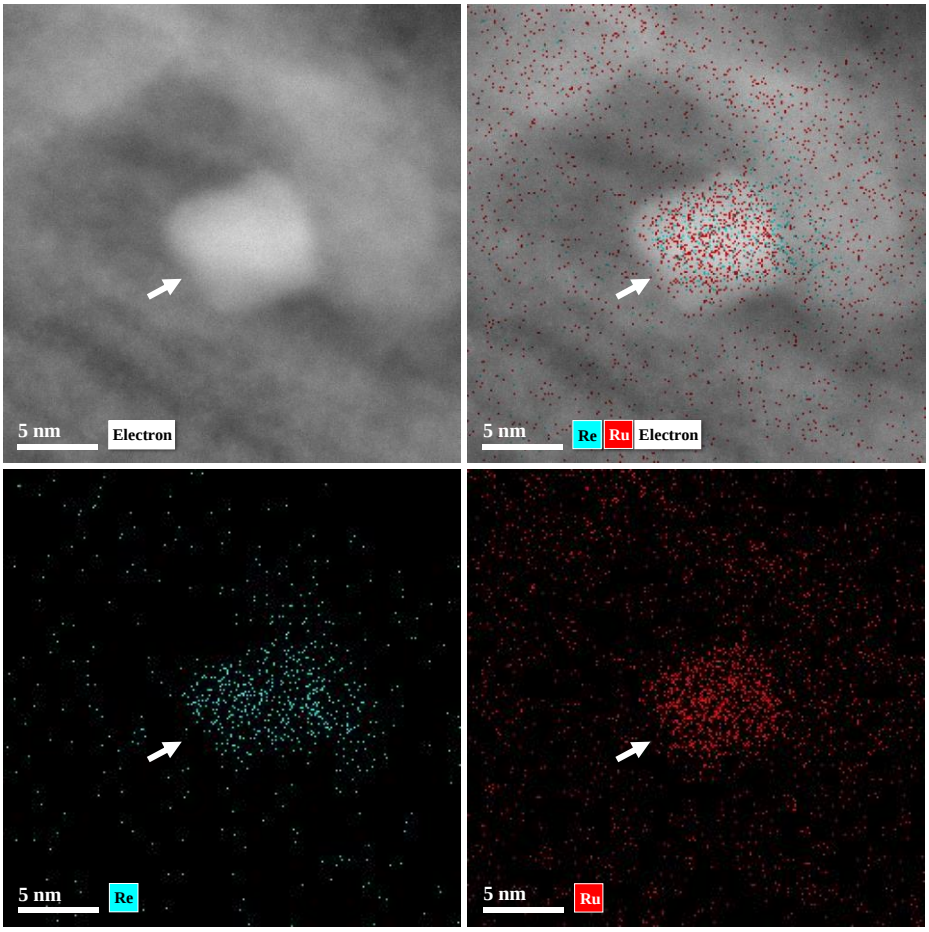

Fig. 3.1.5. STEM-EDX images of reduced 0.3Re-0.3Ru/MC catalyst obtained by mapping on rhenium and ruthenium.

3.1.5. XPS study of reduced catalysts

It is known that the oxidation state of metal species in the catalyst served as an important factor determining the catalytic activity [51,52]. Accordingly, the oxidation states of reduced (0.6-x)Re-xRu/MC (x = 0, 0.15, 0.3, 0.45, and 0.6) catalysts were examined by XPS analyses. Fig. 3.1.6 shows the XPS spectra for Re 4f (Fig. 3.1.6(a)) and Ru $3p_{3/2}$ (Fig. 3.1.6(b)) levels of the catalysts. The Re 4f spectra were deconvoluted into Re $4f_{7/2}$ (solid line in Fig. 3.1.6(a)) and Re $4f_{5/2}$ (dashed line in Fig. 3.1.6(a)) peaks, and then Re $4f_{7/2}$ spectra were divided into Re^0 (40.6 eV), Re^{3+} (41.4 eV), Re^{4+} (42.3 eV), and Re^{6+} (45.3 eV) species [53,54]. On the other hand, the Ru $3p_{3/2}$ spectra were assigned to metallic Ru^0 (462.1 eV) and Ru^{4+} (464.3 eV) species [55]. It was found that the areas of Re 4f and Ru $3p_{3/2}$ spectra decreased with decreasing the rhenium and ruthenium loading, respectively. On the basis of deconvoluted peak areas of Re $3f_{7/2}$ and Ru $3p_{3/2}$ spectra, the oxidation state ratios and surface atomic ratios of rhenium and ruthenium were quantified as summarized in Table 3.1.5. It was found that Re^0/Re_{total} increased in the order of 0.6Re/MC < 0.15Re-0.45Ru/MC < 0.45Re-0.15Ru/MC < 0.3Re-0.3Ru/MC, while Ru^0/Ru_{total} increased in the order of 0.6Ru/MC < 0.15Re-0.45Ru/MC < 0.45Re-0.15Ru/MC < 0.3Re-0.3Ru/MC. It was also found that $(Re^0 + Ru^0)/C$ increased in the order of 0.6Re/MC < 0.6Ru/MC < 0.45Re-0.15Ru/MC < 0.15Re-0.45Ru/MC < 0.3Re-0.3Ru/MC, which was in good agreement with the trend of metal surface area determined by CO chemisorption (Table 3.1.5). This demonstrates that all the catalysts retained different total reduction

degree of rhenium and ruthenium species. In addition, (Re^0 + Ru^0)/C increased with decreasing average metal particle size determined by TEM (Fig. 3.1.4), indicating that total reduction degree of both two metals was closely related to the average particle size of the catalysts. It is important to note that (Re^0 + Ru^0)/C ratios of (0.6-x)Re-xRu/MC (x = 0.15, 0.3, and 0.45) catalysts were higher than those of 0.6Re/MC and 0.6Ru/MC. According to the shrinking core model [56-58], the reduction of a metal particle is limited by the intraparticle hydrogen diffusivity, which means that the reduction degree of metal species can be enhanced by decreasing the particle size. Therefore, it is believed that the Re-Ru bimetallic catalysts with smaller particle size were more effectively reduced than rhenium or ruthenium monometallic catalyst.

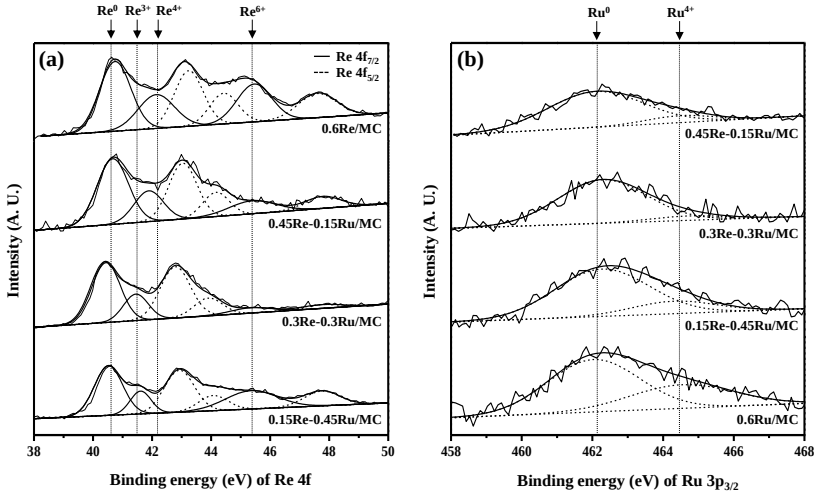

Fig. 3.1.6. XPS spectra of (a) Re 4f and (b) Ru $3p_{3/2}$ levels in the reduced (0.6-x)Re-xRu/MC (x = 0, 0.15, 0.3, 0.45, and 0.6) catalysts.

Table 3.1.5

XPS analyses results of reduced (0.6-x)Re-xRu/MC (x = 0, 0.15, 0.3, 0.45, and 0.6) catalysts

Catalyst	Ratio of Re species[a]			Ratio of Ru species[a]		Surface atomic ratio ($\times 10^3$)		
	Re^0/Re_{total}	$Re^{\alpha+}/Re_{total}$[b]	Re^{6+}/Re_{total}	Ru^0/Ru_{total}	Ru^{4+}/Ru_{total}	Re_{total}/C	Ru_{total}/C	$(Re^0 + Ru^0)/C$
0.6Re/MC	0.46	0.26	0.28	-	-	4.12	-	1.90
0.45Re-0.15Ru/MC	0.61	0.24	0.15	0.88	0.12	5.03	1.81	4.66
0.3Re-0.3Ru/MC	0.67	0.25	0.08	0.92	0.08	4.75	5.46	8.21
0.15Re-0.45Ru/MC	0.53	0.16	0.31	0.81	0.19	1.51	6.65	6.19
0.6Ru/MC	-	-	-	0.65	0.35	-	5.73	3.72

[a] Calculated from deconvoluted peak area of XPS spectra in Fig. 3.6
[b] $3 \leq \alpha \leq 4$

3.1.6. Hydrogen adsorption study of reduced catalysts

It has been reported that the ability of hydrogen adsorption on the active sites plays a crucial role in the catalytic hydrogenation reaction [59,60]. Thus, H_2-TPD measurements were carried out to explain the affinity of metal species toward hydrogen in the reduced (0.6-x)Re-xRu/MC (x =0, 0.15, 0.3, 0.45, and 0.6) catalysts. In this study, hydrogen was injected to the reduced catalysts at 200 ˚C, which was identical to the reaction temperature, to thermally activate the dissociative adsorption of hydrogen molecules on metallic rhenium and ruthenium [61]. Fig. 3.1.7 shows the H_2-TPD profiles of reduced (0.6-x)Re-xRu/MC (x =0, 0.15, 0.3, 0.45, and 0.6) catalysts. For comparison, H_2-TPD profile of MC support was also presented. The H_2-TPD profile of MC support exhibited a broad minor peak at 283 ºC and a main peak at 607 ºC; the former corresponded to the adsorption of hydrogen molecules, while the latter was caused by gaseous products such as H_2, CH_4, C_2H_2, and C_2H_4 formed by reaction of carbon with spillover hydrogen on carbon surface, as evidenced by the TPR results [62]. Interestingly, when rhenium or ruthenium was added into the MC support, new peaks corresponding to the dissociatively adsorbed hydrogen (400-600 ˚C) appeared instead of the peak for molecularly adsorbed hydrogen (<300 ˚C). In order to distinguish dissociatively adsorbed hydrogen in the H_2-TPD profiles of the reduced (0.6-x)Re-xRu/MC catalysts, therefore, H_2-TPD profiles were deconvoluted into three peaks in terms of desorption temperature; weak hydrogen-binding site (400-500 ˚C), strong hydrogen-binding site (500-600

˚C), and the others (>600 ˚C). The other peaks appearing above 600 ˚C might be due to mesoporous carbon. Thus, weak hydrogen-binding sites and strong hydrogen-binding sites were only considered for quantification. The amounts of these two hydrogen-binding sites calculated from the deconvoluted results of H_2-TPD profiles of the catalysts are summarized in Table 3.1.6. Total amount of hydrogen desorbed from the reduced (0.6-x)Re-xRu/MC catalysts increased in the order of 0.6Re/MC < 0.6Ru/MC < 0.45Re-0.15Ru/MC < 0.15Re-0.45Ru/MC < 0.3Re-0.3Ru/MC. This trend was well consistent with the trend of $(Re^0 + Ru^0)/C$ determined by XPS analyses, indicating that larger total amount of desorbed hydrogen resulted from more reduced state of the catalysts. On the other hand, the amount of weak hydrogen-binding sites increased in the order of 0.6Ru/MC < 0.6Re/MC < 0.15Re-0.45Ru/MC < 0.45Re-0.15Ru/MC < 0.3Re-0.3Ru/MC, which was different from the trend of the total amount of hydrogen-binding sites.

From XPS and H_2-TPD results of the reduced (0.6-x)Re-xRu/MC catalysts, it was found that the trend of weak hydrogen-binding sites was well matched with the trend of Re^0/Re_{total} and Ru^0/Ru_{total} ratios. Fig. 3.1.8 shows the relationships between the amount of weak hydrogen-binding sites and Re^0/Re_{total} ratio and between the amount of weak hydrogen-binding sites and Ru^0/Ru_{total} ratio of reduced (0.6-x)Re-xRu/MC (x = 0, 0.15, 0.3, 0.45, and 0.6) catalysts. It was revealed that the amount of weak hydrogen-binding sites increased with increasing Re^0/Re_{total} and Ru^0/Ru_{total} ratios, suggesting that the metallic ratio was a crucial factor determining the hydrogen adsorption behavior of (0.6-x)Re-xRu/MC catalysts. In other words, the synergistic interaction formed by Re-Ru metallic bond increased the amount of weak

hydrogen-binding sites with respect to total active sites in the (0.6-x)Re-xRu/MC catalysts. It is well known that the weakly bound hydrogen atoms on the metallic surface are highly mobile due to their low stability, and therefore, they can be easily and continuatively delivered to the adsorbed reactant molecules [63,64]. Thus, it is expected that a catalyst retaining larger amount of weak hydrogen-binding sites would be more favorable for continuous supply of hydrogen to adsorbed succinic acid.

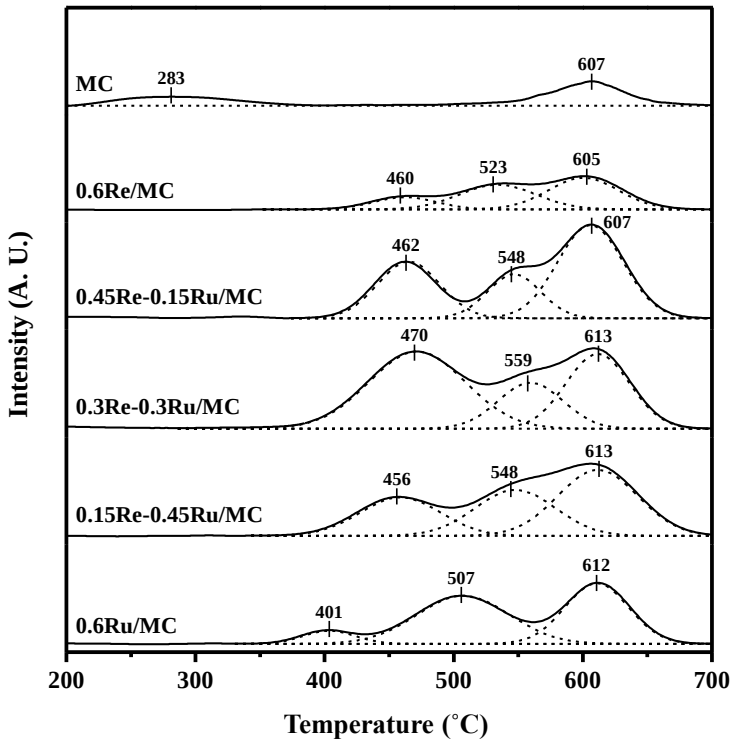

Fig. 3.1.7. H_2-TPD profiles of reduced (0.6-x)Re-xRu/MC (x = 0, 0.15, 0.3, 0.45, and 0.6) catalysts and mesoporous carbon (MC) support.

Table 3.1.6

H_2-TPD results of reduced (0.6-x)Re-xRu/MC (x = 0, 0.15, 0.3, 0.45, and 0.6) catalysts

Catalyst	Amount of desorbed hydrogen (μmol-H_2/g-catalyst)[a]		
	Weak site (400-500 ˚C)	Strong site (500-600 ˚C)	Total
0.6Re/MC	3.15	17.6	7.9
0.45Re-0.15Ru/MC	3.62	20.3	6.8
0.3Re-0.3Ru/MC	4.74	26.9	5.1
0.15Re-0.45Ru/MC	4.09	23.2	5.9
0.6Ru/MC	3.36	19.2	6.9

[a] Calculated from deconvoluted peak area of H_2-TPD profiles in Fig. 3.7

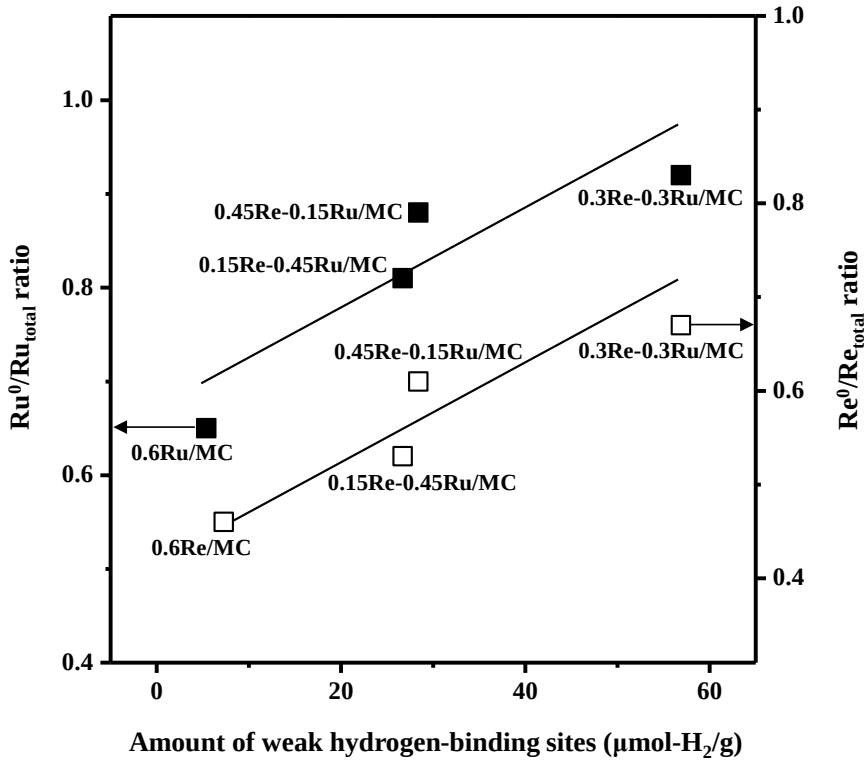

Fig. 3.1.8. Correlations between the amount of weak hydrogen-binding sites and Re_0/Re_{total} ratio and between the amount of weak hydrogen-binding sites and Ru_0/Ru_{total} ratio of reduced (0.6-x)Re-xRu/MC (x = 0, 0.15, 0.3, 0.45, and 0.6) catalysts.

3.1.7. Catalytic performance in the hydrogenation of succinic acid

In order to ensure the reaction pathways, catalytic hydrogenation of succinic acid to BDO was carried out at 200 ˚C and 80 bar with time on stream. 0.3Re-0.3Ru/MC catalyst with the largest amount of weak hydrogen-binding sites was used as a model catalyst for the reaction. Fig. 3.1.9 shows the conversion of succinic acid and yields for GBL, BDO, and THF as a function of time. It was found that succinic acid was completely converted after 5 h, and yield for GBL exhibited a volcano-shaped curve with respect to the reaction time because GBL was transformed to BDO or THF by consecutive hydrogenation. It is noteworthy that BDO was dominantly produced from GBL, indicating that BDO can be selectively formed from succinic acid over 0.3Re-0.3Ru/MC catalyst. The yield for BDO showed the maximum value (71.2%) after 7 h-reaction.

The catalytic performance of (0.6-x)Re-xRu/MC (x = 0, 0.15, 0.3, 0.45, and 0.6) in the liquid-phase hydrogenation of succinic acid to BDO at 200 ˚C and 80 bar for 7 h is summarized in Table 3.1.7. It was found that 0.6Re/MC and 0.6Ru/MC catalysts produced GBL as a major product, while (0.6-x)Re-xRu/MC (x = 0.15, 0.3, and 0.45) catalysts produced BDO as a major product in the reaction. This result indicates that Re-Ru bimetallic catalysts were more effective for consecutive hydrogenation of succinic acid to BDO via GBL than rhenium or ruthenium monometallic catalyst. It should be noted that TOF and TOF_{BDO} of (0.6-x)Re-xRu/MC (x = 0.15, 0.3, and 0.45) catalysts were also higher than those of 0.6Re/MC and 0.6Ru/MC, which means that the Re-

Ru bimetallic catalysts were structure sensitive in the hydrogenation of succinic acid to BDO. In other words, the catalytic activity of (0.6-x)Re-xRu/MC was significantly affected by the ability of active sites rather than by the amount of total active sites. TOF and TOF_{BDO} increased in the order of 0.6Ru/MC < 0.6Re/MC < 0.15Re-0.45Ru/MC < 0.45Re-0.15Ru/MC < 0.3Re-0.3Ru/MC. Among the catalysts tested, 0.3Re-0.3Ru/MC showed the highest TOF (61.2 h^{-1}) and TOF_{BDO} (8.51 h^{-1}). In particular, the catalytic performance of 0.3Re-0.3Ru/MC was comparable to that of reported Re-based bimetallic catalysts [20-24]. This implies that 0.3Re-0.3Ru/MC served as a promising catalyst for the selective formation of BDO from succinic acid.

From the trend of TOF_{BDO} (Table 3.1.7), it was revealed that an optimal Re:Ru molar ratio was required for the maximum BDO production by hydrogenation of succinic acid over (0.6-x)Re-xRu/MC (x = 0, 0.15, 0.3, 0.45, and 0.6) catalysts. It was also found that the trend of TOF_{BDO} was closely related to the hydrogen adsorption behavior of the catalysts. Accordingly, TOF_{BDO} of (0.6-x)Re-xRu/MC catalysts was correlated with the amount of weak hydrogen-binding sites as shown in Fig. 3.1.10. It was revealed that TOF_{BDO} increased with increasing the amount of weak hydrogen-binding sites. This indicates that weak hydrogen-binding sites of the catalysts served as the crucial active sites for the selective formation of BDO from hydrogenation of succinic acid. This is because weak hydrogen-binding site can provide excellent hydrogen supply to the reactants adsorbed on the catalysts, as discussed in the H_2-TPD results. Among the catalysts, 0.3Re-0.3Ru/MC catalyst with the largest amount of weak hydrogen-binding sites showed the highest TOF_{BDO} in the hydrogenation of succinic acid to BDO.

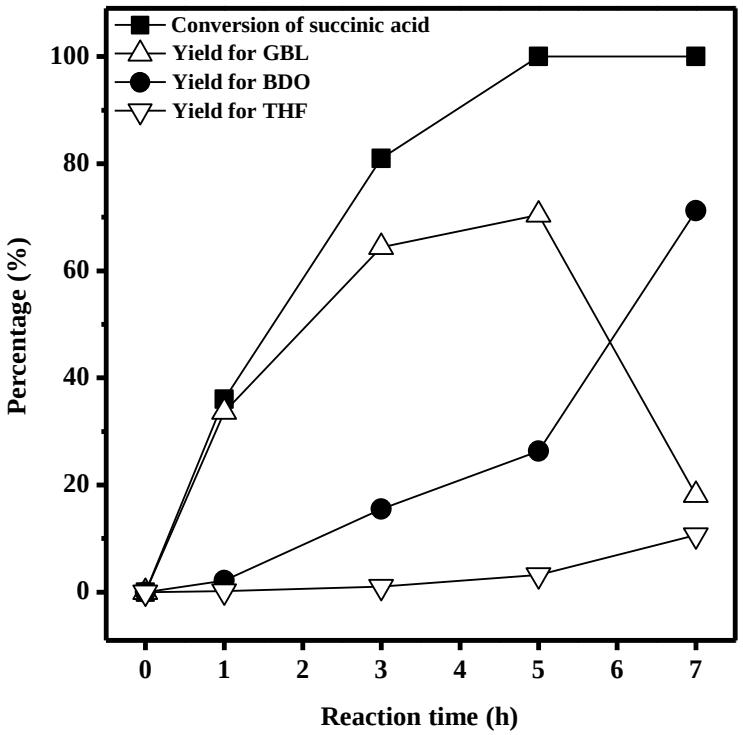

Fig. 3.1.9. Conversion of succinic acid and yields for GBL, BDO, and THF with time on stream in liquid-phase hydrogenation of succinic acid over 0.3Re-0.3Ru/MC catalyst at 200 ˚C and 80 bar.

Table 3.1.7

Performance of (0.6-x)Re-xRu/MC (x = 0, 0.15, 0.3, 0.45, and 0.6) catalysts in liquid-phase hydrogenation of succinic acid at 200 ˚C and 80 bar for 7 h

Catalyst	Conversion of succinic acid (%)	Selectivity (%)			Yield for BDO (%)	TOF (h^{-1})[a]	TOF_{BDO} (h^{-1})[b]
		GBL	BDO	THF			
0.6Re/MC	73.1	88.7	7.7	3.6	5.6	25.4	2.05
0.45Re-0.15Ru/MC	100	39.8	52.2	7.9	52.2	46.1	6.04
0.3Re-0.3Ru/MC	100	18.1	71.2	10.7	71.2	61.2	8.51
0.15Re-0.45Ru/MC	100	44.3	48.9	6.8	48.9	38.6	5.23
0.6Ru/MC	45.2	97.5	1.8	0.7	0.8	13.4	0.29

[a] Calculated as moles of succinic acid converted per moles of surface metal atom per hour (at ca. 10% conversion of succinic acid)
[b] Calculated as moles of BDO produced per moles of surface metal atom per hour (at ca. 70% yield for GBL)

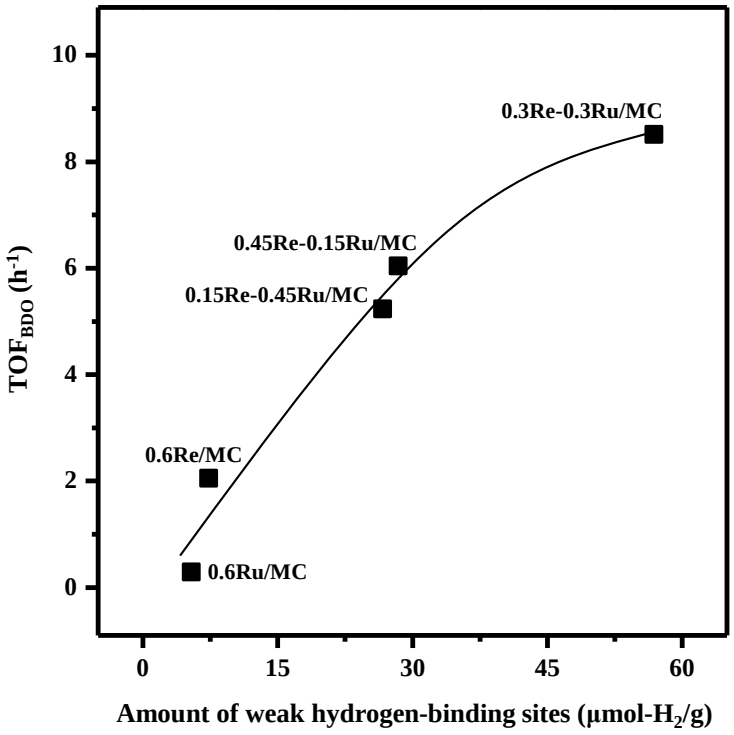

Fig. 3.1.10. A correlation between TOF_{BDO} and the amount of weak hydrogen-binding sites in the reduced (0.6-x)Re-xRu/MC (x = 0, 0.15, 0.3, 0.45, and 0.6) catalysts.

3.1.8. Stability and reusability of catalysts

To investigate the stability of 0.3Re-0.3Ru/MC catalyst, reusability of the catalyst was tested. According to the previous works [18,19], it was revealed that the decrement of catalytic activity in the hydrogenation of succinic acid was mainly attributed to the leaching of active metal species under the harsh reaction conditions. For the recycle test, the spent catalyst was separated from liquid product by filtration, washed with deionized water, and dried in a vacuum oven at 60 ˚C after each reaction test. The remaining liquid containing leached metal species was collected for ICP-MS analysis. Fig. 3.1.11 shows the recycle results of 0.3Re-0.3Ru/MC catalyst in the liquid-phase hydrogenation of succinic acid to BDO at 200 ˚C and 80 bar for 7 h. Fresh and spent 0.3Re-0.3Re/MC catalyst showed complete conversion of succinic acid, and selectivity and yield for BDO over the catalyst remained almost constant. Moreover, no significant metal leaching was observed (less than 2%) after each recycle test, as listed in Table 3.1.8. This implies that the strong interaction of Re-Ru metallic bond effectively suppressed leaching of metal species. Thus, 0.3Re-0.3Ru/MC catalyst served as a stable and reusable catalyst in the hydrogenation of succinic acid to BDO.

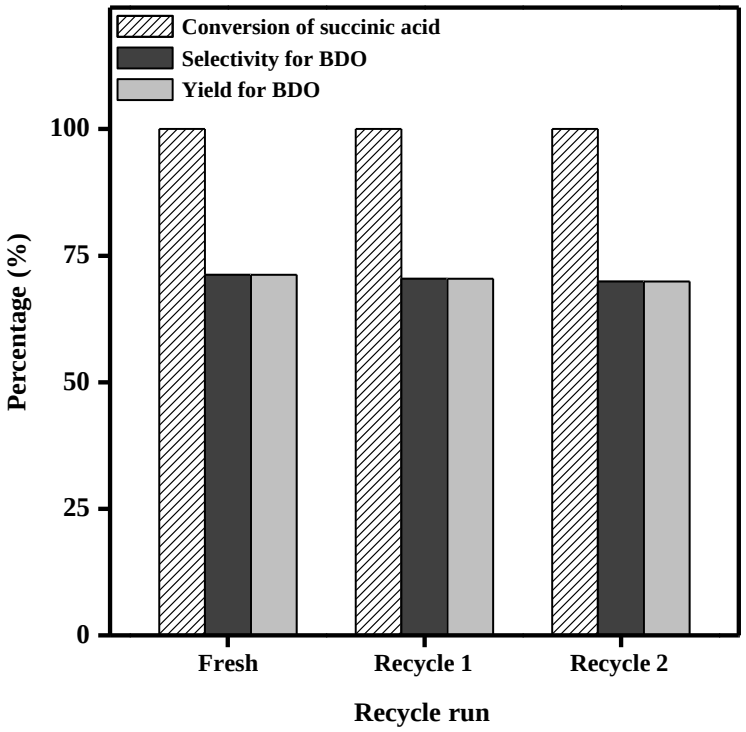

Fig. 3.1.11. Results for liquid-phase hydrogenation of succinic acid to BDO over 0.3Re-0.3Ru/MC catalyst with respect to recycle run at 200 ˚C and 80 bar for 7 h.

Table 3.1.8

Metal leaching in the liquid-phase hydrogenation of succinic acid over 0.3Re-0.3Ru/MC catalyst with respect to recycle run at 200 ˚C and 80 bar for 7 h

Recycle run	Rhenium leaching (%)[a]	Ruthenium leaching (%)[a]
Fresh	1.01	0.28
1	0.96	0.40
2	1.47	0.74

[a] Determined by ICP-MS measurement

3.2. Re-Ru bimetallic catalysts supported on mesoporous boron-modified carbon

3.2.1. Textural properties of catalysts

To investigate textural properties of Re-Ru/xBMC (x = 0, 0.02, 0.04, 0.08, and 0.12) catalysts, nitrogen adsorption-desorption analyses were conducted. Fig. 3.2.1 shows the nitrogen adsorption-desorption isotherms of Re-Ru/xBMC (x = 0, 0.02, 0.04, 0.08, and 0.12) catalysts. All the catalysts showed IV-type isotherm with H3-type hysteresis loop, indicating that well-developed mesopores and slit-shaped carbon structure were formed in the catalysts. Detailed textural properties of Re-Ru/xBMC (x = 0, 0.02, 0.04, 0.08, and 0.12) catalysts is summarized in Table 3.2.1 and Table 3.2.2. Actual Re:Ru and B/C molar ratios in the Re-Ru/xBMC catalysts were in good agreement with the designed values. In addition, all the catalysts retained mesopores larger than 6.3 nm, representing successful preparation of mesoporous boron-modified carbon supports. It was also found that surface area and pore volume of Re-Ru/xBMC catalysts decreased with increasing B/C molar ratio. This is because boron was introduced into carbon framework during the preparation step by retarding the formation of pore structure.

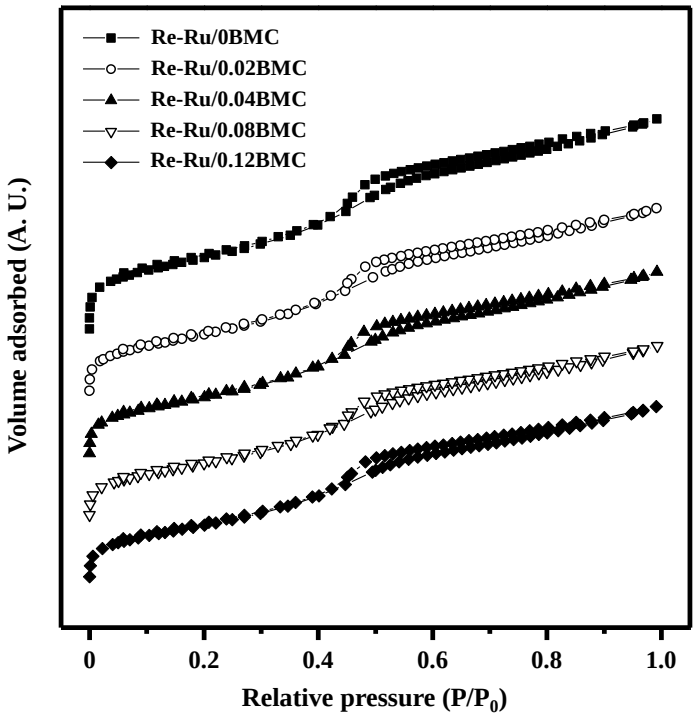

Fig. 3.2.1. Nitrogen adsorption-desorption isotherms of Re-Ru/xBMC (x = 0, 0.02, 0.04, 0.08, and 0.12) catalysts.

Table 3.2.1

ICP-MS results of Re-Ru/xBMC (x = 0, 0.02, 0.04, 0.08, and 0.12) catalysts

Catalyst	Re : Ru molar ratio[a]	B/C molar ratio[a]
Re-Ru/0BMC	0.48 : 0.52	-
Re-Ru/0.02BMC	0.47 : 0.53	0.018
Re-Ru/0.04BMC	0.51 : 0.49	0.038
Re-Ru/0.08BMC	0.48 : 0.52	0.077
Re-Ru/0.12BMC	0.52 : 0.48	0.114

[a] Determined by ICP-MS measurement

Table 3.2.2

Textural properties of Re-Ru/xBMC (x = 0, 0.02, 0.04, 0.08, and 0.12) catalysts

Catalyst	Surface area $(m^2/g)^a$	Pore volume $(cm^3/g)^b$	Pore diameter $(nm)^c$
Re-Ru/0BMC	850	0.81	6.5
Re-Ru/0.02BMC	837	0.72	6.6
Re-Ru/0.04BMC	821	0.71	6.4
Re-Ru/0.08BMC	792	0.67	6.3
Re-Ru/0.12BMC	774	0.67	6.4

[a] Calculated by the BET equation
[b] Total pore volume at $P/P_0 = 0.99$
[c] Average pore diameter

3.2.2. Crystalline structures of reduced catalysts

Fig. 3.2.2 shows the XRD patterns of reduced Re-Ru/xBMC (x = 0, 0.02, 0.04, 0.08, and 0.12) catalysts. All the catalysts exhibited broad diffraction peaks at 23.5˚ and 43.8˚, corresponding to graphitic carbon phase. Interestingly, neither rhenium phase nor ruthenium phase was observed in the XRD patterns of the catalysts. This means that rhenium and ruthenium species were finely dispersed on the surface of the catalysts. Moreover, no distinct boron-related peaks were observed in the XRD patterns, indicating that boron species were homogeneously distributed in the carbon framework.

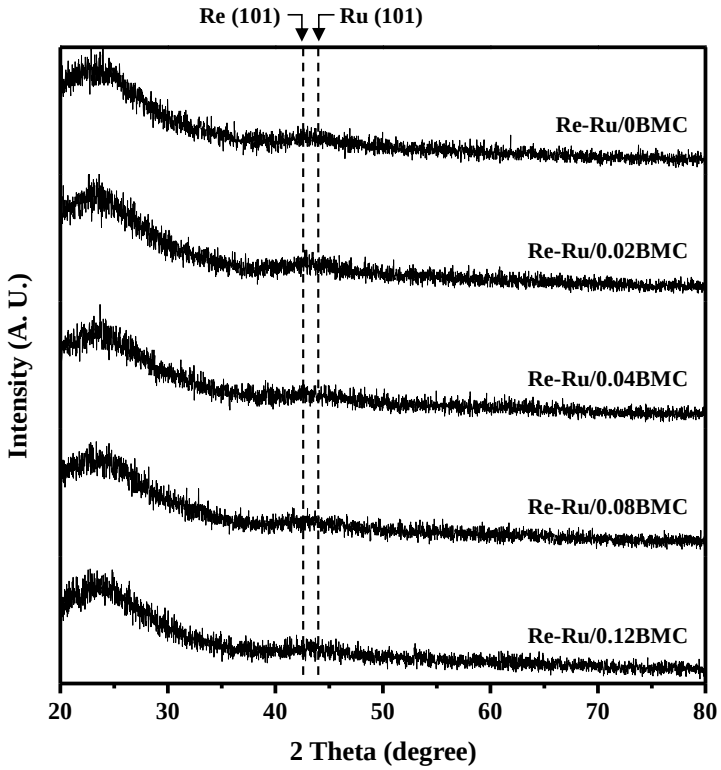

Fig. 3.2.2. XRD patterns of reduced Re-Ru/xBMC (x = 0, 0.02, 0.04, 0.08, and 0.12) catalysts.

3.2.3. Metal dispersion of reduced catalysts

The above result was further confirmed by CO chemisorption analyses of reduced Re-Ru/xBMC (x = 0, 0.02, 0.04, 0.08, and 0.12) catalysts, as listed in Table 3.2.3. It was found that all the catalysts retained metal particles less than 6 nm. It is interestingly to note that metal surface area and metal dispersion decreased while average metal particle size increased with increasing B/C molar ratio of Re-Ru/xBMC catalysts. This might be due to the decrement of surface area with increasing B/C molar ratio, as discussed in Section 3.2.1.

STEM images of Re-Ru/0.04BMC catalyst and EDX mapping images with distributions of rhenium, ruthenium, and boron species are shown in Fig. 3.2.3. It was found that each element was clearly distinguishable in the EDX mapping images. In particular, it was found that boron species were successfully introduced into carbon support during the single-step surfactant-templating preparation step. It was also observed that rhenium and ruthenium atoms were homogeneously distributed throughout the catalyst.

Table 3.2.3

CO chemisorption results of reduced Re-Ru/xBMC (x = 0, 0.02, 0.04, 0.08, and 0.12) catalysts

Catalyst	Metal surface area (m^2/g-cat.)[a]	Metal dispersion (%)[a]	Average metal particle size (nm)[a]
Re-Ru/0BMC	4.70	26.5	5.2
Re-Ru/0.02BMC	4.61	26.0	5.3
Re-Ru/0.04BMC	4.46	25.2	5.5
Re-Ru/0.08BMC	4.18	23.7	5.9
Re-Ru/0.12BMC	4.09	23.1	6.0

[a] Calculated from CO chemisorption measurement by assuming a stoichiometry factor of $CO/metal_{atom} = 1$

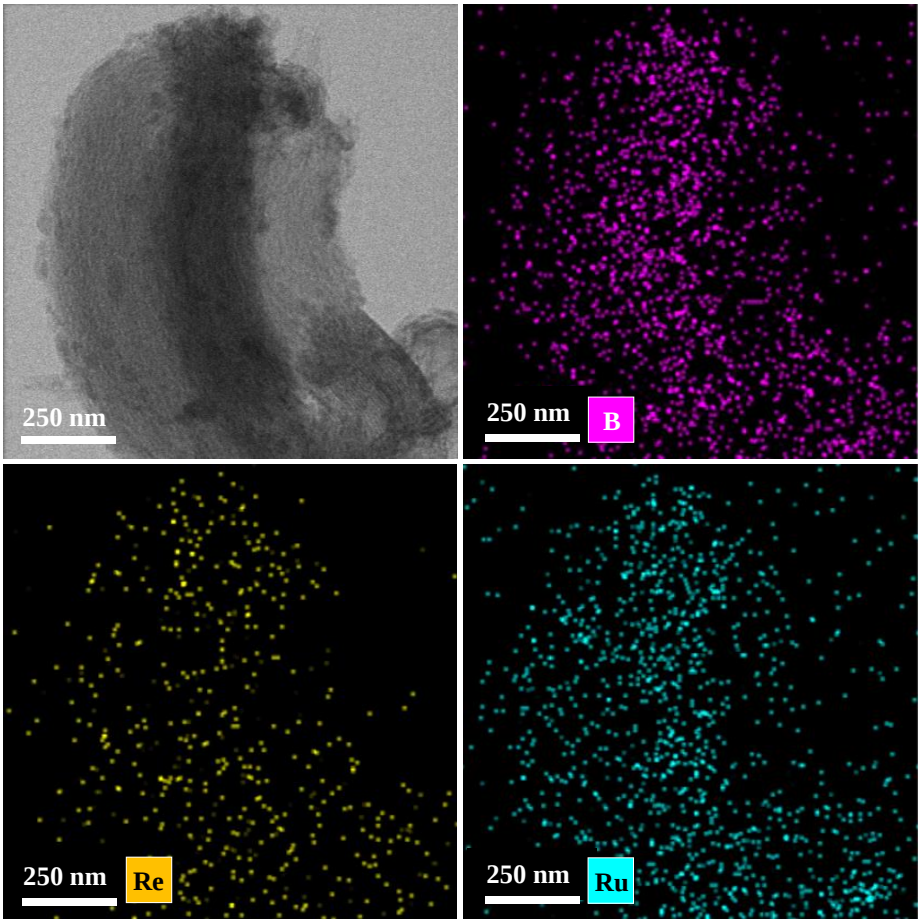

Fig. 3.2.3. STEM-EDX images of reduced Re-Ru/0.04BMC catalyst obtained by mapping on rhenium, ruthenium, and boron.

3.2.4. Reduction behaviors of catalysts

TPR measurements were conducted to examine reduction behavior of Re-Ru/xBMC (x = 0, 0.02, 0.04, 0.08, and 0.12) catalysts, as shown in Fig. 3.2.4. It was observed that all the catalysts showed one reduction peak at around 282-341 ˚C despite the presence of two noble metals. According to the previous work, rhenium and ruthenium species are simultaneously reduced because pre-reduced ruthenium species can transfer hydrogen to unreduced metal species. Therefore, it is believed that rhenium and ruthenium species in the Re-Ru/xBMC catalysts were co-reduced during the reduction process. It is interesting to note that the peak shape became broader with increasing B/C molar ratio. Moreover, the peak moved toward higher temperature with increasing B/C molar ratio. In particular, peak temperature of Re-Ru/xBMC (x = 0.08 and 0.12) was significantly higher than that of Re-Ru/xBMC (x = 0, 0.02, and 0.04). The amount of hydrogen uptake calculated from reduction peak area of Re-Ru/xBMC (x = 0, 0.02, 0.04, 0.08, and 0.12) catalysts is listed in Table 3.2.4. It was found that the amount of hydrogen uptake exceeded the theoretical values for rhenium (3.5) and for ruthenium (2) due to hydrogen spillover by metal species [38]. It is noteworthy that Re-Ru/xBMC (x = 0.08 and 0.12) showed rapid decrement of the amount of hydrogen uptake compared to Re-Ru/xBMC (x = 0, 0.02, and 0.04). From the result, it can be inferred that an excessive boron addition into carbon support aggravated particle distribution and reducibility of rhenium and ruthenium species in the Re-Ru/xBMC catalysts.

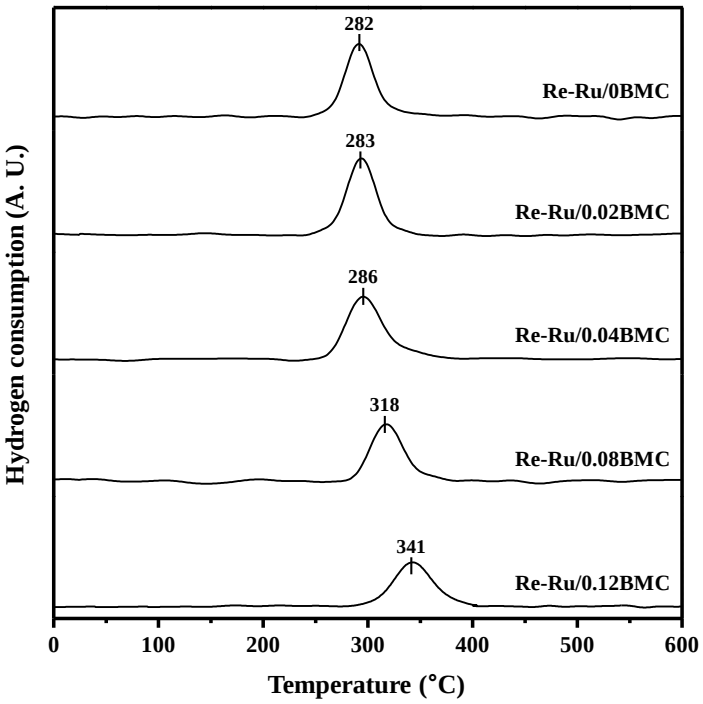

Fig. 3.2.4. TPR profiles of Re-Ru/xBMC (x = 0, 0.02, 0.04, 0.08, and 0.12) catalysts.

Table 3.2.4

TPR chemisorption results of Re-Ru/xBMC (x = 0, 0.02, 0.04, 0.08, and 0.12) catalysts

Catalyst	Amount of hydrogen uptake (mol-H_2/mol-metal)[a]
Re-Ru/0BMC	4.08
Re-Ru/0.02BMC	4.06
Re-Ru/0.04BMC	4.01
Re-Ru/0.08BMC	3.78
Re-Ru/0.12BMC	3.41

[a] Calculated from peak area of TPR profiles in Fig. 3.2.4

3.2.5. Raman and XPS analyses of catalysts

In order to examine boron-modified carbon structure of Re-Ru/xBMC (x = 0, 0.02, 0.04, 0.08, and 0.12) catalysts, Raman spectroscopy analyses were carried out as shown in Fig. 3.2.5. It was found that all the catalysts showed two characteristic peaks at 1350 cm^{-1} and 1600 cm^{-1}; the former corresponds to D band while the latter corresponds to G band of sp^2-carbon material [51,65]. It is known that the ratio of D band/G band intensity (I_D/I_G) represents the degree of sp^2-carbon structure [65-67]. In other words, the decrement of I_D/I_G ratio indicates the increment of substituted boron species in the sp^2-carbon lattice. The I_D/I_G ratio calculated from Raman spectra of Re-Ru/xBMC (x = 0, 0.02, 0.04, 0.08, and 0.12) catalysts is summarized in Table 2. It was revealed that I_D/I_G ratio decreased in the order of Re-Ru/0.12BMC > Re-Ru/0.08BMC > Re-Ru/0BMC > Re-Ru/0.02BMC > Re-Ru/0.04BMC. Therefore, it can be said that Re-Ru/0.04BMC catalyst retaining the smallest I_D/I_G ratio would have more substituted boron species in the carbon lattice.

XPS analyses were carried out to confirm chemical state of boron species of Re-Ru/xBMC (x = 0, 0.02, 0.04, 0.08, and 0.12) catalysts. Fig. 3.2.6 shows the XPS spectra for B 1s level of Re-Ru/xBMC catalysts. The B 1s spectra was deconvoluted by Gaussian curve-fitting method, and the peaks were assigned to substituted boron (BC_3) at 191.2 eV, partially oxidized boron (BN_3, BCO_2, and BC_2O) at 192.6 eV, and boron oxide (BO_x) at 193.6 eV, respectively [68,69]. It was found that the total area of B 1s spectra increased with increasing B/C molar ratio of Re-Ru/xBMC catalysts. The deconvoluted

areas for B 1s spectra of Re-Ru/xBMC (x = 0, 0.02, 0.04, 0.08, and 0.12) catalysts were re-calculated into ratio of boron species and surface atom ratio, as summarized Table 3. It was found that B_{total}/C ratio increased with increasing boron content in the catalysts. It was also revealed that $B_{substituted}$/C ratio increased in the order of Re-Ru/0.12BMC < Re-Ru/0.08BMC < Re-Ru/0.02BMC < Re-Ru/0.04BMC, in good agreement with the result of Raman spectroscopy analyses. Among the catalysts, Re-Ru/0.04BMC catalyst showed the highest $B_{substituted}$/C ratio.

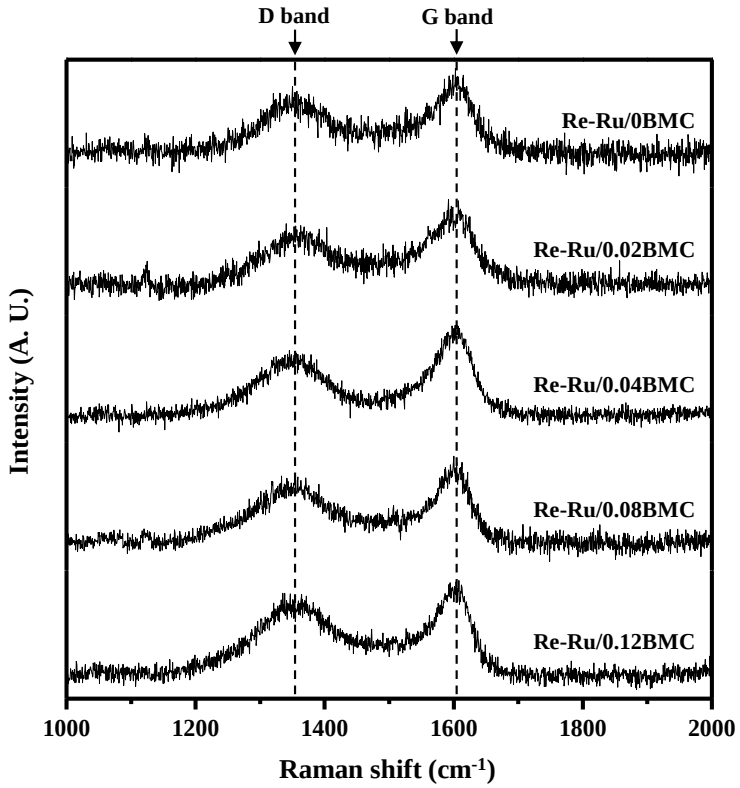

Fig. 3.2.5. Raman spectra of Re-Ru/xBMC (x = 0, 0.02, 0.04, 0.08, and 0.12) catalysts.

Table 3.2.5

A ratio of D band/G band intensity of Re-Ru/xBMC (x = 0, 0.02, 0.04, 0.08, and 0.12) catalysts

Catalyst	I_D/I_G ratio[a]
Re-Ru/0BMC	0.74
Re-Ru/0.02BMC	0.70
Re-Ru/0.04BMC	0.64
Re-Ru/0.08BMC	0.77
Re-Ru/0.12BMC	0.82

[a] Calculated from peak area of TPR profiles in Fig. 3.2.5

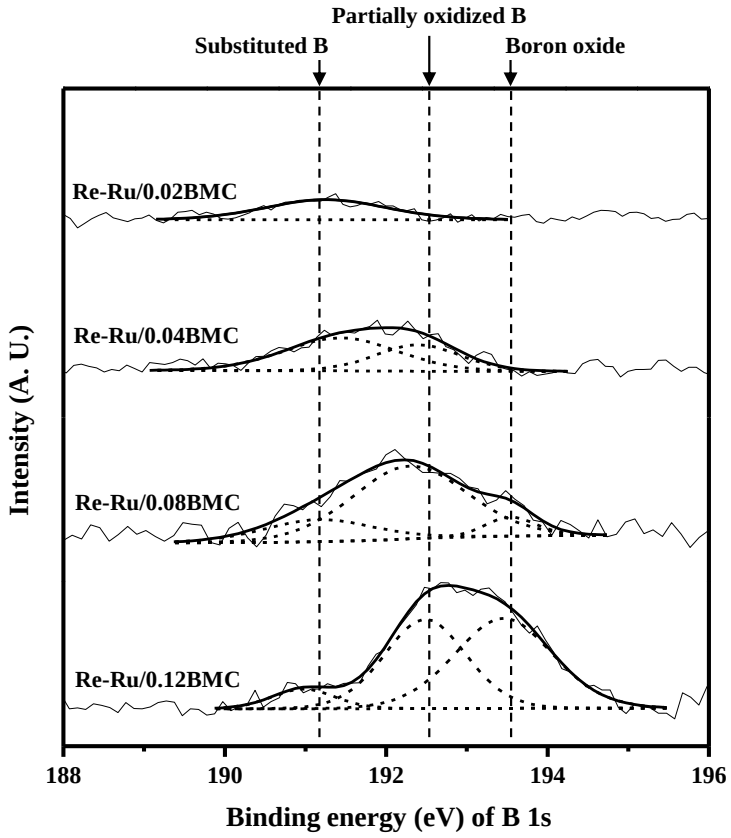

Fig. 3.2.6. XPS spectra of B 1s level in the Re-Ru/xBMC (x = 0, 0.02, 0.04, 0.08, and 0.12) catalysts.

Table 3.2.6

XPS analyses results of Re-Ru/xBMC (x = 0, 0.02, 0.04, 0.08, and 0.12) catalysts

Catalyst	Ratio of boron species[a]			Surface atomic ratio ($\times 10^2$)	
	$B_{substituted}/B_{total}$	$B_{partially\ oxidized}/B_{total}$	$B_{boron\ oxide}/B_{total}$	B_{total}/C	$B_{substituted}/C$
Re-Ru/ 0.02BMC	1.0	0	0	1.61	1.61
Re-Ru/ 0.04BMC	0.62	0.38	0	3.59	2.26
Re-Ru/ 0.08BMC	0.20	0.71	0.09	7.64	1.53
Re-Ru/ 0.12BMC	0.07	0.59	0.34	11.9	0.83

[a] Calculated from deconvoluted peak area of XPS spectra in Fig. 3.2.6

3.2.6. Hydrogen adsorption study of reduced catalysts

For quantitative comparison of hydrogen adsorption capacity of Re-Ru/xBMC (x = 0, 0.02, 0.04, 0.08, and 0.12) catalysts, H_2-TPD measurements were conducted. Fig. 3.2.7 shows the H_2-TPD profiles of reduced Re-Ru/xBMC catalysts. According to the previous study, the peak above 600 ˚C in the H_2-TPD profiles was due to hydrogen spillover or gaseous products such as methane, ethylene, and acetylene formed by thermal reaction of carbon material. On the other hand, hydrogen desorption peaks below 600 ˚C were attributed to dissociatively adsorbed hydrogen on the reduced rhenium and ruthenium species. Thus, H_2-TPD profiles of the catalysts were deconvoluted into weak hydrogen-binding site (400-500 ˚C), strong hydrogen-binding site (500-600 ˚C), and the others (>600 ˚C). The two peaks below 600 ˚C were only considered for the calculation of hydrogen uptake capacity by metal species. The amount of desorbed hydrogen calculated from H_2-TPD profiles of Re-Ru/xBMC (x = 0, 0.02, 0.04, 0.08, and 0.12) catalysts is summarized in Table 3.2.7. It was found that total amount of desorbed hydrogen decreased with increasing B/C molar ratio of the catalysts. This trend was well consistent with the trend of metal surface area and metal dispersion in Table 3.2.3. It was also found that the amount of weak hydrogen-binding sites increased in the order of Re-Ru/0.12BMC < Re-Ru/0.08BMC < Re-Ru/0BMC < Re-Ru/0.02BMC < Re-Ru/0.04BMC, in good agreement with the trends of Raman and XPS results. Among the catalysts, Re-Ru/0.04BMC showed the largest amount of weak hydrogen-

binding sites. This indicates that hydrogen can be weakly bound and easily diffused to adsorbed reactant on the metal surface of Re-Ru/0.04BMC catalyst.

On the basis of XPS and H_2-TPD results of Re-Ru/xBMC (x = 0, 0.02, 0.04, 0.08, and 0.12) catalysts, it is suggested that hydrogen adsorption behavior of active metal species was closely related to the amount of substituted boron species in the catalysts. Fig. 3.2.8 shows the relationship between the amount of weak hydrogen-binding sites and $R_{substituted}$/C ratio of reduced Re-Ru/xBMC (x = 0, 0.02, 0.04, 0.08, and 0.12) catalysts. It was revealed that the amount of weak hydrogen-binding sites increased with increasing $B_{substituted}$/C ratio of the catalysts. It is known that the substitution of boron into carbon lattice induces negatively charged carbon atom due to lower electronegativity of boron (2.04) than carbon (2.55), which increases electron density of active metal species [70]. Therefore, it is believed that electron-rich rhenium and ruthenium induced by boron-containing carbon support became more favorable for the formation of weak hydrogen-binding sites.

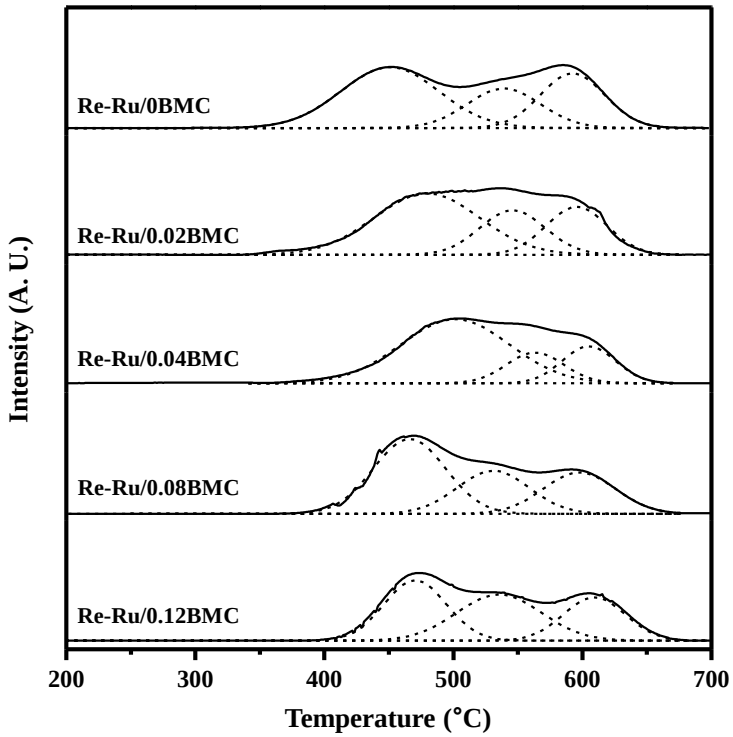

Fig. 3.2.7. H_2-TPD profiles of reduced Re-Ru/xBMC (x = 0, 0.02, 0.04, 0.08, and 0.12) catalysts.

Table 3.2.7

H_2-TPD results of reduced Re-Ru/xBMC (x = 0, 0.02, 0.04, 0.08, and 0.12) catalysts.

Catalyst	Amount of desorbed hydrogen (μmol-H_2/g-catalyst)[a]		
	Weak site (400-500 ˚C)	Strong site (500-600 ˚C)	Total
Re-Ru/0BMC	52.6	30.0	82.6
Re-Ru/0.02BMC	56.5	25.6	82.1
Re-Ru/0.04BMC	63.3	16.8	80.2
Re-Ru/0.08BMC	48.7	29.1	77.8
Re-Ru/0.12BMC	39.9	34.9	74.8

[a] Calculated from deconvoluted peak area of H_2-TPD profiles in Fig. 3.2.7

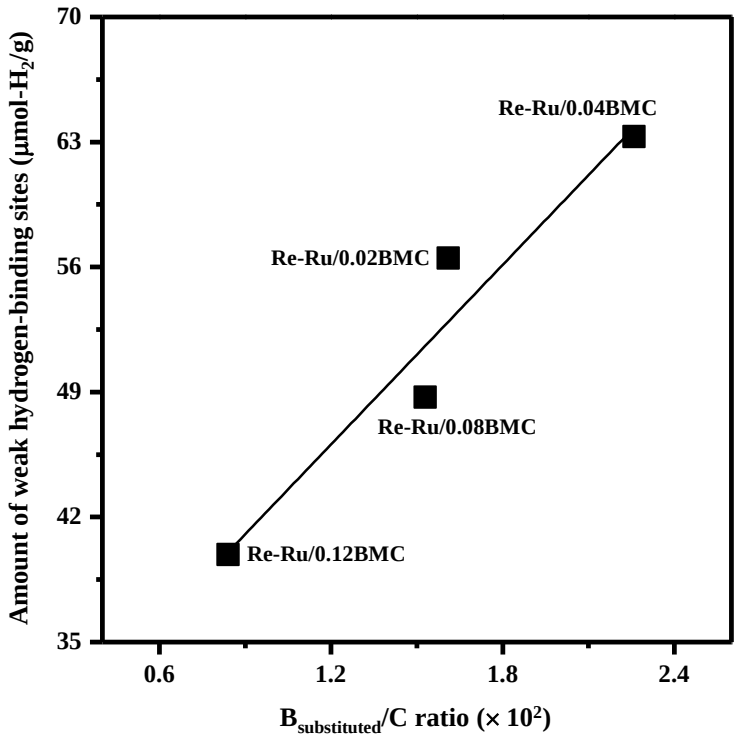

Fig. 3.2.8. A correlation between $B_{substituted}$/C ratio and the amount of weak hydrogen-binding sites of Re-Ru/xBMC (x = 0, 0.02, 0.04, 0.08, and 0.12) catalysts.

3.2.7. Catalytic performance in the hydrogenation of succinic acid

Catalytic performance of Re-Ru/xBMC (x = 0, 0.02, 0.04, 0.08, and 0.12) in the liquid-phase hydrogenation of succinic acid to BDO at 200 ˚C and 80 bar after a 5 h-reaction is summarized in Table 3.2.8. It was found that all the catalysts selectively produced BDO rather than THF due to the synergistic effect between rhenium and ruthenium species. However, only Re-Ru/0.04BMC catalyst yielded BDO as a major product while the other catalysts produced GBL as a major product in the reaction. TOF and TOF_{BDO} were calculated to evaluate the active sites of the catalysts, as listed in Table 3.2.8. Fig. 3.2.9 shows the yield for BDO and TOF_{BDO} over Re-Ru/xBMC (x = 0, 0.02, 0.04, 0.08, and 0.12) catalysts plotted as a function of B/C molar ratio. It was revealed that yield for BDO and TOF_{BDO} showed volcano-shaped curves with respect to B/C molar ratio. Yield for BDO and TOF_{BDO} increased in the order of Re-Ru/0.12BMC < Re-Ru/0.08BMC < Re-Ru/0BMC < Re-Ru/0.02BMC < Re-Ru/0.04BMC. This indicates that an optimal B/C molar ratio was required for maximum BDO production by hydrogenation of succinic acid over Re-Ru/xBMC catalysts. Moreover, TOF_{BDO} of Re-Ru/xBMC (x = 0, 0.02, 0.04, 0.08, and 0.12) catalysts was well correlated with the amount of weak hydrogen-binding sites, as shown in Fig. 3.2.10. It was found that TOF_{BDO} increased with increasing weak hydrogen-binding sites of Re-Ru/xBMC catalysts. This indicates that hydrogen adsorption capacity of the catalysts plays an important role in determining the catalytic performance. In other words, weakly adsorbed hydrogen can be easily

diffused on the metal surface, and consecutively, can be easily supplied to the adsorbed reactant, which promotes the selective production of BDO via GBL in the hydrogenation of succinic acid. Among the catalysts, Re-Ru/0.04BMC with the largest amount of weak hydrogen-binding sites showed the highest TOF_{BDO}. Thus, Re-Ru/0.04BMC catalyst served as an effective catalyst in the hydrogenation of succinic acid to BDO.

Table 3.2.8

Performance of Re-Ru/xBMC (x = 0, 0.02, 0.04, 0.08, and 0.12) catalysts in liquid-phase hydrogenation of succinic acid at 200 ˚C and 80 bar for 7 h

Catalyst	Conversion of succinic acid (%)	Selectivity (%)			Yield for BDO (%)	TOF (h^{-1})[a]	TOF_{BDO} (h^{-1})[b]
		GBL	BDO	THF			
Re-Ru/ 0BMC	98.8	66.9	27.2	2.8	26.9	62.2	8.6
Re-Ru/ 0.02BMC	100	48.2	42.8	3.0	42.8	78.0	10.9
Re-Ru/ 0.04BMC	100	23.6	64.7	3.2	64.7	93.5	12.4
Re-Ru/ 0.08BMC	78.1	67.8	25.4	2.5	19.9	57.4	8.0
Re-Ru/ 0.12BMC	64.2	75.3	19.0	2.1	12.2	50.9	6.2

[a] Calculated as moles of succinic acid converted per moles of surface metal atom per hour (at ca. 10% conversion of succinic acid)
[b] Calculated as moles of BDO produced per moles of surface metal atom per hour (at ca. 70% yield for GBL)

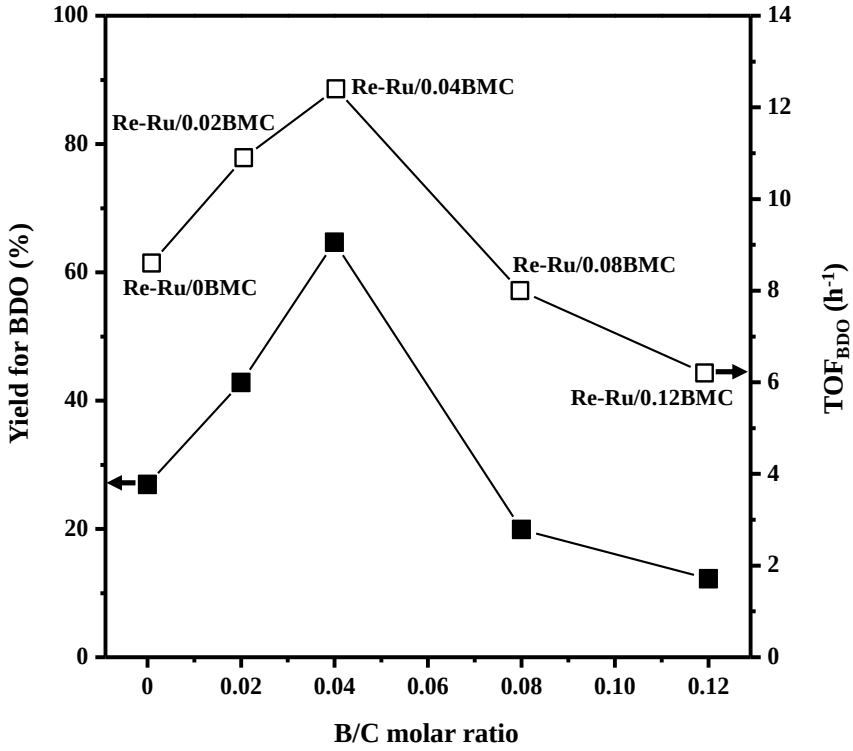

Fig. 3.2.9. Correlations between B/C molar ratio and yield for BDO and between B/C molar ratio and TOF_{BDO} of Re-Ru/xBMC (x = 0, 0.02, 0.04, 0.08, and 0.12) catalysts.

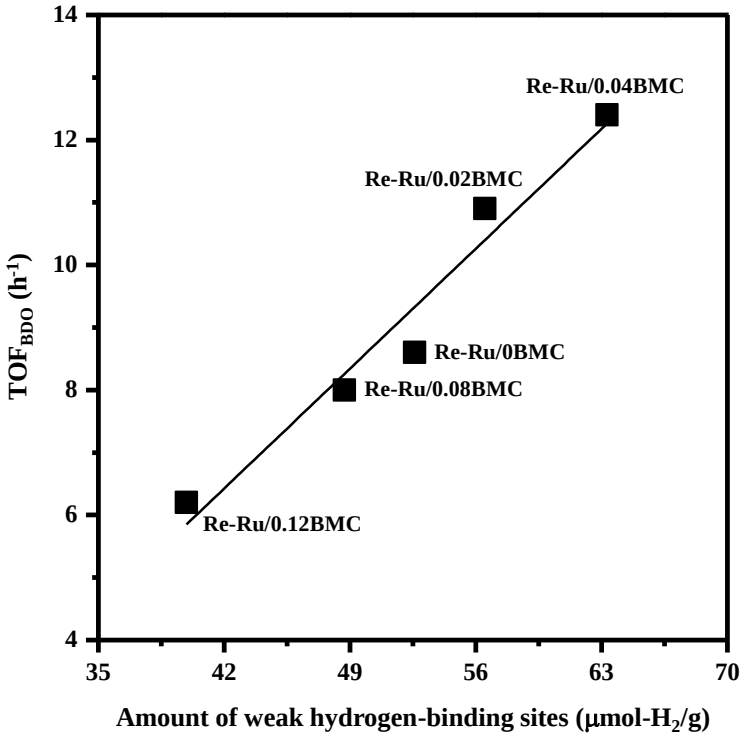

Fig. 3.2.9. A correlation between TOF_{BDO} and the amount of weak hydrogen-binding sites in the Re-Ru/xBMC (x = 0, 0.02, 0.04, 0.08, and 0.12) catalysts.

3.3. Mesoporous Re-Cu-carbon composite catalysts

3.3.1. Textural properties of catalysts

Fig. 3.3.1 shows the nitrogen adsorption-desorption isotherms of the catalysts (Re-Cu-MC, Re/Cu-MC, Cu/Re-MC, and Re-Cu/MC). For comparison, isotherm of mesoporous carbon support (MC) is also presented. All the samples showed IV-type isotherms with H3-type hysteresis loops, indicating the existence of well-developed mesopores [71,72]. Detailed physicochemical properties of the catalysts (Re-Cu-MC, Re/Cu-MC, Cu/Re-MC, and Re-Cu/MC) and mesoporous carbon support (MC) are listed in Table 3.3.1 and Table 3.3.2. Actual Re and Cu contents in all the catalysts were well matched with the designed values. Average pore diameters of the samples were in the range of 3.6-4.4 nm, indicating successful formation of mesoporous carbon structure. It is interesting to note that average pore diameter decreased in the order of Re-Cu/MC > Cu/Re-MC > Re/Cu-MC > Re-Cu-MC. This was because pore size of mesoporous carbon decreased with increasing the amount of metal precursor located on silica wall during the single-step preparation [73]. On the other hand, surface area and pore volume of the catalysts decreased with increasing impregnated metal content due to pore blockage by metal particles. It should be noted that Re-Cu-MC catalyst showed higher surface area (1169 m^2/g) and larger pore volume (1.04 cm^3/g) than the other catalysts.

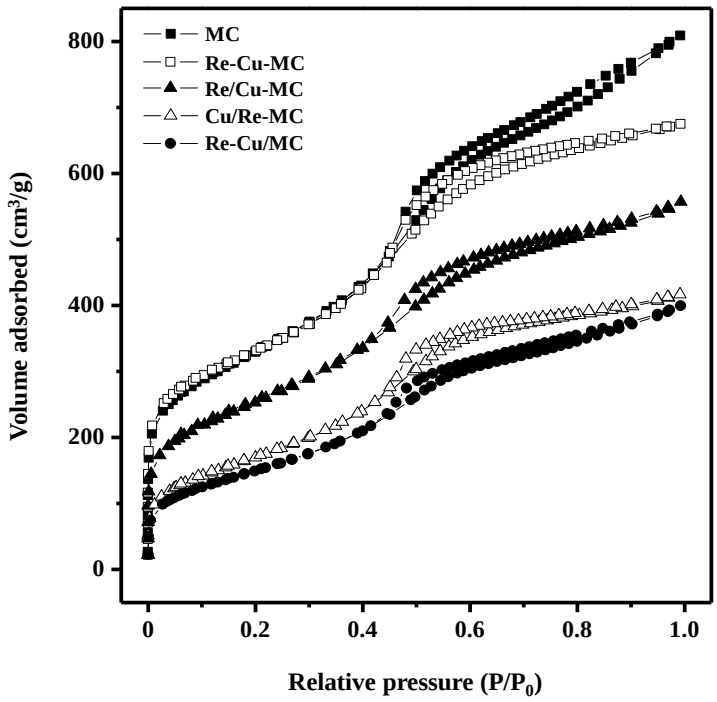

Fig. 3.3.1. Nitrogen adsorption-desorption isotherms of the catalysts (Re-Cu-MC, Re/Cu-MC, Cu/Re-MC, and Re-Cu/MC) and mesoporous carbon support (MC).

Table 3.3.1

ICP-MS results of of the catalysts (Re-Cu-MC, Re/Cu-MC, Cu/Re-MC, and Re-Cu/MC) and mesoporous carbon support (MC)

Sample	Re content (wt%)[a]	Cu content (wt%)[a]
MC	-	-
Re-Cu-MC	4.6	17.9
Re/Cu-MC	4.8	18.0
Cu/Re-MC	4.8	18.6
Re-Cu/MC	4.7	18.4

[a] Determined by ICP-MS measurement

Table 3.3.2

Textural properties of the catalysts (Re-Cu-MC, Re/Cu-MC, Cu/Re-MC, and Re-Cu/MC) and mesoporous carbon support (MC)

Catalyst	Surface area (m^2/g)[a]	Pore volume (cm^3/g)[b]	Pore diameter (nm)[c]
MC	1189	1.18	4.3
Re-Cu-MC	1169	1.04	3.6
Re/Cu-MC	898	0.86	3.8
Cu/Re-MC	624	0.64	4.1
Re-Cu/MC	555	0.62	4.4

[a] Calculated by the BET equation
[b] Total pore volume at $P/P_0 = 0.99$
[c] Average pore diameter

3.3.2. Crystalline structures of reduced catalysts

Crystalline structures of the reduced catalysts (Re-Cu-MC, Re/Cu-MC, Cu/Re-MC, and Re-Cu/MC) were examined by XRD measurements as shown in Fig. 3.3.2. All the catalysts showed a broad peak at $2\theta = 23^{o}$ due to their graphitic carbon structure [50]. It is noteworthy that no characteristic diffraction peaks indicative of metallic rhenium (closed circles) were detected in all the catalysts, because only a small amount (<5 wt%) of rhenium was used for the catalyst preparation. In case of metallic copper, diffraction peaks (dashed lines) were observed without a shift of diffraction angle. It has been reported that rhenium and copper are immiscible in the metallic phase due to their different lattice structure; rhenium has a hexagonal closed-packed structure with nearest-neighbor distance of 2.7609 Å, while copper has a face-centered cubic structure with nearest-neighbor distance of 2.5509 Å [74]. Therefore, it can be said that rhenium and copper species in all the catalysts did not form a phase transitional structure such as substitutional solid-solution. Interestingly, the catalysts based on copper-carbon composites (Re-Cu-MC and Re/Cu-MC) showed weaker intensity for metallic copper than carbon-supported copper catalysts (Cu/Re-MC and Re-Cu/MC). This means that copper particles in these catalysts based on copper-carbon composites (Re-Cu-MC and Re/Cu-MC) were finely incorporated into the carbon framework during the single-step preparation.

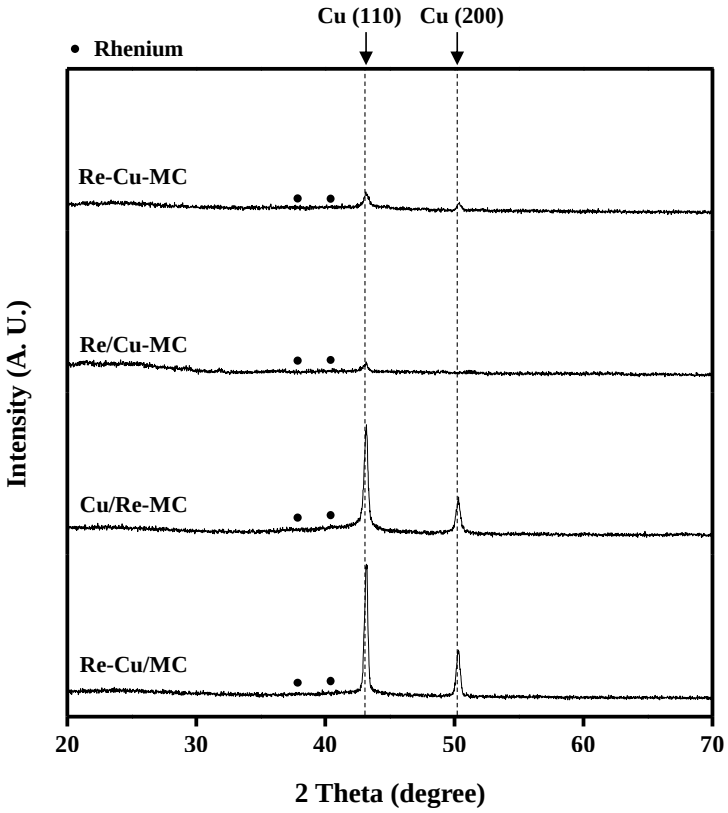

Fig. 3.3.2. XRD patterns of the reduced catalysts (Re-Cu-MC, Re/Cu-MC, Cu/Re-MC, and Re-Cu/MC).

3.3.3. Reduction behaviors of catalysts

In order to investigate metal-support interaction of the catalysts (Re-Cu-MC, Re/Cu-MC, Cu/Re-MC, and Re-Cu/MC), TPR experiments were conducted as shown in Fig. 3.3.3. All the catalysts exhibited two reduction peaks at around 300-340 ˚C and 550-650 ˚C; the former corresponded to reduction of rhenium species, while the latter corresponded to reduction of copper species. It was found that the reduction peak temperatures of rhenium species increased in the order of Re-Cu/MC < Re/Cu-MC < Re-Cu-MC < Cu/Re-MC, and the reduction peak temperature of copper species increased in the order of Re-Cu/MC < Cu/Re-MC < Re-Cu-MC < Re/Cu-MC. It should be noted that the reduction peak temperatures of rhenium species in the catalysts based on rhenium-carbon composites (Re-Cu-MC and Cu/Re-MC) were higher than those of carbon-supported rhenium catalysts (Re/Cu-MC and Re-Cu/MC). Moreover, the reduction peak temperatures of copper species in the catalysts based on copper-carbon composites (Re-Cu-MC and Re/Cu-MC) were also higher than those of carbon-supported copper catalysts (Cu/Re-MC and Re-Cu/MC). This indicates that the metal species in the metal-carbon composite catalysts more strongly interacted with carbon framework than the impregnated metal species.

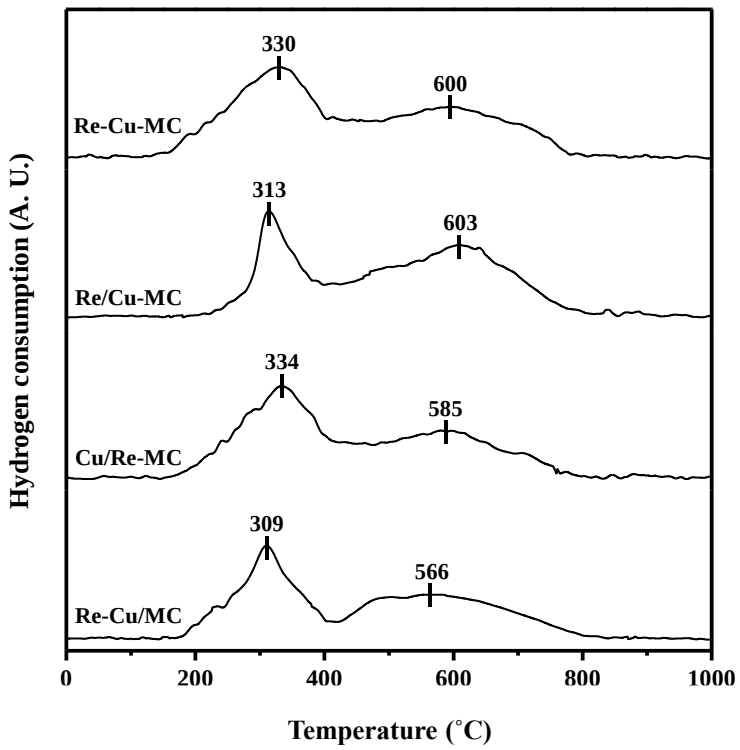

Fig. 3.3.3. TPR profiles of the catalysts (Re-Cu-MC, Re/Cu-MC, Cu/Re-MC, and Re-Cu/MC).

3.3.4. XPS study of reduced catalysts

XPS analyses were further performed to elucidate interaction between reduced metal particles and carbon framework in the catalysts. Fig. 3.3.4 shows the XPS spectra of Re $4f_{7/2}$ and Cu $2p_{3/2}$ levels in the reduced catalysts (Re-Cu-MC, Re/Cu-MC, Cu/Re-MC, and Re-Cu/MC). All the catalysts exhibited Re $4f_{7/2}$ peaks at 40.3-40.7 eV and Cu $2p_{3/2}$ peaks at 932.2-932.7 eV in the XPS spectra, corresponding to zerovalent rhenium and copper species, respectively [54,75]. Rhenium and copper are known to have little metal-metal interaction, because polarization of Re-Cu bonding is suppressed by their identical Pauling electronegativities [76]. Thus, any shift of binding energies by rhenium-copper interaction was not detected in the XPS spectra. It was found that binding energy of Re $4f_{7/2}$ increased in the order of Re-Cu/MC < Re/Cu-MC < Re-Cu-MC < Cu/Re-MC, while binding energy of Cu $2p_{3/2}$ increased in the order of Re-Cu/MC < Cu/Re-MC < Re-Cu-MC < Re/Cu-MC. It is interesting to note that these trends for two metal species were well consistent with trends of TPR peak temperatures (Fig. 3.3.3). This result can be explained by the fact that interaction between metal species and carbon framework was induced by electron transfer effect at the interfacial region [77-79]. In other words, the metal atom on the carbon framework serves as an electron donor to the carbon atom, leading to the shift of binding energy for metal species toward higher value in XPS spectra. From these results, it is believed that the metal-carbon composite catalysts (Re-Cu-MC, Re/Cu-MC, and Cu/Re-MC) were more favorable than the impregnated catalyst (Re-

Cu/MC) for effective electron transfer, resulting in strong metal-support interaction in these three catalysts.

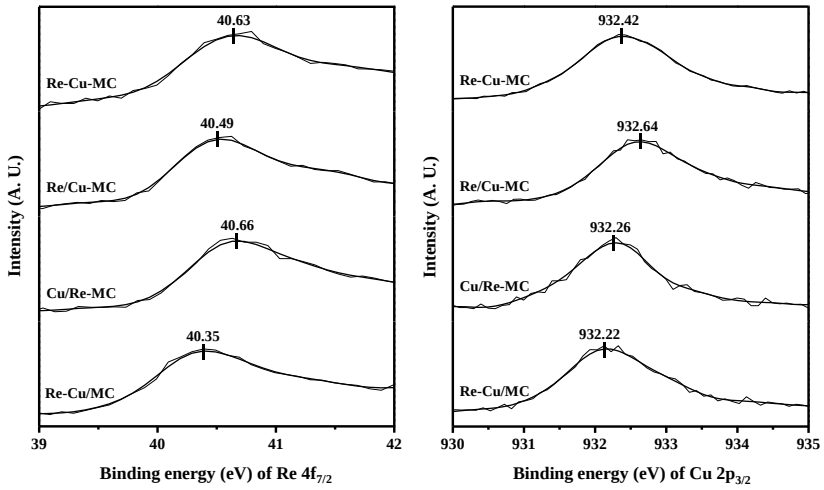

Fig. 3.3.4. XPS spectra of Re $4f_{7/2}$ and Cu $2p_{3/2}$ levels in the reduced catalysts (Re-Cu-MC, Re/Cu-MC, Cu/Re-MC, and Re-Cu/MC).

3.3.5. Metal dispersion of reduced catalysts

In order to measure the amount of rhenium and copper atoms on the catalyst surface, quantitative XPS analyses of the reduced catalysts (Re-Cu-MC, Re/Cu-MC, Cu/Re-MC, and Re-Cu/MC) were conducted. Surface atomic ratios of rhenium and copper with respect to carbon are summarized in Table 3.3.3. Surface Cu/Re atomic ratios of Re/Cu-MC and Cu/Re-MC were quite different from bulk atomic ratios due to relatively non-uniform dispersion of each metal species on the catalyst surface. It was observed that Re/C atomic ratio increased in the order of Re-Cu/MC < Re/Cu-MC < Re-Cu-MC < Cu/Re-MC, while Cu/C atomic ratio increased in the order of Re-Cu/MC < Cu/Re-MC < Re-Cu-MC < Re/Cu-MC. Interestingly, these trends were in good agreement with the trends of TPR peak temperatures (Fig. 3.3.3) and binding energies (Fig. 3.3.4). It is known that the amount of surface metal atom measured by XPS analyses decreases with increasing metal particle size, due to limited XPS penetration depth [80,81]. Therefore, it is inferred that the aggregation of metal particles was effectively suppressed with increasing metal-support interaction of the catalyst. It was found that (Re+Cu)/C atomic ratio increased in the order of Re-Cu/MC < Cu/Re-MC < Re/Cu-MC < Re-Cu-MC. This indicates that Re-Cu-MC composite catalyst retained the largest total amount of metal atoms exposed on the catalyst surface.

CO chemisorption measurements were carried out to measure metal surface area, metal dispersion, and average metal particle size of the reduced catalysts (Re-Cu-MC, Re/Cu-MC, Cu/Re-MC, and Re-Cu/MC). As

summarized in Table 3.3.4, metal surface area and metal dispersion increased in the order of Re-Cu/MC < Cu/Re-MC < Re/Cu-MC < Re-Cu-MC, which was consistent with the trend of (Re+Cu)/C atomic ratio. This means that metal species in the catalysts based on metal-carbon composite were finely dispersed on both external and internal surfaces of carbon framework. It was also revealed that average metal particle size decreased in the order of Re-Cu/MC > Cu/Re-MC > Re/Cu-MC > Re-Cu-MC. This result was further confirmed by HR-TEM analyses.

Fig. 3.3.5 shows the HR-TEM images of the reduced catalysts (Re-Cu-MC, Re/Cu-MC, Cu/Re-MC, and Re-Cu/MC) and carbon support (MC). All the samples retained a highly ordered mesoporous carbon structure. It should be noted that metallic rhenium and copper species were more aggregated with increasing impregnated metal content of the catalysts, which was well matched with the results of quantitative XPS analyses (Table 3.3.3) and CO chemisorption (Table 3.3.4). It was revealed that Re-Cu-MC composite catalyst showed smaller metal particle size and more uniform metal dispersion than the other catalysts.

In order to confirm the dispersion of metallic rhenium and copper in the Re-Cu-MC catalyst, STEM-EDX analyses were conducted. Fig. 3.3.6 shows the STEM images and EDX mapping images of Re-Cu-MC catalyst. Metallic rhenium and copper were indistinguishable in the STEM images (Fig. 3.3.6(a) and Fig. 3.3.6(c)) in spite of the difference in atomic number, because of similar shape, contrast, and size distribution under the blurred background by carbon framework. On the other hand, each metal species was clearly identified in the EDX mapping images (Fig. 3.3.6(b) and Fig. 3.3.6(d)). It was

revealed that rhenium and copper particles with a size of 4-8 nm were uniformly distributed in the Re-Cu-MC catalyst, which was well matched with average metal particle size determined by CO-chemisorption. Furthermore, it was found that rhenium and copper were distributed as separate particles. On the basis of XRD, XPS, and EDX mapping results, it can be inferred that rhenium and copper species served as independent active sites. Therefore, it is expected that Re-Cu-MC catalyst, which retained smaller rhenium and copper particles than the other catalysts, would be more active in the hydrogenation of succinic acid to GBL and BDO.

Table 3.3.3

Surface atomic ratios of the reduced catalysts (Re-Cu-MC, Re/Cu-MC, Cu/Re-MC, and Re-Cu/MC)

Catalyst	Cu/Re[a]	Re/C	Cu/C	(Re+Cu)/C
Re-Cu-MC	10.6 (11.4)	0.0030	0.0319	0.0349
Re/Cu-MC	12.9 (11.0)	0.0025	0.0321	0.0346
Cu/Re-MC	9.1 (11.4)	0.0032	0.0291	0.0323
Re-Cu/MC	10.8 (11.5)	0.0022	0.0238	0.0260

[a] Values in parentheses indicate the bulk atomic ratios determined by ICP-MS measurement

Table 3.3.4

CO chemisorption results for the reduced catalysts (Re-Cu-MC, Re/Cu-MC, Cu/Re-MC, and Re-Cu/MC)

Catalyst	Metal surface area (m^2/g-metal)[a]	Metal dispersion (%)[a]	Average metal particle size (nm)[a]
Re-Cu-MC	97.9	17.9	6.1
Re/Cu-MC	45.6	8.4	13.2
Cu/Re-MC	24.8	4.5	24.2
Re-Cu/MC	19.6	3.6	30.7

[a] Calculated from CO chemisorption measurement by assuming a stoichiometry factor of $CO/metal_{atom} = 1$

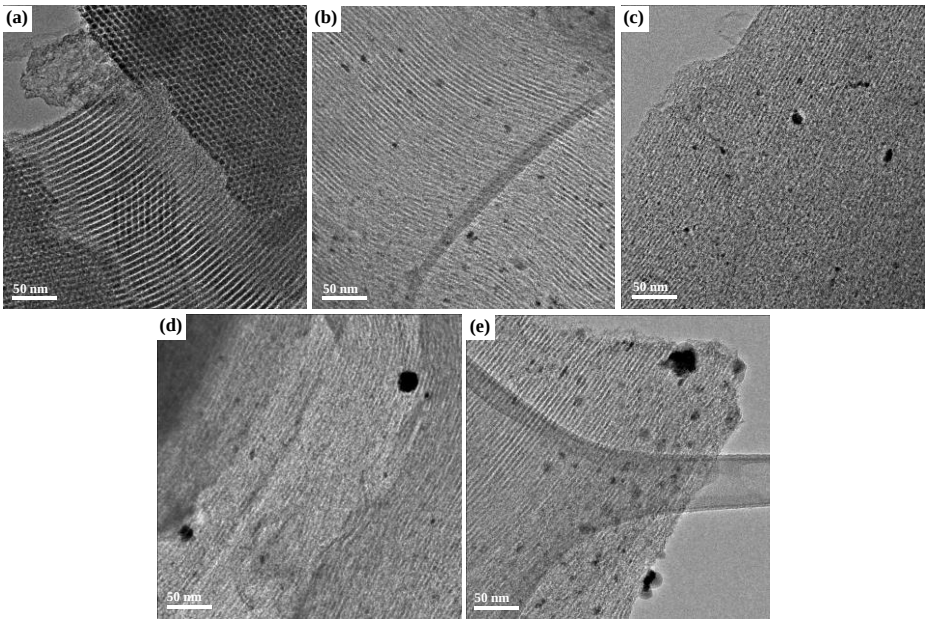

Fig. 3.3.5. HR-TEM images of (a) MC, (b) Re-Cu-MC, (c) Re/Cu-MC, (d) Cu/Re-MC, and (e) Re-Cu/MC catalysts. The catalysts were reduced at 600 ˚C.

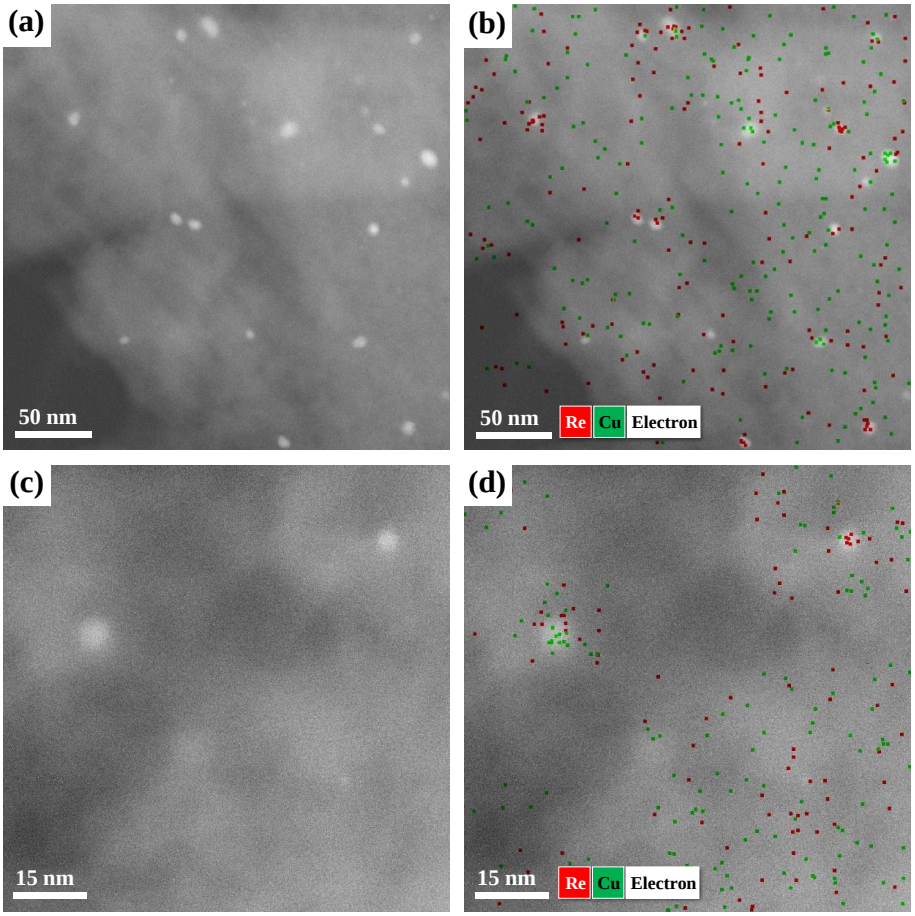

Fig. 3.3.6. STEM images ((a) and (c)) of reduced Re-Cu-MC catalyst and EDX images ((b) and (d)) obtained by mapping on rhenium and copper.

3.3.6. Catalytic performance in the hydrogenation of succinic acid

Performance of the catalysts (Re-Cu-MC, Re/Cu-MC, Cu/Re-MC, and Re-Cu/MC) in the liquid-phase hydrogenation of succinic acid is summarized in Table 3.3.5. In the reaction, GBL and BDO were produced as major final products. Small amount of THF was also formed. In addition, DMS was produced as a major intermediate through the reaction of succinic acid with methanol. All the catalysts showed complete conversion of succinic acid. Yield for GBL and BDO increased in the order of Re-Cu/MC < Cu/Re-MC < Re/Cu-MC < Re-Cu-MC, and yield for DMS decreased in the order of Re-Cu/MC > Cu/Re-MC > Re/Cu-MC > Re-Cu-MC. Among the catalysts, Re-Cu-MC catalyst showed the highest total yield for GBL and BDO (41.9%). The catalytic performance of Re-Cu-MC catalyst was comparable to that of noble metal-based catalysts such as Pd-Re/C and Pt-Re/C, demonstrating that Re-Cu-MC catalyst served as a promising bifunctional catalyst. It is believed that average metal particle size of rhenium and copper of the catalyst was closely related to the formation of GBL and BDO in the hydrogenation of succinic acid.

Fig. 3.3.7 shows the correlation between average metal particle size and catalytic activity of the catalysts (Re-Cu-MC, Re/Cu-MC, Cu/Re-MC, and Re-Cu/MC) in the liquid-phase hydrogenation of succinic acid to GBL and BDO. It should be noted that total yield for GBL and BDO increased with decreasing average metal particle size (with increasing metal dispersion) of the catalysts. Interestingly, although average metal particle size of the

catalysts was quite different, TOFs were nearly identical as listed in Table 3.3.5. This result indicates that hydrogenation of succinic acid over the catalysts (Re-Cu-MC, Re/Cu-MC, Cu/Re-MC, and Re-Cu/MC) was structure-insensitive. Among the catalysts tested, Re-Cu-MC composite catalyst with the smallest average metal particle size (with the highest metal dispersion) exhibited the best catalytic performance in the reaction. Thus, rhenium and copper particle size of the catalysts played an important role in determining catalytic performance in the hydrogenation of succinic acid to GBL and BDO.

Table 3.3.5

Performance of the catalysts (Re-Cu-MC, Re/Cu-MC, Cu/Re-MC, and Re-Cu/MC) in the liquid-phase hydrogenation of succinic acid to GBL and BDO at 200 ˚C and 80 bar for 20 h

Catalyst	Conversion of succinic acid (%)	Yield (%)				Total yield for GBL and BDO (%)	TOF (h^{-1})[a]
		GBL	BDO	THF	DMS		
Re-Cu-MC	100	22.5	19.4	3.2	53.6	41.9	14.0
Re/ Cu-MC	100	18.5	16.2	2.8	55.4	34.7	13.6
Cu/ Re-MC	100	19.7	9.3	3.0	63.1	29.0	13.8
Re-Cu/ MC	100	13.9	6.5	1.0	66.2	20.4	13.8

[a] Calculated as moles of succinic acid converted per moles of surface metal atom per hour

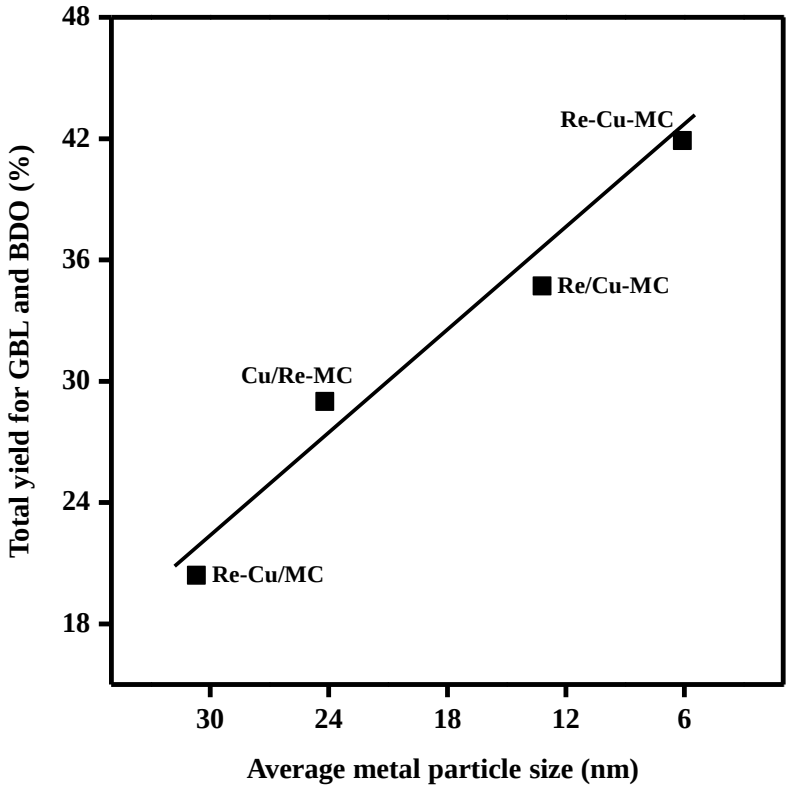

Fig. 3.3.7. A correlation between average metal particle size of the catalysts and catalytic activity in the hydrogenation of succinic acid to GBL and BDO.

3.3.7. Stability and reusability of catalysts

In the liquid-phase hydrogenation of succinic acid, stability of active metal species under the acidic condition is very important. Thus, recycle tests for hydrogenation of succinic acid were conducted three times to investigate stability and reusability of the catalyst. Fig. 3.3.8 shows the results for liquid-phase hydrogenation of succinic acid to GBL and BDO over Re-Cu-MC and Re-Cu/MC catalysts with respect to recycle run. Importantly, fresh and spent Re-Cu-MC catalysts retained similar catalytic performance. In case of Re-Cu/MC catalyst, however, total yield for GBL and BDO significantly decreased with recycle run. This indicates that Re-Cu-MC catalyst was stable and reusable under the acidic condition. In conclusion, Re-Cu-MC catalyst with the highest catalytic activity and stability served as the most efficient catalyst in the hydrogenation of succinic acid to GBL and BDO.

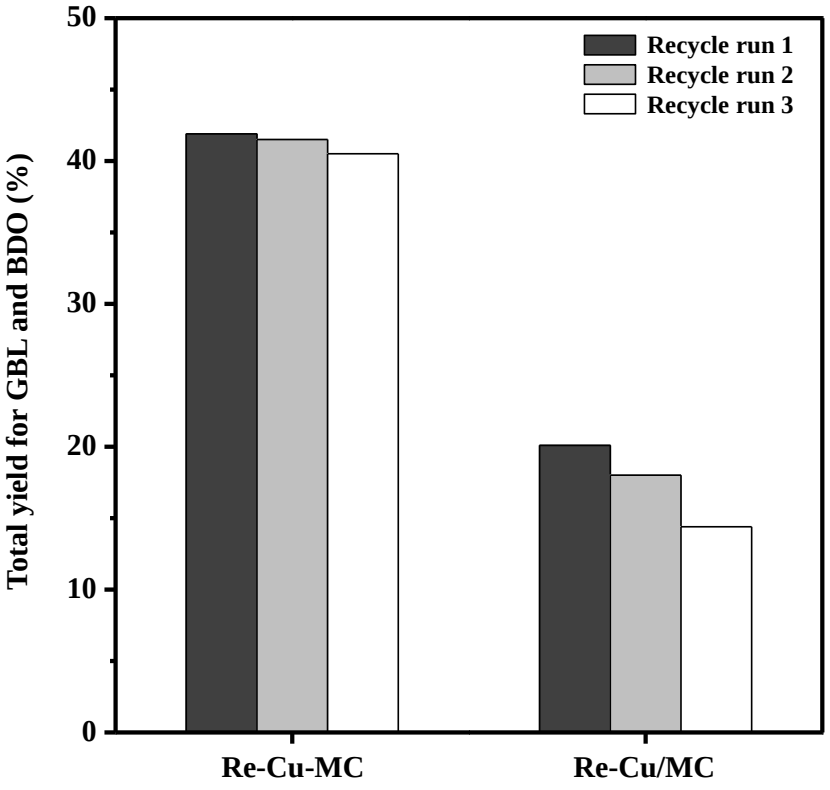

Fig. 3.3.8. Results for liquid-phase hydrogenation of succinic acid over Re-Cu-MC and Re-Cu/MC catalysts with respect to recycle run at 200 ˚C and 80 bar for 20 h.

Chapter 4. Conclusions

In this work, various Re-based bimetallic catalysts were prepared and physicochemically modified, and they were applied to the liquid-phase hydrogenation of succinic acid to BDO.

A series of Re-Ru bimetallic catalysts supported on mesoporous carbon ((0.6-x)Re-xRu/MC, x = 0, 0.15, 0.3, 0.45, and 0.6 mol%) were prepared by a single-step surfactant-templating method and a subsequent incipient wetness impregnation method, and they were used for liquid-phase hydrogenation of succinic acid to BDO. The effect of metal content on the catalytic activities and physicochemical properties of (0.6-x)Re-xRu/MC was investigated. All the catalysts showed a well-developed mesoporous structure. It was found that a Re-Ru solid-solution phase was formed in the catalysts during the reduction process, facilitating the synergistic interaction between rhenium and ruthenium. It was also revealed that reducibility, metal dispersion, and oxidation state of (0.6-x)Re-xRu/MC catalysts were strongly influenced by Re:Ru molar ratio. In particular, the ratios of Re^0/Re_{total} and Ru^0/Ru_{total} were closely related to the hydrogen adsorption behavior of the reduced (0.6-x)Re-xRu/MC catalysts. The amount of weak hydrogen-binding sites of the catalysts increased with increasing Re^0/Re_{total} and Ru^0/Ru_{total} ratios. Catalytic performance in the hydrogenation of succinic acid to BDO over (0.6-x)Re-xRu/MC showed a volcano-shaped trend with respect to Re:Ru molar ratio. TOF_{BDO} increased with increasing the amount of weak hydrogen-binding sites of the reduced (0.6-x)Re-xRu/MC catalysts. Among the catalysts tested,

0.3Re-0.3Ru/MC with the largest amount of weak hydrogen-binding sites showed the highest TOF_{BDO}. Furthermore, 0.3Re-0.3Ru/MC served as a stable and reusable catalyst in the selective formation of BDO by hydrogenation of succinic acid.

A series of Re-Ru bimetallic catalysts supported on mesoporous boron-modified carbon (Re-Ru/xBMC, x = B/C molar ratio) were prepared for use in the liquid-phase hydrogenation of succinic acid to BDO. The effect of boron addition on the catalytic activities and physicochemical properties of Re-Ru/xBMC was investigated. All the catalysts retained well-developed mesopores and slit-shaped carbon structure. Metal surface area and metal dispersion decreased with decreasing B/C molar ratio due to the decrement of surface area of Re-Ru/xBMC catalysts. It was found that an excessive addition of boron into carbon structure decreased reducibility of rhenium and ruthenium species in the Re-Ru/xBMC catalysts. Raman and XPS analyses showed that the amount of substituted boron species was changed with a variation of B/C molar ratio. It was revealed that the trend of $B_{substituted}$/C ratio was in good agreement with the trend of weak hydrogen-binding sites of Re-Ru/xBMC catalysts. The amount of weak hydrogen-binding sites increased with increasing $B_{substituted}$/C ratio of the catalysts. Yield for BDO and TOF_{BDO} in the hydrogenation of succinic acid to BDO over Re-Ru/xBMC showed volcano-shaped curves with respect to B/C molar ratio. It was also found that TOF_{BDO} increased with increasing the amount of weak hydrogen-binding sites of Re-Ru/xBMC catalysts. This indicates that catalytic performance of Re-Ru/xBMC was closely related to the amount of weak hydrogen-binding sites. Among the catalysts, Re-Ru/0.04BMC with the largest amount of weak

hydrogen-binding sites showed the highest TOF_{BDO}.

A mesoporous rhenium-copper-carbon composite catalyst (Re-Cu-MC) was prepared by a facile single-step surfactant-templating method. For comparison, a series of mesoporous carbon-supported catalysts (Re/Cu-MC, Cu/Re-MC, and Re-Cu/MC) were also prepared. The prepared catalysts were applied to the liquid-phase hydrogenation of succinic acid to GBL and BDO. The effect of preparation method on the physicochemical properties and catalytic activities was investigated. Although all the catalysts retained a well-developed mesoporous structure, Re-Cu-MC composite catalyst exhibited excellent textural properties compared to the other catalysts. It was found that metallic copper and rhenium effectively interacted with carbon framework by electron transfer effect. Surface atomic ratios of metal species (Re/C and Cu/C) on the catalyst surface increased with increasing metal-support interaction. Yield for GBL and BDO increased with decreasing average metal particle size (with increasing metal dispersion) of the catalysts. Among the catalysts tested, Re-Cu-MC composite catalyst with the smallest average metal particle size showed the best catalytic performance with excellent reusability. Thus, metal particle size of the catalysts played a crucial role in determining the catalytic activity and stability in the reaction. It is concluded that Re-Cu-MC composite catalyst prepared by a facile single-step surfactant-templating method served as an efficient catalyst in the hydrogenation of succinic acid to GBL and BDO.

Bibliography

[1] I. Bechthold, K. Bretz, S. Kabasci, R. Kopitzky, A. Springer, "Succinic acid: a new platform chemical for biobased polymers from renewable resources", *Chem. Eng. Technol.* **31** (2008) 647-654.

[2] R.H. Roth, J.M.R. Delgado, N.J. Giarman, "γ-Butyrolactone and γ-hydroxybutyric acid - II. The pharmacologically active form", *Int. J. Neuropharmacol*. **5** (1966) 421-428.

[3] C. Delhomme, D. Weuster-Botz, F.E. Kuhn, "Succinic acid from renewable resources as a C_4 building-block chemical - a review of the catalytic possibilities in aqueous media", *Green Chem.* **11** (2009) 13-26.

[4] P. Gallezot, "Conversion of biomass to selected chemical products", *Chem. Soc. Rev*. **41** (2012) 1538-1558.

[5] J. Kanetaka, T. Asano, S. Masamune, "New process for production of tetrahydrofuran", *Ind. Eng. Chem*. **62** (1970) 24-32.

[6] T. Haas, B. Jaeger, R. Weber, S.F. Mitchell, C.F. King, "New diol processes: 1,3-propanediol and 1,4-butanediol", *Appl. Catal. A* **280** (2005) 83-88.

[7] M. Aghaziarati, M. Kazemeini, M. Soltanieh, S. Sahebdelfar, "Evaluation of zeolites in production of tetrahydrofuran from 1,4-butanediol: Performance tests and kinetic investigations", *Ind. Eng. Chem. Res.* **46** (2007) 726-733.

[8] J.G. Zeikus, M.K. Jain, P. Elankovan, "Biotechnology of succinic acid production and markets for derived industrial products", *Appl. Microbiol. Biotechnol.* **51** (1999) 545-552.

[9] A. Cukalovic, C.V. Stevens, "Feasibility of production methods for succinic acid derivatives: a marriage of renewable resources and chemical

technology", *Biofuels Bioprod. Bioref.* **2** (2008) 505-529.

[10] M. Seitz, O. Reiser, "Synthetic approaches towards structurally diverse γ-butyrolactone natural-product-like compounds", *Curr. Opin. Chem. Biol*. **9** (2005) 285-292.

[11] M.L. Morgan, "The rapidly changing world of 1,4-butanediol", *Chem. Ind.* **3** (1997) 166-168.

[12] S.M. Jung, E. Godard, S.Y. Jung, K.-C. Park, J.U. Choi, "Liquid-phase hydrogenation of maleic anhydride over Pd/SiO_2: effect of tin on catalytic activity and deactivation", *J. Mol. Catal. A* **198** (2003) 297-302.

[13] S.-H. Chung, Y.-M. Park, M.-S. Kim, K.-Y. Lee, "The effect of textural properties on the hydrogenation of succinic acid using palladium incorporated mesoporous supports", *Catal. Today* **185** (2012) 205-210.

[14] B. Tapin, F. Epron, C. Especel, B.K. Ly, C. Pinel, M. Besson, "Study of monometallic Pd/TiO_2 catalysts for the hydrogenation of succinic acid in aqueous phase", *ACS Catal*. **3** (2013) 2327-2335.

[15] U.G. Hong, J. Lee, S. Hwang, I.K. Song, "Hydrogenation of succinic acid to γ-butyrolactone (GBL) over palladium-alumina composite catalyst prepared by a single-step sol–gel method", Catal. Lett. 141 (2011) 332-338.

[16] R. Luque, J.H. Clark, K. Yoshida, P.L. Gai, "Efficient aqueous hydrogenation of biomass platform molecules using supported metal nanoparticles on Starbons®", *Chem. Commun*. **35** (2009) 5305-5307.

[17] L. Rosi, M. Frediani, P. Frediani, "Isotopomeric diols by "one-pot" Ru-catalyzed homogeneous hydrogenation of dicarboxylic acids", *J. Organomet. Chem*. **695** (2010) 1314-1322.

[18] U.G. Hong, J.K. Kim, J. Lee, J.K. Lee, J.H. Song, J. Yi, I.K. Song, "Hydrogenation of succinic acid to tetrahydrofuran (THF) over ruthenium-carbon composite (Ru-C) catalyst", *Appl. Catal. A* **469** (2014) 466-471.

[19] U.G. Hong, H.W. Park, J. Lee, S. Hwang, J. Yi, I.K. Song, "Hydrogenation of succinic acid to tetrahydrofuran (THF) over rhenium catalyst supported on H_2SO_4-treated mesoporous carbon", *Appl. Catal. A* **415** (2012) 141-148.

[20] S. Varadarajan, D.J. Miller, "Catalytic upgrading of fermentation-derived organic acids", *Biotechnol. Prog.* **15** (1999) 845-854.

[21] R.M. Deshpande, V.V. Buwa, C.V. Rode, R.V. Chaudhari, P.L. Mills, "Tailoring of activity and selectivity using bimetallic catalyst in hydrogenation of succinic acid", *Catal. Commun*. **3** (2002) 269-274.

[22] L. Corbel-Dimailly, B.-K. Ly, D.-P. Minh, B. Tapin, C. Especel, F. Epron, A. Cabiac, E. Guillon, M. Besson, C. Pinel, "Heterogeneous Catalytic Hydrogenation of Biobased Levulinic and Succinic Acids in Aqueous Solutions", *ChemSusChem* **6** (2013) 2388-2395.

[23] D.P. Minh, M. Besson, C. Pinel, P. Fuertes, C. Petitjean, "Aqueous-phase hydrogenation of biomass-based succinic acid to 1,4-butanediol over supported bimetallic catalysts", *Top. Catal*. **53** (2010) 1270-1273.

[24] B.K. Ly, D.P. Minh, C. Pinel, M. Besson, B. Tapin, F. Epron, C. Especel, "Effect of addition mode of Re in bimetallic Pd-Re/TiO_2 catalysts upon the selective aqueous-phase hydrogenation of succinic acid to 1,4-butanediol", *Top. Catal*. **55** (2012) 466-473.

[25] R.V. Chaudhari, C.V. Rode, R.M. Deshpande, R. Jaganathan, T.M. Leib, P.L. Mills, "Kinetics of hydrogenation of maleic acid in a batch slurry reactor using a bimetallic Ru-Re/C catalyst", *Chem. Eng. Sci.* **58** (2003) 627-632.

[26] G. Beamson, A.J. Papworth, C. Phillipps, A.M. Smith, R. Whyman, "Selective hydrogenation of amides using bimetallic Ru/Re and Rh/Re catalysts" *J. Catal*. **278** (2011) 228-238.

[27] T.B. Massalski, "Binary Alloy Phase Diagrams", ASM International, Materials Park, 1990.

[28] H.C. Yao, M. Shelef, “Surface interactions in the system Re γ-Al_2O_3”, *J. Catal*. **44** (1976) 392-403.

[29] J. Okal, L. Kepinski, L. Krajczyk, M. Drozd, “Oxidation and redispersion of a Re/γ-Al_2O_3 catalyst”, *J. Catal*. **188** (1999) 140-153.

[30] A. Pintar, M. Besson, P. Gallezot, “Catalytic wet air oxidation of kraft bleach plant effluents in a trickle-bed reactor over a Ru/TiO_2 catalyst”, *Appl. Catal. B* **31** (2001) 275-290.

[31] R.M. Deshpande, V.V. Buwa, C.V. Rode, R.V. Chaudhari, P.L. Mills, “Tailoring of activity and selectivity using bimetallic catalyst in hydrogenation of succinic acid”, *Catal. Commun.* **3** (2002) 269-274.

[32] D.N. Hendrickson, J.M. Hollander, W.L. Jolly, “Core-electron binding energies for compounds of boron, carbon, and chromium”, *Inorg. Chem.* **9** (1970) 612-615.

[33] C.H. Choi, S.H. Park, S.I. Woo, “Binary and ternary doping of nitrogen, boron, and phosphorus into carbon for enhancing electrochemical oxygen reduction activity”, *ACS Nano* **6** (2012) 7084-7091.

[34] C.A. Davis, Y. Yin, D.R. Mckenzie, L.H. Hall, E. Kravtchinskaia, V. Keast, G.A.J. Amaratunga, V.S. Veerasamy, “The structure of boron-, phosphorus- and nitrogen-doped tetrahedral amorphous carbon deposited by cathodic arc”, *J. Non Cryst Solids* **170** (1994) 46-50.

[35] Y. Cao, H. Yu, J. Tan, F. Peng, H. Wang, J. Li, W. Zheng, N.-B. Wong, “Nitrogen-, phosphorous- and boron-doped carbon nanotubes as catalysts for the aerobic oxidation of cyclohexane”, *Carbon* **57** (2013) 433-442.

[36] H.N. Yang, D.C. Lee, K.W. Park, W.J. Kim, “Platinum-boron doped graphene intercalated by carbon black for cathode catalyst in proton exchange membrane fuel cell”, *Energy* **89** (2015) 500-510.

[37] J.S. Yoo, Z-.J. Zhao, J.K. Norskov, F. Studt, “Effect of Boron Modifications of Palladium Catalysts for the Production of Hydrogen from Formic Acid”, *ACS Catal*. **5** (2015) 6579-6586.

[38] B. Wei, R. Spolenak, P. Kohler-Redlich, M. Ruhle, E. Arzt, “Electrical transport in pure and boron-doped carbon nanotubes”, *Appl. Phys. Lett.* **74** (1999) 3149-3151.

[39] U.G. Hong, H.W. Park, J. Lee, S. Hwang, J. Kwak, J. Yi, I.K. Song, “Hydrogenation of succinic acid to 1,4-butanediol over rhenium catalyst supported on copper-containing mesoporous carbon”, *J. Nanosci. Nanotechnol*. **13** (2013) 7448-7453.

[40] S.J. Tauster, S.C. Fung, R.L. Garten, “Strong metal-support interactions. Group 8 noble metals supported on TiO_2”, *J. Am. Chem. Soc*. **100** (1978) 170-175.

[41] G.K. Wertheim, S.B. Dicenzo, D.N.E. Buchanan, P.A. Bennett, “Core electron binding energy shifts in metal clusters: Tin on amorphous carbon”, *Solid State Commun*. **53** (1985) 377-381.

[42] P. Arnoldy, E.M. Van-Oersa, O.S.L. Bruinsma, V.H.J. De-Beer, J.A. Moulijn, “Temperature-Programmed Reduction of Al_2O_3-, SiO_2-, and carbon-supported Re_2O_7 catalysts”, *J. Catal*. **93** (1985) 231-245.

[43] P. Betancourt, A. Rives, R. Hubaut, C.E. Scott, J. Goldwaser, “A study of the ruthenium-alumina system”, *Appl. Catal. A* **170** (1998) 307-314.

[44] M. Bonarowska, A. Malinowski, Z. Karpinski, “Hydrogenolysis of C-C and C-Cl bonds by Pd-Re/Al_2O_3 catalysts”, *Appl. Catal. A* **188** (1999) 145-154.

[45] B.H. Isaacs, E.E. Petersen, “The effect of drying temperature on the temperature-programmed reduction profile of a platinum/rhenium/alumina catalyst”, *J. Catal*. **77** (1982) 43-52.

[46] L. Ma, D. He, “Hydrogenolysis of glycerol to propanediols over highly active ru-re bimetallic catalysts”, *Top. Catal*. **52** (2009) 834-844.

[47] Y. Amada, Y. Shimi, S. Koso, T. kubota, Y. Nakagawa, K. Tomishige, “Reaction mechanism of the glycerol hydrogenolysis to 1,3-propanediol over Ir-ReOx/SiO_2 catalyst”, *Appl. Catal. B* **105** (2011) 117-127.

[48] K. Aika, K.Shimazaki, Y. Hattori, A. Ohya, S. Ohshima, K. Shirota, A. Ozaki, “Support and promoter effect of ruthenium catalyst. I. Characterization of alkali-promoted ruthenium/alumina catalysts for ammonia synthesis”, *J. Catal*. **92** (1985) 296-304.

[49] P. Badenes, L. Daza, I. Rodriguez-Ramos, A. Guerrero-Ruiz, “Mechanism of hydrogen spillover over carbon supported metal catalysts”, *Stud. Surf. Sci. Catal*. **112** (1997) 241-250.

[50] Z.Q. Li, C.J. Lu, Z.P. Xia, Y. Zhou, Z. Luo, “X-ray diffraction patterns of graphite and turbostratic carbon”, *Carbon* **45** (2007) 1686-1695.

[51] Y. Zhu, W. Lu, H. Li, H. Wan, “Selective modification of surface and bulk V^{5+}/V^{4+} ratios and its effects on the catalytic performance of Mo{single bond}V{single bond}Te{single bond}O catalysts”, *J. Catal.* **246** (2007) 382-389.

[52] Y. Yazawa, H. Yoshida, N. Takagi, S. Komai, A. Satsuma, T. Hattori, “Acid strength of support materials as a factor controlling oxidation state of palladium catalyst for propane combustion”, *J. Catal*. **187** (1999) 15-23.

[53] Y. Yuan, T. Shido, Y. Iwasawa, “The new catalytic property of supported rhenium oxides for selective oxidation of methanol to methylal”, *Chem. Commun*. **15** (2000) 1421-1422.

[54] W.T. Tysoe, F. Zaera, G.A. Somorjai, “An XPS study of the oxidation and reduction of the rhenium-platinum system under atmospheric conditions”, *Surf. Sci*. **200** (1988) 1-14.

[55] P.C.H. Mitchell, C.E. Scott, J.-P. Bonnelle, J.G. Grimblot, “Ru/alumina and RuMo/alumina catalysts: An XPS study”, *J. Catal*. **107** (1987) 482-489.

[56] S. Yagi, D. Kuni, “Fluidized-solid reactors with continuous solid feed (II)”, *Chem. Eng. Sci.* **16** (1961) 372-379.

[57] J.Y. Park, O. Levenspiel, “The crackling core model for the reaction of

solid particles", *Chem. Eng. Sci.* **30** (1975) 1207-1214.

[58] S.C. Su, J.N. Carstens, A.T. Bell, "A study of the dynamics of Pd oxidation and PdO reduction by H_2 and CH_4", *J. Catal*. **176** (1998) 125-135.

[59] P. Claus, "Heterogeneously catalysed hydrogenation using gold catalysts", *Appl. Catal. A* **291** (2005) 222-229.

[60] J.-P. Tessonnier, L. Pesant, G. Ehret, M.J. Ledoux, C. Pham-Huu, "Pd nanoparticles introduced inside multi-walled carbon nanotubes for selective hydrogenation of cinnamaldehyde into hydrocinnamaldehyde", *Appl. Catal. A* **288** (2005) 203-210.

[61] K. Baranowska, J. Okal, N. Miniajluk, "Effect of rhenium on ruthenium dispersion in the Ru-Re/λ-Al_2O_3catalysts", *Catal. Lett*. **144** (2014) 447-459.

[62] X. Dong, H.-B. Zhang, G.-D. Lin, Y.-Z. Yuan, K.R. Ysai, "Highly active CNT-promoted Cu-ZnO-Al_2O_3 catalyst for methanol synthesis from H_2/CO/CO_2", *Catal. Lett*. **85** (2003) 237-246.

[63] C. Zupanc, A. Hornung, O. Hinrichsen, M. Muhler, "The interaction of hydrogen with Ru/MgO catalysts", *J. Catal*. **209** (2002) 501-514.

[64] D.P. Vanderwiel, M. Pruski, T.S. King, "A kinetic study on the adsorption and reaction of hydrogen over silica-supported ruthenium and silver-ruthenium catalysts during the hydrogenation of carbon monoxide", *J. Catal.* **188** (1999) 186-202.

[65] Z.R. Ismagilov, A.E. Shalagina, O.Y. Podyacheva, A.V. Ischenko, L.S. Kibis, A.I. Boronin, Y.A. Chesalov, D.I. Kochubey, A.I. Romanenko, O.B. Anikeeva, T.I. Buryakov, E.N. Tkachev, "Structure and electrical conductivity of nitrogen-doped carbon nanofibers", *Carbon* **47** (2009) 1922-1929.

[66] A.A. Onoprienko, I.B. Yanchuk, "Structural studies of materials: Effects of deposition conditions on carbon-film resistivity and microstructure",

Powder Metall. Met. Ceram. **44** (2005) 499-504.

[67] H.S. Myung, Y.S. Park, B. Hong, J.G. Han, Y.H. Kim, J.Y. Lee, L.R. Shaginyan, "Effect of the target power density on the synthesis and physical properties of sputtered nc-C films", *Thin Solid Films* **494** (2006) 123-127.

[68] M. Koh, T. Nakajima, "Synthesis of well crystallized boron-carbon filament by chemical vapor deposition using a nickel catalyst", *Carbon* **36** (1998) 913-920.

[69] J. Ozaki, N. Kimura, T. Anahara, A. Oya, "Preparation and oxygen reduction activity of BN-doped carbons", *Carbon* **45** (2007) 1847-1853.

[70] K.P. Gong, F. Du, Z.H. Xia, M. Durstock, L.M. Dai, "Nitrogen-doped carbon nanotube arrays with high electrocatalytic activity for oxygen reduction", *Science* **323** (2009) 760-764.

[71] M. Kruk, M. Jaroniec, Y. Bereznitski, "Adsorption study of porous structure development in carbon blacks", *J. Colloid Interface Sci.* **182** (1996) 282-288.

[72] I. Matos, S. Fernandes, L. Guerreiro, S. Barata, A.M. Ramos, J. Vital, I.M. Fonseca, "The effect of surfactants on the porosity of carbon xerogels", *Microporous Mesoporous Mater*. **92** (2006) 38-46.

[73] A. Galarneau, H. Cambon, F.D. Renzo, R. Ryoo, M. Choi, F. Fajula, "Microporosity and connections between pores in SBA-15 mesostructured silicas as a function of the temperature of synthesis", *New J. Chem.* **27** (2003) 73-79.

[74] R. Wagner, D. Schlatterbeck, K. Christmann, "Interaction of copper with a rhenium(0001) surface: structure, energetics, and growth modes", *Surf. Sci.* **440** (1999) 231-251.

[75] G. Ertl, R. Hierl, H. Knozinger, N. Thiele, H.P. Urbach, "XPS study of copper aluminate catalysts", *Appl. Surf. Sci*. **5** (1980) 49-64.

[76] W.R. Tyson, W.A. Miller, "Surface free energies of solid metals:

Estimation from liquid surface tension measurements", *Surf. Sci.* **62** (1977) 267-276.

[77] L.J. Hillenbrand, J.W. Lacksonen, "The Platinum-on-Carbon Catalyst System for Hydrogen Anodes", *J. Electrochem. Soc*. **112** (1965) 249-252.

[78] F. Coloma, A. Sepulveda, J. Fierro, F. Rodriguez-Reinoso, "Crotonaldehyde hydrogenation over bimetallic Pt-Sn catalysts supported on pregraphitized carbon black. Effect of the preparation method", *Appl. Catal. A* **148** (1996) 63-80.

[79] A.K. Shukla, M.K. Ravikumar, A. Roy, S.R. Barman, D.D. Sarma, A.S. Arico, V. Antonucci, L. Pino, N. Giordano, "Electro-Oxidation of Methanol in Sulfuric Acid Electrolyte on Platinized-Carbon Electrodes with Several Functional-Group Characteristics", *J. Electrochem. Soc.* **141** (1994) 1517-1522.

[80] J.P. Espinos, J. Morales, A. Barranco, A. Caballero, J.P. Holgado, A.R. Gonzalez-Elipe, "Interface effects for Cu, CuO, and Cu_2O deposited on SiO_2 and ZrO_2. XPS determination of the valence state of copper in Cu/SiO_2 and Cu/ZrO_2 catalysts", *J. Phys. Chem. B* **106** (2002) 6921-6929.

[81] M. Gilbert, I. Sutherland, A. Guest, "Characterization of coated particulate fillers", *J. Mater. Sci.* **35** (2000) 391-397.

초 록

1,4-부탄디올은 다양한 산업 분야에서 활용되고 있는 유용한 화학물질로서 유기용매에서부터 접착제, 섬유, 고분자의 제조 등 광범위한 분야에 사용된다. 특히 1,4-부탄디올은 폴리뷰티렌 숙시네이트 혹은 폴리뷰티렌테레프탈레이트와 같은 열가소성 고분자의 원료로 주로 사용되며 최근 전자 및 자동차 소재 산업이 빠르게 발달함에 따라 그 수요량 역시 급증하고 있는 추세이다.

1,4-부탄디올은 종래에 말레산무수물의 수소화, 프로필렌 옥사이드의 이성질화, 그리고 부타디엔의 아세톡실화 등의 반응을 통해 제조되었으며 상기 공정들은 화석연료를 기반으로 한 석유화학 반응물에 의존한다. 그러나 화석 연료의 유한한 자원량으로 인해 그 사용량이 감소됨에 따라 바이오매스와 같은 재생 에너지를 활용하는 새로운 연구 방안이 중요시되고 있다. 특히 최근 바이오-리파이너리 공정의 발달로 인해 저렴한 바이오 숙신산의 공급이 가능해지면서 숙신산의 수소화를 통한 1,4-부탄디올을 제조하는 공정이 크게 각광받고 있다.

숙신산의 수소화 반응은 두 단계의 연속 반응으로 진행된다. 먼저 숙신산의 수소화로 인해 감마부티로락톤이 생성되고 연속적인 수소화로 1,4-부탄디올 혹은 사수소화퓨란이 형성된다. 촉매의 종류에 따라 상기 생성물의 선택도가 변화하므로 1,4-부탄디올의 선택적인 생산을 위해서는 적절한 반응성을 가진 촉매를 제조하는

것이 중요하다. 상기 반응은 수소 흡착이 용이한 귀금속 촉매 상에서 진행되며 대표적인 촉매로는 팔라듐, 백금, 로듐, 루세늄, 그리고 레늄 등이 보고된 바 있다. 상기 금속 중에서 로듐은 단일금속 촉매로는 1,4-부탄디올의 선택적 제조에 가장 효과적이나 가격이 매우 비싸서 활용이 어렵다. 레늄의 경우 가격 대비 가장 효율적인 단일금속이지만 로듐에 비해서 반응활성이 부족하다는 단점이 있으므로 이를 극복하기 위하여 레늄 기반 촉매의 반응성 향상 연구가 전세계적으로 수행되고 있다.

레늄 촉매 상에서 1,4-부탄디올의 제조량을 향상시키기 위하여 Re-Pt/C, Re-Pd/C, Re-Pd/TiO_2 등 다양한 이종금속 촉매에 대한 연구가 수행되었다. 그러나 아직까지 레늄 기반 이종금속 촉매의 활성점 및 조성 최적화에 대한 연구는 미흡한 실정이다. 이는 레늄의 특성 중 팔라듐이나 루세늄과 같은 다른 귀금속들과 유사한 원자 크기, 표면 에너지 등으로 인해 쉽게 고용체를 형성하여 촉매의 특성분석이 까다롭기 때문이다. 또한 레늄의 경우 저온에서 수소의 해리 흡착이 어려우므로 개선된 수소 흡착실험이나 일산화탄소의 흡착실험이 요구 된다.

숙신산의 수소화 반응에 사용되는 촉매의 지지체로는 탄소 담체나 티타니아와 같음 금속산화물 담체가 있으며 산 저항성이나 활성금속의 분산도 등의 이점으로 인해 탄소 담체가 가장 효과적인 것으로 알려져 있다. 또한, 금속과 탄소 사이의 전하 전달 효과를 조절함으로써 활성금속의 반응성을 쉽게 조절할 수 있다는 장점이

있다. 따라서 탄소 담체에 담지된 레늄 기반의 금속 촉매의 물리화학적 특성을 적절히 조절한다면 숙신산의 수소화 반응에 우수한 반응성을 보일 것으로 판단된다.

본 연구에서는 다양한 레늄 기반의 촉매를 제조하여 숙신산의 수소화 연구에 적용시켰다. 먼저 단일 단계 주형법 및 습윤 함침법으로 제조된 탄소 담체에 담지된 레늄-루세늄 촉매를 숙신산의 수소화 반응에 적용시켰다. 이때 레늄과 루세늄의 비율 변화가 상기 촉매의 물리화학적 특성과 촉매 활성에 미치는 영향을 조사하였다. 촉매의 환원과정 동안 레늄-루세늄 혼합상이 생성되는 것으로 나타났으며 이로 인해 레늄과 루세늄의 강한 상호작용이 발생하는 것으로 나타났다. 또한, 촉매의 환원성, 금속 분산도, 레늄과 루세늄의 산화상태 등이 레늄과 루세늄의 비율에 영향을 받는 것으로 드러났으며 상기 금속종의 산화상태에 따라 촉매의 수소흡착능력이 변화하였다. 특히 수소흡착점 중 약한 흡착력을 가진 활성점의 경우 레늄과 루세늄의 비율이 1:1에서 가장 많은 양을 보였다. 약한 수소흡착점과 1,4-부탄디올의 생성량은 직접적인 상관관계를 보였으며 약한 수소흡착점이 증가할수록 1,4-부탄디올의 생성량은 증가하였다. 제조된 촉매 중에서 약한 수소흡착점이 가장 많은 0.3Re-0.3Ru/MC 촉매의 반응활성이 가장 높은 것으로 나타났다.

상기 레늄-루세늄 촉매의 반응활성을 향상시키기 위하여 붕소가 함유된 탄소 담체에 레늄과 루세늄을 담지한 촉매를

제조하였다. 먼저 단일 단계 주형법으로 붕소가 함유된 탄소 담체를 제조한 후 레늄과 루세늄을 습윤 함침법으로 담지하여 촉매를 제조하고 숙신산의 수소화 반응에 사용하였다. 그리고 탄소 대비 붕소의 함유량이 촉매의 물리화학적 특성과 반응활성에 미치는 영향을 조사하였다. 그 결과 붕소의 양에 따라 촉매의 표면적, 금속 분산도, 환원성 등이 변하는 것을 확인하였다. 특히 붕소는 함유량에 따라 치환종, 부분산화종, 완전산화종으로 분류되었으며 치환된 붕소의 양이 촉매의 수소흡착거동에 영향을 미치는 것으로 나타났다. 이때 촉매의 약한 수소흡착점은 치환된 붕소의 양이 많아질수록 증가하였다. 1,4-부탄디올의 수율은 붕소의 함유량에 따라 변화하였으며 약한 수소흡착점이 많아질수록 증가하였다. 제조된 촉매 중에서 약한 수소흡착점이 가장 많은 Re-Ru/0.04BMC 촉매가 1,4-부탄디올 제조에 가장 효과적인 것으로 나타났다.

숙신산으로부터 1,4-부탄디올을 제조하는 방법으로 메탄올을 반응물로 추가하여 디메틸숙시네이트를 경유하는 경로가 본 연구를 통해 제시되었다. 디메틸숙시네이트의 제조를 위하여 저렴한 구리를 활성상으로 사용하여 레늄-구리-탄소 복합체 촉매를 제조하였다. 복합체 촉매는 단일 단계 주형법으로 제조되었으며 비교를 위하여 레늄과 구리가 각각 담지된 촉매도 제조되었다. 분석 결과, 금속-담체 상호작용이 증가할수록 레늄과 구리의 표면 분산도는 증가하였으며 금속의 입자 크기가 작아질수록 감마부티로락톤과 1,4-부탄디올의 수율은 증가하였다. 제조된 촉매 중에서

평균입자크기가 가장 작은 레늄-구리-탄소 복합체 촉매가 가장 우수한 반응활성을 보였다.

주요어: 숙신산의 수소화, 1,4-부탄디올, 이종금속 촉매, 중형기공성 탄소, 레늄-루세늄 촉매, 붕소 함유 탄소, 레늄-구리 촉매, 디메틸숙시네이트, 이종기능 촉매

학번: 2014-30247

List of publications

Papers

International papers published (First author)

1. **K.H. Kang**, S.J. Han, J.W. Lee, T.H. Kim, I.K. Song, "Effect of Boron Content on 1,4-Butanediol Production by Hydrogenation of Succinic Acid over Re-Ru/BMC (Boron-modified Mesoporous Carbon) Catalysts", *Applied Catalysis A: General*, 524, pp.206-213 (2016).

2. **K.H. Kang**, T.H. Kim, W.C. Choi, Y.-K. Park, U.G. Hong, D.S. Park, C.-J. Kim, I.K. Song, "Dehydrogenation of Propane to Propylene over CrO_y-CeO_2-K_2O/γ-Al_2O_3 Catalysts: Effect of Cerium Content", *Catalysis Communications*, 72, pp.69-72 (2015).

3. **K.H. Kang**, J.O. Jun, S.J. Han, K. Kwon, O.-S. Kwon, B. Jang, I.K. Song, "Direct Synthesis of Diphenyl Carbonate from Phenol and Carbon Dioxide over Ti-salen-based Catalysts", *Journal of Nanoscience and Nanotechnology*, 15(10), pp.8353-8358 (2015).

4. **K.H. Kang**, U.G. Hong, Y. Bang, J.H. Choi, J.K. Kim, J.K. Lee, S.J. Han, I.K. Song, "Hydrogenation of Succinic Acid to 1,4-Butanediol over Re-Ru Bimetallic Catalysts Supported on Mesoporous Carbon", *Applied Catalysis A: General*, 490, pp.153-162 (2015).

5. **K.H. Kang**, U.G. Hong, J.O. Jun, J.H. Song, Y. Bang, J.H. Choi, S.J. Han, I.K. Song, "Hydrogenation of Succinic Acid to γ-Butyrolactone and 1,4-Butanediol over Mesoporous Rhenium-copper-carbon Composite Catalyst", *Journal of Molecular Catalysis A: Chemical*, 395, pp.234-242 (2014).

6. **K.H. Kang**, C.H. Lee, D.B. Kim, B. Jang, I.K. Song, "NiO/CeO_2-ZnO Nano-catalysts for Direct Synthesis of Dimethyl Carbonate from Methanol and Carbon Dioxide", *Journal of Nanoscience and Nanotechnology*, 14(11), pp.8693-8698 (2014).

7. **K.H. Kang**, W. Joe, C.H. Lee, M. Kim, D.B. Kim, B. Jang, I.K. Song, "Direct Synthesis of Dimethyl Carbonate from Methanol and Carbon Dioxide over CeO_2(X)-ZnO(1-X) Nano-Catalysts",*Journal of Nanoscience and Nanotechnology*, 13(12), pp.8116-8120 (2013).

International papers published (Co-author)

1. T.H. Kim, **K.H. Kang**, M.S. Baek, J.H. Song, U.G Hong, D.S. Park, W.C. Choi, Y.-K. Park, I.K. Song, "Dehydrogenation of Propane to Propylene with Lattice Oxygen over CrO_y/Al_2O_3-ZrO_2 Catalysts", *Journal of Molecular Catalysis A: Chemical* (In Press).

2. J.K. Lee, J.K. Kim, **K.H. Kang**, I.K. Song, "Direct Dehydrogenation of n-Butane over Platinum-tin Catalysts Supported on Alumina', *Journal of Nanoscience and Nanotechnology*, 16(10), pp.10816-10822 (2016).

3. J.H. Song, J.O. Jun, **K.H. Kang**, S.J. Han, J. Yoo, S. Park, D.H. Kim, I.K. Song, "Synthesis of Dimethyl Carbonate from Propylene Carbonate and Methanol over Y_2O_3/CeO_2-La_2O_3 Catalysts",*Journal of Nanoscience and Nanotechnology*, 16(10), pp.10810-10815 (2016).

4. U.G. Hong, **K.H. Kang**, J.H. Song, T.H. Kim, I.K. Song, "Hydrogenation of Succinic Acid to Tetrahydrofuran over Ruthenium-carbon Composite Catalyst: Effect of Catalyst Preparation Condition", *Journal of Nanoscience and Nanotechnology*, 16(10), pp.10841-10845 (2016).

5. S.J. Han, J.H. Song, Y. Bang, J. Yoo, S. Park, **K.H. Kang**, I.K. Song, "Hydrogen Production by Steam Reforming of Ethanol over Mesoporous Cu-Ni-Al_2O_3-ZrO_2 Xerogel Catalysts", *International Journal of Hydrogen Energy*, 41(4), pp.2554-2563 (2016).

6. S.J. Han, Y. Bang, J.H. Song, J. Yoo, S. Park, **K.H. Kang**, I.K. Song, "Hydrogen Production by Steam Reforming of Ethanol over Dual-templated Ni-Al_2O_3 Catalyst", *Catalysis Today*, 265, pp.103-110 (2016).

7. Y. Bang, S. Park, S.J. Han, J. Yoo, J.H. Song, J.H. Choi, **K.H. Kang**, I.K. Song, "Hydrogen Production by Steam Reforming of Liquefied Natural Gas (LNG) over Mesoporous Ni/Al_2O_3Catalyst Prepared by an EDTA-assisted

Impregnation Method", *Applied Catalysis B: Environmental*, 180, pp.179-188 (2016).

8. J.K. Kim, J.K. Lee, **K.H. Kang**, J.W. Lee, I.K. Song, "Catalytic Decomposition of Phenethyl Phenyl Ether to Aromatics over Pd-Fe Bimetallic Catalysts Supported on Ordered Mesoporous Carbon", *Journal of Molecular Catalysis A: Chemical*, 410, pp.184-192 (2015).

9. J.K. Kim, J.K. Lee, **K.H. Kang**, J.C. Song, I.K. Song, "Selective Cleavage of C-O Bond in Benzyl Phenyl Ether to Aromatics over Pd-Fe Bimetallic Catalyst Supported on Ordered Mesoporous Carbon", *Applied Catalysis A: General*, 498, pp.142-149 (2015).

10. J.O. Jun, J. Lee, **K.H. Kang**, I.K. Song, "Synthesis of Dimethyl Carbonate from Ethylene Carbonate and Methanol over Nano-catalysts Supported on CeO_2-MgO", *Journal of Nanoscience and Nanotechnology*, 15(10), pp.8330-8325 (2015).

11. S.J. Han, Y. Bang, J. Yoo, S. Park, **K.H. Kang**, J.H. Choi, J.H. Song, I.K. Song, "Hydrogen Production by Steam Reforming of Ethanol over P123-assisted Mesoporous Ni-Al_2O_3-ZrO_2 Xerogel Catalysts", *International Journal of Hydrogen Energy*, 39(20), pp.10445-10453 (2014).

12. S.J. Han, Y. Bang, J. Yoo, **K.H. Kang**, J.H. Song, J.G. Seo, I.K. Song, "Hydrogen Production by Steam Reforming of Ethanol over Mesoporous Ni-Al_2O_3-ZrO_2 Aerogel Catalysts", *International Journal of Hydrogen Energy*, 38(35), pp.15119-15127 (2013).

13. Y. Bang, S.J. Han, J. Yoo, J.H. Choi, **K.H. Kang**, J.H. Song, J.G. Seo, J.C. Jung, I.K. Song, "Hydrogen Production by Steam Reforming of Liquefied Natural Gas (LNG) over Trimethylbenzene-assisted Ordered Mesoporous Nickel-alumina Catalyst", *International Journal of Hydrogen Energy*, 38(21), pp.8751-8758 (2013).

Patents

Registered patents

1. 송인규, 김정권, 홍웅기, **강기혁**, 이종권, "술폰산기 ($-SO_3H$) 가 도입된 산점을 포함한 정렬된 구조의 중형기공성탄소에 담지된 귀금속 촉매, 그 제조방법 및 상기 촉매를 이용한 리그닌 모델 화합물 분해 방법", 대한민국 특허출원 10-2014-0057290 (2014), 대한민국특허 제 1,536,623호 (2015).

2. 송인규, **강기혁**, 홍웅기, 방용주, "규칙적인 중형기공구조를 갖는 레늄-구리-탄소 복합체 촉매, 그 제조방법 및 상기 촉매를 이용한 1,4-부탄디올의 생산 방법", 대한민국 특허출원 10-2014-0032557, 대한민국특허 제 1,572,846호 (2015).

Applied patents

1. 최원춘, 박용기, 공수진, 송인규, **강기혁**, 홍웅기, 박덕수, 김철진 "탄화수소의 탈수소화를 통해 올레핀을 제조하기 위한 촉매 및 그 제조방법", 대한민국 특허출원 10-2015-0098248 (2015).

2. 권기혁, 김동백, 송수정, 이연주, 권오성, **강기혁**, 송인규, "살렌형 촉매, 이의 제조방법 및 이를 이용한 방향족 탄산에스테르의 제조방법", 대한민국 특허출원 10-2013-0149723 (2013).

3. 이창훈, 권오성, 김동백, 이연주, 장복남, **강기혁**, 송인규, "담지촉매를 이용한 디메틸카보네이트의 제조방법", 대한민국 특허출원 10-2013-0048909 (2013).

4. 이창훈, 김동백, 장복남, **강기혁**, 송인규, “담지촉매, 이의 제조방법 및 이를 이용한 디메틸카보네이트의 제조방법”, 대한민국 특허출원 10-2012-0152621 (2012).

Conferences

International conferences (First author)

1. **K.H. Kang**, T.H. Kim, J.K. Lee, S.J. Han, W.C. Choi, Y.-K. Park, I.K. Song, "Dehydrogenation of Propane to Propylene over Cr-based Catalysts", *NANO KOREA 2015*, P1503_101, COEX, Seoul, Korea (2015/7/1-3).

2. **K.H. Kang**, J.K. Kim, J.K. Lee, S.J. Han, I.K. Song, "Re-Ru Bimetallic Catalysts for Hydrogenation of Succinic Acid to 1,4-Butanediol", *The 15th Korea-Japan Symposium on Catalysis*, GP59, Busan, Korea (2015/05/26-28).

3. **K.H. Kang**, J.O. Jun, S.J. Han, K. Kwon, O.-S. Kwon, B. Jang, I.K. Song,"Direct Synthesis of Diphenyl Carbonate from Phenol and Carbon Dioxide over Ti-salen-based Catalysts", *NANO KOREA 2014*, P1403_168, COEX, Seoul, Korea (2014/7/2-4).

4. **K.H. Kang**, J.O. Jun, S.J. Han, K. Kwon, D.B. Kim, Y. Lee, O.-S. Kwon, I.K. Song, "Direct Synthesis of Diphenyl Carbonate from Methanol and Carbon Dioxide over Metal-Salen Catalysts",*Seventh Tokyo Conference on Advanced Catalytic Science and Technology*, GP2028, Kyoto, Japan (2014/6/1-6).

5. **K.H. Kang**, C.H. Lee, D.B. Kim, B. Jang, I.K. Song, "NiO/CeO_2-ZnO Nano-catalysts for Direct Synthesis of Dimethyl Carbonate from Methanol and Carbon Dioxide", *NANO Korea 2013 Symposium*, P1303_011, Coex, Seoul, Korea (2013/7/10-12).

6. **K.H. Kang**, W. Joe, M. Kim, D.B. Kim, B. Jang, I.K. Song, "Direct Synthesis of Dimethyl Carbonate from Methanol and Carbon Dioxide over CeO_2(X)-ZnO(1-X) Nano-catalysts", *The 10thNANO KOREA 2012 Symposium*, P1208_002, COEX, Korea (2012/8/16-18).

International conferences (Co-author)

1. T.H. Kim, S. Park, **K.H. Kang**, E.J. Lee, W.C. Choi, Y.-K. Park, U.G. Hong, D.S. Park, C.-J. Kim, I.K, Song, "Oxidative Dehydrogenation of Propane to Propylene with Lattice Oxygen over CrO_y-CeO_2-K_2O/γ-Al_2O_3 Catalysts", *The 16th International Congress on Catalysis*, PC109, Beijing, China (2016/07/3-8).

2. T.H. Kim, **K.H. Kang**, M.S. Baek, J.H. Song, U.G. Hong, W.C. Choi, Y.-K. Park, I.K. Song, "CrOy/Al2O3-ZrO2 Catalysts for Oxidative Dehydrogenation of Propane to Propylene", NANO KOREA 2016, P1605_0543, KINTEX, Korea (2016/7/13-15).

3. J.K. Lee, J.K. Kim, **K.H. Kang**, I.K. Song, "Direct Dehydrogenation of n-Butane over Platinum-tin Catalysts Supported on Alumina", *NANO KOREA 2015*, P1503_099, COEX, Seoul, Korea (2015/7/1-3).

4. U.G. Hong, **K.H. Kang**, J.H. Song, T.H. Kim, I.K. Song, "Hydrogenation of Succinic Acid to Tetrahydrofuran over Ruthenium-carbon Composite Catalyst: Effect of Catalyst Preparation Condition", *NANO KOREA 2015*, P1503_123, COEX, Seoul, Korea (2015/7/1-3).

5. S.J. Han, Y. Bang, J.H. Song, J. Yoo, S. Park, **K.H. Kang**, I.K. Song, "Hydrogen Production by Steam Reforming of Ethanol over Dual-templated Ni-Al2O3 Catalyst", NANO KOREA 2015, P1503_097, COEX, Seoul, Korea (2015/7/1-3).

6. J.K. Kim, **K.H. Kang**, J.K. Lee, J.W. Lee, I.K. Song, "Catalytic Decomposition of Phenethyl Phenyl Ether to Aromatics over Pd-Fe Bimetallic Catalysts Supported on Ordered Mesoporous Carbon", *NANO KOREA 2015*, P1506_104, COEX, Seoul, Korea (2015/7/1-3).

7. J.H. Song, J.O. Jun, **K.H. Kang**, S.J. Han, J. Yoo, S. Park, D.H. Kim, I.K. Song, "Synthesis of Dimethyl Carbonate from Propylene Carbonate and Methanol over Y_2O_3/CeO_2-La_2O_3 Catalysts",*NANO KOREA 2015*, P1503_098, COEX, Seoul, Korea (2015/7/1-3).

8. S.J. Han, Y. Bang, S. Park, **K.H. Kang**, J.H. Choi, J.H. Song, I.K. Song, "Ethanol Steam Reforming over P123-assisted Mesoporous Ni-Al_2O_3-ZrO_2 Xerogel Catalysts", *The 15th Korea-Japan Symposium on Catalysis*, YO A14, Busan, Korea (2015/05/26-28).

9. J.O. Jun, J. Lee, **K.H. Kang**, I.K. Song, "Synthesis of Dimethyl Carbonate from Ethylene Carbonate and Methanol over Nano-catalysts Supported on CeO2-MgO", NANO KOREA 2014, P1403_029, COEX, Seoul, Korea (2014/7/2-4).

10. S.J. Han, Y. Bang, J. Yoo, **K.H. Kang**, J.H. Song, J.G. Seo, I.K. Song, "Ethanol Steam Reforming over a Mesoporous Ni-Al2O3-ZrO2 Aerogel Catalyst", Seventh Tokyo Conference on Advanced Catalytic Science and Technology, GP2035, Kyoto, Japan (2014/6/1-6).

11. Y. Bang, S.J. Han, J. Yoo, J.H. Choi, **K.H. Kang**, I.K. Song, "Preparation of Structure-modified Ordered Mesoporous Nickel-alumina Catalyst for Hydrogen Production by Steam Reforming of Liquefied Natural Gas (LNG)", International Conference on Hydrogen Production - 2014, P-45, Fukuoka, Japan (2014/2/2-5).

Domestic conferences (First author)

1. **강기혁**, 한승주, 이종원, 유재경, 박승원, 이어진, 송인규, “붕소가 첨가된 Re-Ru/C 촉매 상에서 숙신산의 수소화를 통한 1,4-부탄디올의 제조”, 2016 년 한국화학공학회 추계학회, P 촉매금-94, 대전 DCC (2016/10/19-21).

2. **강기혁**, 한승주, 이종원, 강태훈, 유재경, 송인규, “중형기공성 탄소 담체에 담지된 귀금속 촉매 상에서 숙신산의 수소화를 통한 1,4-부탄디올의 제조”, 2016 년 한국화학공학회 춘계학회, O 촉매 J 목-1, 부산 BEXCO (2016/4/27-29).

3. **강기혁**, 김정권, 이종권, 한승주, 김태협, 송인규, “레늄-루세늄 이중금속 촉매 상에서 숙신산의 수소화를 통한 1,4-부탄디올의 제조”, 2015 년 한국화학공학회 춘계학술회의, P 촉매목-6, 제주 ICC (2015/4/22-24).

4. **강기혁**, 김정권, 이종권, 한승주, 김태협, 송인규, “레늄-루세늄 이중금속 촉매 상에서 숙신산의 수소화를 통한 1,4-부탄디올의 제조”, 2015 년 한국화학공학회 춘계학술회의, P 촉매목-6, 제주 ICC (2015/4/22-24).

5. **강기혁**, 홍웅기, 전진오, 방용주, 최정호, 한승주, 송인규, “레늄-구리-카본 복합체 촉매 상에서 숙신산의 수소화를 통한 감마부티로락톤과 1,4-부탄디올의 제조”, 2014 년 한국화학공학회 추계학술회의, P 촉매금-2, 대전 DCC (2014/10/22-24).

6. **강기혁**, 권기혁, 김동백, 이연주, 권오성, 송인규, “이산화탄소와 페놀로부터 디페닐카보네이트의 직접합성을 위한 균일계 Ti-salen

촉매의 제조 및 특성분석", 2014 년 한국공업화학회 춘계학술회의, 1P-255, 제주 ICC (2014/4/30-5/2).

7. **강기혁**, 권기혁, 김동백, 이연주, 권오성, 송인규, "티타늄-살렌 촉매를 이용한 이산화탄소와 페놀로부터 디페닐카보네이트의 직접합성", 2014 년 한국화학공학회 춘계학술회의, P 촉매금-100, 창원 컨벤션센터 (2014/4/23-25).

8. **강기혁**, 조왕래, 김미옥, 김동백, 장복남, 송인규, "NiO/CeO_2(0.7)-ZnO(0.3) 촉매를 이용한 메탄올과 이산화탄소로부터 Dimethyl Carbonate 의 직접합성", 2012 년 한국공업화학회 추계학술회의, 2P-185, 대전컨벤션센터 (2012/10/31-11/2).

9. **강기혁**, 조왕래, 김미옥, 김동백, 장복남, 송인규, "Methanol 과 Carbon Dioxide 로부터 Dimethyl Carbonate 의 직접합성 공정에서 NiO/CeO_2-ZnO 촉매의 산-염기 특성이 반응 활성에 미치는 영향", 2012 년 한국화학공학회 추계학술회의, P 촉매수-11, 부산 BEXCO (2012/10/24-26).

10. **강기혁**, 조왕래, 김미옥, 김동백, 송인규, "CeO_2 기반의 복합 금속산화물 촉매를 이용한 메탄올과 이산화탄소로부터 Dimethyl Carbonate 의 직접합성", 2012 년 한국공업화학회 춘계학술회의, 2P-158, 김대중컨벤션센터 (2012/5/9-11).

Domestic conferences (Co-author)

1. 한승주, 송지환, 유재경, 박승원, **강기혁**, 송인규, "정렬된 중형기공을 갖는 니켈-알루미나-지르코니아 상의 에탄올의 수증기 개질 반응을 통한 수소 가스 생산", 2016 년 한국화학공학회 추계학회, P 촉매금-82, 대전 DCC (2016/10/19-21).

2. 김태협, **강기혁**, 김민영, 최원춘, 박용기, 홍웅기, 박덕수, 송인규, "CrO_y/γ-Al_2O_3 촉매 상에서 프로판 탈수소화 반응을 통한 프로필렌의 제조", 2016 년 한국화학공학회 추계학회, P 촉매금-84, 대전 DCC (2016/10/19-21).

3. 이종원, **강기혁**, 이어진, 송인규, "산특성이 조절된 중형기공 카본에 팔라듐이 담지된 촉매에 의한 과산화수소 직접 합성 반응에 관한 연구", 2016 년 한국화학공학회 추계학회, P 촉매금-74, 대전 DCC (2016/10/19-21).

4. 한승주, 송지환, 유재경, 박승원, **강기혁**, 송인규, "칼슘이 도입된 중형기공성 코발트-알루미나 제로젤 촉매의 제조 및 에탄올 수증기 개질 반응으로의 적용", 2016 년 한국화학공학회 춘계학회, P 촉매금-80, 부산 BEXCO (2016/4/27-29).

5. 김태협, **강기혁**, 송지환, 김민영, 홍웅기, 최원춘, 박용기, 송인규, "알루미나-지르코니아에 담지된 크로미아 촉매 상에서 프로판 탈수소화 반응을 통한 프로필렌의 제조", 2016 년 한국화학공학회 춘계학회, P 촉매금-49, 부산 BEXCO (2016/4/27-29).

6. 김민영, 한승주, **강기혁**, 강태훈, 김태협, 송인규, "텅스텐 산화물이 담지된 제올라이트 촉매상에서 메탄의 직접탈수소방향족화 반응을

통한 BTX 생산", 2016 년 한국화학공학회 춘계학회, P 촉매금-50, 부산 BEXCO (2016/4/27-29).

7. 한승주, 송지환, 유재경, 박승원, **강기혁**, 송인규. "스피넬 구조를 갖는 복합 알루미나 담체에 담지된 코발트 촉매 상의 에탄올 수증기 개질 반응을 통한 수소 가스 생산", 2015 년 한국화학공학회 추계학술회의, P 촉매금-9, 일산 KINTEX (2015/10/21-23).

8. 김정권, 이종권, **강기혁**, 이종원, 송인규, "중형기공성 탄소에 담지된 Pd-Fe 촉매를 통한 리그닌 내부의 선택적인 탄소-산소 분해반응 및 리그닌 모델 화합물의 분해경로 규명", 2015 년 한국화학공학회 추계학술회의, O 촉매 D 목-2, 일산 KINTEX (2015/10/21-23).

9. 김태협, **강기혁**, 이종권, 한승주, 최원춘, 박용기, 송인규, "크로미아 기반 금속 산화물 촉매 상에서 프로판의 탈수소화 반응을 통한 프로필렌의 제조", 2015 년 한국화학공학회 추계학술회의, P 촉매금-14, 일산 KINTEX (2015/10/21-23).

10. 이종권, 김정권, **강기혁**, 이진석, 장호식, 송인규, "노르말-부탄의 직접 탈수소화 반응에서 소성온도가 다른 알루미나에 담지된 백금-주석 촉매가 노르말-부텐과 1,3-부타디엔 생성에 미치는 영향", 2015 년 한국화학공학회 춘계학술회의, P 촉매목-2, 제주 ICC (2015/4/22-24).

11. 김정권, **강기혁**, 이종권, 송인규, "전이금속 복합 촉매상에서 리그닌 내부의 선택적인 탄소-산소 분해반응을 통한방향족 생성 및 리그닌 모델 화합물의 분해경로 규명", 2015 년 한국화학공학회 춘계학술회의, P 촉매목-7, 제주 ICC (2015/4/22-24).

12. 전진오, **강기혁**, 송인규, "메탄올과 프로필렌카보네이트의 에스테르교환반응을 통한 디메틸카보네이트 합성에서의 복합 금속 산화물 촉매의 영향", 2014 년 한국화학공학회 추계학술회의, P 촉매금-7, 대전 DCC (2014/10/22-24).

13. 전진오, 이중원, **강기혁**, 송인규, "CeO_2(X)-MgO(1-X) 복합 금속 산화물에 알칼리 및 알칼리 토금속이 도입된 촉매를 이용한 메탄올과 에틸렌카보네이트로부터 디메틸카보네이트의 합성", 2014 년 한국공업화학회 춘계학술회의, 1P-264, 제주 ICC (2014/4/30-5/2).

14. 홍웅기, **강기혁**, 김정권, 이중원, 이종권, 이종협, 송인규, "염산을 조절한 단일공정 계면활성-주형법으로 제조된 귀금속-탄소 복합체 촉매의 숙신산 수소화 반응활성", 2014 년 한국공업화학회 춘계학술회의, 1P-266, 제주 ICC (2014/4/30-5/2).

15. 전진오, 이중원, **강기혁**, 송인규, "알칼리 및 알칼리 토금속 산화물이 도입된 복합 금속 산화물 촉매를 이용한 메탄올과 에틸렌카보네이트로부터 디메틸카보네이트의 합성", 2014 년 한국화학공학회 춘계학술회의, P 촉매금-7, 창원 컨벤션센터 (2014/4/23-25).

16. 홍웅기, **강기혁**, 김정권, 이중원, 이종권, 이종협, 송인규, "숙신산으로부터 사수소화퓨란 생성 반응에서 촉매 표면 형태에 따른 루테늄-탄소 복합체 촉매의 반응 활성", 2014 년 한국화학공학회 춘계학술회의, P 촉매금-53, 창원 컨벤션센터 (2014/4/23-25).

17. 전진오, 이중원, **강기혁**, 백제범, 공명식, 최철호, 송인규, "메탄올과 에틸렌카보네이트의 에스테르교환반응을 통한 디메틸카보네이트 합성에서의 복합 금속 산화물 및 담지촉매의 영향", 2013 년 한국공업화학회 추계학술회의, 2P-177, 대전 컨벤션센터 (2013/10/30-11/1).

18. 최정호, 강태훈, 방용주, **강기혁**, 송인규, "4 주기 전이금속이 배위된 Keggin 형 헤테로폴리산 촉매의 산화환원 특성에 관한 연구", 2013 년 한국공업화학회 추계학술회의, 2P-181, 대전 컨벤션센터 (2013/10/30-11/1).

19. 전진오, 이중원, **강기혁**, 백제범, 공명식, 최철호, 송인규, "리튬 산화물이 도입된 복합 금속 산화물 촉매를 이용한 메탄올과 에틸렌카보네이트로부터 디메틸카보네이트의 합성", 2013 년 한국화학공학회 추계학술회의, P 촉매목-6, 대구 EXCO (2013/10/23-25).

20. 최정호, 강태훈, 방용주, **강기혁**, 송인규, "Keggin 형 α-$K_5PW_{11}O_{39}$(M?OH_2) (M=Mn^{2+}, Co^{2+}, Ni^{2+}, Zn^{2+}) 헤테로폴리산 촉매의 산화환원 및 반응활성에 관한 연구", 2013 년 한국화학공학회 추계학술회의, P 촉매목-10, 대구 EXCO (2013/10/23-25).

21. 조왕래, **강기혁**, 안영수, 송찬주, 권범진, 송인규, "Urea methanolysis 반응에서 XCo_3O_4/ZnO-CeO_2-La_2O_3 촉매의 Co_3O_4 담지량이 DMC 생성 수율에 미치는 영향", 2012 년 한국공업화학회 추계학술회의, 1P-18, 대전컨벤션센터 (2012/10/31-11/2).

22. 조왕래, **강기혁**, 안영수, 송찬주, 권범진, 송인규, "XCo_3O_4/ZnO(0.64)-CeO_2(0.26)-La_2O_3(0.1) 촉매를 이용한 Urea 와 Methanol 로부터

Dimethyl Carbonate 의 합성", 2012 년 한국화학공학회 추계학술회의, P 촉매수-13, 부산 BEXCO (2012/10/24-26).

23. 조왕래, **강기혁**, 안영수, 송찬주, 권범진, 송인규, "Urea methanolysis 반응에서 $ZnO-CeO_2-La_2O_3$ 촉매의 La_2O_3 조성이 DMC 생성 수율에 미치는 영향", 2012 년 한국공업화학회 춘계학술회의, 2P-198, 김대중컨벤션센터 (2012/5/9-11).

24. 조왕래, **강기혁**, 안영수, 송찬주, 권범진, 송인규, "$ZnO(0.64)-CeO_2(0.26)-MO(0.1)$(MO=Metal Oxide) 촉매를 이용한 Urea 와 Methanol 로부터 Dimethyl Carbonate 의 합성", 2012 년 한국화학공학회 춘계학술회의, P 촉매금-29, 제주 ICC (2012/4/25-27).